学位論文

Delineating species of two glaucophyte genera, on the basis of molecular data and comparative ultrastructures

（灰色藻 2 属の分子情報と微細形態比較に基づく種分類学的研究）

平成 27 年 12 月博士（理学）申請

東京大学大学院理学系研究科

生物科学専攻

高橋　紀之

CONTENTS

ABSTRACT

A heterotrophic organism 1–2 billion years ago enslaved a cyanobacterium to become the first photosynthetic eukaryote and has diverged globally, evolving into species of three major lineages; namely, red algae, Chloroplastida [Viridiplantae (green algae and land plants)] and glaucophytes. Within the three, glaucophytes are the most expected candidate that may have retained ancestral features of the first photosynthetic eukaryote. The motile genus *Cyanophora* and immotile genus *Glaucocystis* represent two divergent clades of glaucophytes. *Cyanophora* is an important glaucophyte genus of unicellular biflagellates whose nuclear genome was recently sequenced. The coccoid genus *Glaucocystis* is characterised by having a thick cell wall, which has to date prohibited examination of the native ultrastructural features of the protoplast periphery. Although the type species of these two genera have been reported from various localities of the world, taxonomic studies using more than two cultured strains are lacking for the glaucophyte algae. Furthermore, no taxonomic study has used molecular methods to delineate species. Very recently during my graduate course to complete the present doctoral dissertation, genetic diversity within *Cyanophora* and *Glaucocystis* was reported using several DNA markers and many worldwide strains to demonstrate multiple cryptic species within each genus; but no morphological difference between strains has been reported within each of the glaucophyte genera.

The present dissertation aimed to delimit the species within the two glaucophyte genera based upon combination of light microscopy (LM), several electron microscopic (EM) methods and molecular analyses, from many globally distributed strains including my several novel strains. In order to reveal detailed ultrastructural diversity above morphological difference observed by LM and conventional EM, I applied advanced EM methodologies for comparative morphology to delineate the *Cyanophora* and

Glaucocystis species. Recent advances in ultra-high resolution (UHR) field emission (FE)-scanning electron microscopy (SEM) have enabled the ultrafine observation of entire cell surface; besides, a lot of cells are observable at once. Although the *Cyanophora* algae have been widely studied as a model organism of primitive phototrophs, surface ornamentations of the naked vegetative cells have not been examined using UHR FE-SEM. FE-SEM, however, cannot be applied for the native protoplast surfaces when enclosed by cell wall or extracellular matrix as in immotile *Glaucocystis*. Transmission electron microscopy (TEM) has also not previously unveiled the ultrastructural diversity in this genus. Recent advancements in ultra-high voltage electron microscopy (UHVEM) have enabled thick-section micrographs in biological samples. Based on three-dimensional (3D) UHVEM tomography, the *in situ* peripheral ultrastructure of protoplasts can be observed, even when enclosed by a cell wall tightly. However, 3D UHVEM has not previously been applied to algae or protozoa. Here, the present dissertation was undertaken to reveal detailed surface ornamentation of *Cyanophora* by UHR FE-SEM and native 3D peripheral ultrastructure of protoplasts of the walled *Glaucocystis* cells.

In Chapter 2, vegetative cells of *Cyanophora* species were examined by UHR FE-SEM; it was revealed under low accelerating voltage (LV) that the cell surface was ornamented with angular fenestrations framed by ridges. TEM showed that the ridge was formed by the edges of overlapping or attaching outermost plate vesicles at the cell periphery. The present LM and SEM clearly distinguished three species with ovoid to ellipsoidal cells (*C. paradoxa* Korshikov, *C. cuspidata* Tos.Takah. sp. nov. and *C. kugrensii* Tos.Takah. sp. nov.) and two species with broad, bean-shaped cells (*C. biloba* Kugrens, B.L.Clay, C.J.Mey. & R.E.Lee and *C. sudae* Tos.Takah. sp. nov.) on the basis

of differences in cell shape and surface ornamentations of the vegetative cells under the LV FE-SEM. Molecular phylogenetic analyses of concatenated photosystem I P700 chlorophyll *a* apoprotein A2 (*psaB*) and photosystem II P680 chlorophyll *a* apoprotein D1 (*psbA*) gene sequences and internal transcribed spacer (ITS) regions of nuclear ribosomal DNA (*r*DNA) as well as a comparison of secondary structures of nuclear *r*DNA ITS-2 and genetic distances of *psaB* genes, supported the delineation of five morphological species of *Cyanophora*.

In Chapter 3, the 3D ultrastructure in species of *Glaucocystis* was examined using UHVEM. The present 3D-modelling of *Glaucocystis* cells using UHVEM tomography clearly showed that numerous, leaflet-like flattened vesicles are distributed throughout the protoplast periphery just underneath a single-layered plasma membrane. Besides, *Glaucocystis* species exhibited morphological diversity in terms of their 3D ultrastructural features based upon the UHVEM tomography. On the basis of the 3D ultrastructures of the protoplast periphery, three periphery types were distinguished within *Glaucocystis* strains even by ultrathin section TEM. Furthermore, two types of cellulose filament arrangements of the mother cell wall were recognised within the *Glaucocystis* strains examined, based on the LV FE-SEM. Combined with these ultrastructural features and LM differences in cell wall at the poles of a vegetative cell and the degree of expansion of a mother cell wall, the *Glaucocystis* strains were clearly classified into six species: *G. nostochinearum* Itzigs. *ex* Rabenh., *G. oocystiformis* Prescott, *G. incrassata* (Lemmerm.) Tos.Takah. comb. & stat. nov., *G. geitleri* E.G.Pringsh. *ex* Tos.Takah. sp. nov., *G. miyajii* Tos.Takah. sp. nov. and *G. bhattacharyae* Tos.Takah. sp. nov. The delineation of these six morphological species was supported by molecular phylogenetic analyses as well as a comparison of

secondary structures of nuclear *r*DNA ITS-2 and genetic distances of *psaB* genes.

The ultrastructures of cell coverings are very important because they might reflect the evolutionary processes and present lifestyles of each organism. The present multiple EM methods in each genus also unveiled the native feature of cell periphery. The 3D peripheral ultrastructures of immotile glaucophyte genus *Glaucocystis* were essentially identical to that of the motile glaucophyte genus *Cyanophora* as well as the secondary phototrophs in haptophytes and alveolates. Thus, the common ancestor of glaucophytes and the first photosynthetic eukaryote might have shown similar 3D structures. On the other hand, morphological difference between the two genera may reflect the presence or absence of a cell wall. Through evolutionary processes from the ancestral *Cyanophora*-like biflagellate to the immotile *Glaucocystis* cells enclosed by a cell wall, the peripheral feature has evolved and diverged losing the cell motility.

The immotile glaucophyte divergent clade, to which *Glaucocystis* belongs, also includes two palmelloid colonial genera *Cyanoptyche* and *Gloeochaete*. Their feature or lifestyle might exhibit the evolutionary intermediate stage between *Cyanophora* and *Glaucocystis* because their naked zoospores resemble *Cyanophora* vegetative cells whereas their vegetative cells are immotile and enclosed by a non-cellulosic extracellular matrix. However, their ultrastructural diversity has not been reported and cultured strains available are limited within the genera although they have been collected globally and considered as a cosmopolitan species. These worldwide records may indicate several cryptic species within each genus, as the case of *Cyanophora* and *Glaucocystis* shown by this dissertation. Thus, taxonomic studies based upon molecular methods and comparative ultrastructures using global strains are also required for each of the palmelloid colonial genera. The application of LV FE-SEM to their zoospores

lacking extracellular matrix as well as 3D UHVEM tomography to their vegetative cells would unveil the peripheral ultrastructures and other essential structures within the each genus, leading to the species diversity and taxonomy of the palmelloid colonial glaucophytes. Based upon taxonomy of the each glaucophyte genus, the novel classification of glaucophytes will be reconstructed, as well as that of eukaryotes.

Since such 3D UHVEM tomography and FE-SEM surface observations can provide the *global* information of characters entirely, they will become the mainstream methods in illuminating such a native feature of microorganism and reconstructing the microbial taxonomy. The present dissertation will become a model case of the methods.

ABBREVIATIONS

3D, three-dimensional

CBC, compensatory base change

CCAP, Culture Collection of Algae and Protozoa

CCMP, Provasoli-Guillard National Center for Culture of Marine Phytoplankton

EM, electron microscopy

FE, field emission

FH, Farlow Herbarium, University of Harvard

FS, freeze-substitution

HPF, high-pressure freezing

ICN, International Code of Nomenclature for algae, fungi, and plants

ICNP, International Code of Nomenclature of Prokaryotes

ICZN, International Code of Zoological Nomenclature

ITS, internal transcribed spacer

LM, light microscopy

LV, low accelerating voltage

ML, maximum likelihood

NIES, National Institute for Environmental Studies

NJ, neighbour-joining

OTU, operational taxonomic unit

PCR, polymerase chain reaction

psaB, photosystem I P700 chlorophyll *a* apoprotein A2 gene

psbA, photosystem II P680 chlorophyll *a* apoprotein D1 gene

SAG, Sammlung von Algenkulturen der Universität Göttingen

SEM, scanning electron microscopy

TEM, transmission electron microscopy

TNS, Department of Botany, National Museum of Nature and Science

UHVEM, ultra-high voltage electron microscopy

UHR, ultra-high resolution

UTEX, Culture Collection of Algae at the University of Texas at Austin

1. GENERAL INTRODUCTION

1.1. THE PHYLOGENY AND CLASSIFICATION OF GLAUCOPHYTES

Approximately 1–2 billion years ago during the Proterozoic Aeon, a heterotrophic eukaryote enslaved a cyanobacterium to obtain the ability for photosynthesis and become the common ancestor of the primary photosynthetic eukaryotes [Archaeplastida (Adl *et al.*, 2005, 2012) or Kingdom Plantae *sensu* Cavalier-Smith (1981) (Cavalier-Smith, 1981, 1998)] (Figure 1.1). Primary photosynthetic eukaryotes have ruled this planet as primary producers, evolving into species of three major lineages (Adl *et al.*, 2005, 2012; Price *et al.*, 2012; Spiegel, 2012); namely, red algae, Chloroplastida [Viridiplantae (green algae and land plants)] and glaucophytes (Figure 1.2). The evolutionary scenario that the eukaryotes and the primary photosynthetic eukaryotes were established by a series of endosymbioses with an α-proteobacterium and a cyanobacterium as mitochondrial and plastidial ancestors, respectively, is widely accepted after Sagan (1967) introduced the endosymbiotic theory (Schimper, 1883; Mereschkowsky, 1905; Geitler, 1923) (Figure 1.1). Whilst no organisms have been known as a primitive eukaryote that retains the very features of the first eukaryote with endosymbiotic α-proteobacteria, the glaucophytes are considered enigmatic phototrophs retaining the ancestral archaeplastidal features that may have been lost in red algae and Chloroplastida (Pascher, 1914; Hall & Claus, 1963, 1967; Kies, 1992; Spiegel, 2012). For this reason, the flagellate glaucophyte species *Cyanophora paradoxa* Korshikov (1924) (Figure 1.2) has been examined extensively by morphological and molecular data for elucidating the early evolutionary facets of Archaeplastida (e.g., Bohnert *et al.*, 1985; Sato *et al.*, 2009; Watanabe *et al.*, 2012; Facchinelli *et al.*, 2013; Gross *et al.*, 2013; Kern *et al.*, 2013; Miyagishima *et al.*, 2014; Smith *et al.*, 2014) and recently its nuclear

genome has been sequenced (Price *et al.*, 2012). However, recognition and taxonomy of glaucophytes had been extremely confused until the consensus of recognition of plastids in the glaucophyte cells based on the endosymbiotic theory (Geitler, 1923; Bhattacharya & Schmidt, 1997) (Figure 1.1).

Today glaucophyte plastids are *not* considered as endosymbiotic cyanobacteria but photosynthetic organelles (Herdman & Stanier, 1977; Lambert *et al.*, 1985; Bayer, 1986; Stirewalt *et al.*, 1995) and proposed to term them cyanoplasts or muroplasts (Schenk *et al.*, 1987; Schenk, 1992, 1994, 2002) (Figure 1.2). The plastids resemble the putative cyanobacterial symbionts of ancestral Archaeplastida, represented by a putative carboxysome, central body, containing ribulose-l,5-bisphosphate carboxylase/oxygenase (RuBisCO) (Mangeney *et al.*, 1987; Kies, 1992; Burey *et al.*, 2005, 2007; Fathinejad *et al.*, 2008) as well as by the bacterial cell wall remnant which is lysozyme-sensitive and consists of peptidoglycan (Schenk, 1970; Aitken & Stanier, 1979; Scott *et al.*, 1984; Kies, 1988) surrounding the plastids demonstrated by transmission electron microscopy (TEM) (Schnepf & Koch, 1966; Kies, 1984, 1989, 1992).

Historically, however, because of the morphological resemblance to free-living cyanobacteria (Pascher, 1914), the term “cyanelles (cyanellae)” was taken for glaucophyte plastids, meaning endosymbiotic cyanobacteria (Pascher, 1929), and finally the “cyanelles” was raised to the rank of cyanobacterial species: *Cyanocyta korschikoffiana* Hall & Claus (1963) [Cyanocytaceae Hall & Claus (1963)] for “endosymbiotic cyanelles” in *Cyanophora paradoxa* and *Skujapelta nuda* Hall & Claus (1967) [Skujapeltaceae Hall & Claus (1967)] in *Glaucocystis nostochinearum* Itzigs. *ex* Rabenh. (1866) (Figure 1.2). Pascher (1914, 1929) defined the term “syncyanosis” or “endocyanosis” for symbiosis or endosymbiosis between those symbiotic or

endosymbiotic cyanelles (cyanobacteria) and other organisms whereas the whole consortia consisted of both organisms are termed “cyanomes”. As a result, the syncyanotic *host cells* of glaucophytes are polyphyletic and assumed to be green algae lacking chloroplasts, plastid-lacking cryptophytes or dinophytes (Pascher, 1929). Therefore, the classification of glaucophytes was confused; glaucophyte genera were classified as the green algae (e.g., *Glaucocystis* and *Gloeochaete*; Komárek & Fott, 1983) or cryptophytes (e.g., *Cyanophora*; Bourrelly, 1960, 1985) on the basis of the putative *host* phylogeny and simultaneously they were classified into a cyanobacterial lineage (West, 1904; Borzì, 1914; Schaffner, 1922) based on the putative phylogeny of their cyanelles.

Skuja (1948), however, proposed glaucophytes as an independent division Glaucophyta Skuja (1954) (Table 1.1) and Skuja (1954, 1956) classified immotile glaucophytes into Glaucophyta on the basis of the endocyanosis (*not* by their phylogeny, however), whereas motile glaucophyte *Cyanophora* was classified into cryptophytes. On the other hand, Kies & Kremer (1986) redefined the division Glaucocystophycota L.Kies & B.P.Kremer (1986) (Table 1.1) at the light of common characters of “*host*” cells for the first time on the basis of the observations using three strains of three glaucophyte genera (*Glaucocystis*, *Gloeochaete* and *Cyanophora*) (Kies, 1979); within Glaucocystophycota, they recognised three orders, each of which comprises one of the three genera (Table 1.1). Although some classification systems regard this division as higher rank (e.g., Cavalier-Smith, 1998) (Table 1.1), glaucophyte classification itself is not above that of Kies & Kremer (1986). In their classification system, whereas the other two orders are monotypic, Gloeochaetales are composed of two families. Kies (1989) observed another strain identified as *Cyanoptyche* belonging to the other family

than Gloeochaetaceae (Table 1.1). As a result, each family recognised by Kies & Kremer (1986) includes a single cultured strain but no taxonomic study at species rank has been performed using the four strains. On the other hand, Kugrens *et al.* (1999) performed a taxonomic study using two *Cyanophora* strains but above their works, no species taxonomy has been depended upon cultured strains within each glaucophyte genus or family (discussed below). Furthermore, no taxonomic study has used molecular methods.

1.2. THE TAXONOMY OF GLAUCOPHYTE SPECIES AS A MICROALGAL LINEAGE

Within Archaeplastida, red algae thrive throughout the oceans and Chloroplastida have advanced even onto land globally. The glaucophytes comprise the smallest number of taxa among the three lineages of Archaeplastida and are rare microalgae that live only in inland freshwater (Kies & Kremer, 1986, 1990; Kies, 1992) (Table 1.1; Figure 1.2). Thus, taxonomic studies at species rank in glaucophytes have fallen behind to those in the other archaeplastidal lineages, red algae and Chloroplastida, thoroughly classified at species level since or even before the establishment of Linnaean system (Theophrastus, 1483; Tao, 718; Li, 1596; Linnaeus, 1753). In taxonomy of land plants, macroalgae and metazoans, “type specimens” have been used as objective criteria for classification. In bacterial and archaeal taxonomy, “type strains” have been used under International Code of Nomenclature of Prokaryotes (ICNP, formerly ICNB, International Code of Nomenclature of Bacteria). Similarly, under the International Code of Zoological Nomenclature (ICZN), a protist strain can be holotypified as a hapantotype. In microalgal taxonomy, however, cultured strains cannot be typified but figures and specimens, under International Code of Nomenclature for algae, fungi, and plants (ICN, formerly ICBN, International Code of Botanical Nomenclature). Figures cannot provide information above the original description whereas in specimens only preservative characters are comparable after long time passed. Although cultured strains are far more useful than the fixed specimens for taxonomical examination, historically phycological taxonomy has been developed lacking cultured strains (Nakada, 2010). Nowadays a lot of microalgae have become cultivable as cultured strains in media (Pringsheim, 1946), including glaucophytes (Geitler, 1923; Pringsheim, 1958) (Figure 1.2). Under current

ICN, cryopreserved strains are acceptable as nomenclatural types and "*ex typo* strains"[1] (strains derived from cryopreserved type specimens) are very useful for phycological research based on cultured materials; cryopreservation, however, has not applicable or established for most of the algal species including glaucophyte species (Mori *et al.*, 2002; Day *et al.*, 2010). Alternatively, based upon holotypification of the specimens made from a clonal strain (referred to as an "authentic strain"[2]) as well as upon supports of previously designated a nomenclatural type lacking cultured strain by epitypifying the material made from a new authentic strain, microalgal taxonomy has established objective and reproducible criteria even under ICN, corresponding to type strains under ICNP: *authentic strains associated with types*. In glaucophyte designations, however, no authentic strains have existed but that of *Cyanophora biloba* Kugrens, B.L.Clay, C.J.Mey. & R.E.Lee (1999) (Kugrens *et al.*, 1999).

In my master's thesis (Takahashi, 2013), I tried to delineate species of *Cyanophora* on the basis of molecular phylogenetic analyses and comparative morphology using several clonal strains worldwide including one newly established. However, taxonomic characters observed by light microscopy (LM) were insufficient to clearly characterise *Cyanophora* species, and evaluating the species concept based only upon conventional electron microscopy (EM) was extremely difficult. During my graduate course to complete the present doctoral dissertation, Chong *et al.* (2014) reported the cryptic diversity within glaucophyte species using molecular phylogenetic analyses and showed

---

[1]According to ICN, they should be referred to as "ex-type" (*ex typo*), "ex-holotype" (*ex holotypo*), "ex-isotype" (*ex isotypo*), etc., in order to make it clear they are derived from the type but are not themselves the nomenclatural type (Recommendation 8B).

[2]In this thesis, I proposal to refer authentic strain as "holotypic authentic strain" for one corresponding to holotype, "epitypic authentic strain" for one corresponding to epitype, etc., in order to distinguish "authentic strain" from which type specimens are made.

that *Cyanophora* represents one of the two divergent clades of glaucophytes; the other clade includes *Cyanoptyche*, *Gloeochaete* and *Glaucocystis*. However, Chong *et al.* (2014) did not delimit the species within each genus using morphological data (see also Section 2.7 Addendum).

1.3. MICROSCOPY AND MICROBIOLOGY

"Microorganisms" did not *exist* for scientists before van Leeuwenhoek discovered and observed them in 1674 by LM, starting microbiology (van Leewenhoek, 1677; Smit & Heniger, 1975; Palm, 2008). Various types of LM, the essential tool for microbiology, have been devised since 19th century and the LM resolution has also been improved to reach the very theoretical limit by the end of the 19th century (Kojima, 2008). This improvement of the LM resolution brought the starting point of modern taxonomy on microorganisms (Nakada, 2010). However, delimitation between unicellular related species only by LM has been far more limited in microorganisms than in macroorganisms whose characters have been unveiled by the naked eye or by LM (Li, 1596; Linnaeus, 1753). The first turning point has come by invention of EM based on the nature of electron in the 20th century (de Broglie, 1924; Kojima, 2008). Indeed, TEM already had enough high resolution to elucidate the characters precisely even in 10-μm-scale microalgae. Conventional TEM, however, can reveal only limited parts of cells, *locally*, because the electron beam can transmit only into ultrathin samples (Kojima, 2008; Cyranoski, 2009). On the other hand, scanning electron microscopy (SEM) provides the whole characters of an entire cell, *globally*, as for cell surface. Conventional SEM, however, had not got enough high resolution to observe the ultrastructures precisely (Nagatani, 1991; Kojima, 2008).

Recent advances in ultra-high resolution (UHR) field emission (FE)-SEM have enabled the ultrafine observation of entire cell surface; besides, a lot of cells are observable all at once (Nagatani, 1991; Osumi, 1998). Here, in the present thesis, as supported by ultrathin section and freeze-fracture TEM, UHR FE-SEM showed that the

whole peripheral surface of naked vegetative cells in several species of *Cyanophora* is ornamented with angular fenestrations formed by ridges structured by overlapping, leaflet-like flattened vesicles underneath the plasma membrane (see Chapter 2). However, this leaflet-like three-dimensional (3D) morphology of the flattened vesicles has not been unambiguously demonstrated in other glaucophyte genera, possibly because FE-SEM cannot reveal surface ultrastructures of the periphery of the protoplast that is enclosed by a cell wall or extracellular matrix in these genera (Kies & Kremer, 1986).

Meanwhile, thick-section micrographs in biological samples have been obtainable by ultra-high voltage electron microscopy (UHVEM): UHR TEM with ultra-high accelerating voltage (Cyranoski, 2009). Based on 3D UHVEM tomography, the *in situ* peripheral ultrastructure of protoplasts can be observed, even when enclosed by extracellular structures (Nishida *et al.*, 2013). 3D UHVEM, however, has not previously been applied to phycology or taxonomy. Here, in the present thesis, the 3D ultrastructure of the protoplast periphery was revealed in the species of *Glaucocystis* by UHVEM tomography combined with high-pressure freezing (HPF) and freeze-substitution (FS) fixation (see Chapter 3). The species had a fundamentally identical peripheral 3D ultrastructure but exhibited morphological diversity in terms of their 3D peripheral ultrastructure.

For microbial taxonomy, entire or *global* observations of a character are required to delineate species. Now that the performance of EM has reached atomic resolution (Kojima, 2008; Akashi *et al.*, 2015), any cellular ultrastructures and their 3D arrangements are comparable in principle; this comparison based upon the extreme morphology shall bring a big turning point in microbial taxonomy, I guess. As

microscopy like UHVEM or UHR FE-SEM become more and more general, such *global* and ultrafine observations will become mainstream in taxonomy or another fields in the new age. In the present thesis, I applied ultrastructural observations based on 3D EM to microalgal taxonomy for the first time. Combining the *global* ultrastructural data with molecular data, I could clearly distinguish cultured strains of two glaucophyte genera, *Cyanophora* and *Glaucocystis*, into five and six species, respectively, and new taxonomic systems of species within these two genera are proposed: *C. paradoxa*, *C. biloba*, *C. cuspidata* Tos.Takah. sp. nov., *C. kugrensii* Tos.Takah. sp. nov. and *C. sudae* Tos.Takah. sp. nov. (Chapter 2); *G. nostochinearum*, *G. oocystiformis* Prescott (1944), *G. incrassata* (Lemmerm.) Tos.Takah. comb. & stat. nov., *G. geitleri* E.G.Pringsh. *ex* Tos.Takah. sp. nov., *G. miyajii* Tos.Takah. sp. nov. and *G. bhattacharyae* Tos.Takah. sp. nov. (Chapter 3).

1.4. TABLE AND FIGURES

Table 1.1. Glaucophyte species and supraspecific taxa previously recognised*.

Rank	Taxon name
Subkingdom	Glaucocystobiotina Doweld (in Prosyll. tracheoph.: LXXIII. 2001)
	= Biliphyta[a] (Caval.-Sm. in BioSys. 14: 479. 1981) *sensu* Saunders & Hommersand (2004)
	= Glaucobionta[a] Bresinsky & Kaderkit (in Sys.-Pos. Bot. 2. Aufl.: 2001; 3. Aufl.: 2006) *nom. nud.*
Infrakingdom	Glaucophyta[a] (Skuja) Caval.-Sm. (in Biol. Rev. 73: 209, 250. 1998)
Division	Glaucophyta[a] Skuja (in Melchior & Werdermann (eds.), Syllab. Pflanzenfam. 1: 56. 1954)
	≡ Glaucophyta[a] Skuja (in Symb. Bot. Upsal. 9(3): 6, 7, 63. 1948) *nom. nud.*
	= Glaucocystophycota[b] L.Kies & B.P.Kremer (in Taxon 35(1): 130. 1986, 'Glaucocystophyta')
Class	Glaucophyceae[a] Skuja (in Melchior & Werdermann (eds.), Syllab. Pflanzenfam. 1: 56. 1954)
	= Glaucophyceæ[a] Bohlin (in Utkast Grön. Alg.: 16, 25, fig. 1901) *nom. nud.*
	= Glaucocystophyceae[b] J.H.Schaffn. (in Classif. Pl.: 131. 1922, 'Glaucocysteæ')
	= Holoplastideae[a] Bessey (in Synop. Pl. Ph.: 6. 1907)
Subclass	Glaucocystophycidae[b] G.S.West (in Brit. Fres. Alg.: 316. 1904, 'Glaucocystideæ')
Order	Glaucocystales Bessey (in Synop. Pl. Ph.: 6. 1907)
	= Glaucystinae Borzì (in Nuovo Giorn. Bot. Ital. 21: 360. 1914)
Family	Glaucocystaceae[b] G.S.West (in Brit. Fres. Alg.: 317. 1904, 'Glaucocystaceæ')
	≡ Glaucocystaceæ Bohlin (in Utkast Grön. Alg.: 25. 1901) *nom. nud.*
	≡ Glaucocysteae L.Gross & A.Kneucker (in Allg. Bot. Zeitschrift: 126. 1901) *nom. nud.*
Subfamily	Glaucocystidea Pascher (in SitzBer. Deutsch. Naturw.-Med. Ver. Böhmen "Lotos" 54: 175. 1906) *nom. nud.*
	≡ Glaucocystoideae Komárek & Fott (in Chlorophyceae Grünalgen: 550. 1983) *nom. prov.*
	≡ Glaucocystidoideae Komárek & Fott (in Chlorophyceae Grünalgen: 446, 552. 1983) *nom. nud.*
Genus	*Glaucocystis* Itzigs. *ex* Rabenh. (in Alg. Eur. 94–5: no. 1935. 1866)
	= *Glaucocystis* Itzigs. (1854) *in litt.*, *ined.*
	Glaucocystis nostochinearum Itzigs. *ex* Rabenh. (in Alg. Eur. 94–5: no. 1935. 1866)
	≡ *Skujapelta nostochinearum* (Itzigs. *ex* Rabenh.) Hirose & M.Akiyama (in Illust. Jpn. fresh. Alg.: 155. 1977) *inval.*
	= *Glaucocystis nostochinearum* Itzigs. (1854) *ined.*
	= *Oocystis cyanea* Nägeli *in litt., ined.*
	= *Cyanocystis itzigsohniana* Rabenh. *in litt., ined.*

Table 1.1. Continued.

	= *Glaucocystis molochinearum* Geitler (in Arch. Hydrobiol. 15: 280. 1924) *nom. nud.*
	Glaucocystis bullosa (Kütz.) Wille (in Nyt Mag. Naturv. 56: 38. 1919)
	≡ *Palmella bullosa* Kütz. (in Alg. Aq. Dulc. Ger. 16: no. 154., sp. p. 243, Tab. Phyc. I, t. 14, f. III, 1836)
	Glaucocystis oocystiformis Prescott (in Farlowia 1(3): 372. 1944)
	= *Glaucocystis caucasica* Tarnogr. (in Rab. Severo-Kavkaz. Gidrobiol. Stancij Ordžonikidze 6: 1957)
	Glaucocystis duplex Prescott (in Farlowia 1(3): 371–2. 1944)
	Glaucocystis cingulata Bohlin (in Bid. K. Svensk. Vet. Akad. Handl. 23, 3(7): 13. 1897)
	Glaucocystis reniformis B.N.Prasad, R.K.Mehrotra & P.K.Misra (in Cryptogam. Algol. 5: 79. 1984)
	Glaucocystis indica R.J.Patel (in Geophytol. 11(2): 259. 1981)
	Glaucocystis simplex Tarnogr. (in Rab. Severo-Kavkaz. Gidrobiol. Stancij Ordžonikidze 8: 18. 1959) *nom. nud.*
	Glaucocystis geitleri E.G.Pringsh. (in Prad, Stud. Pl. Physiol.: 177–8. 1958) *nom. provis., inval.*
	≡ *Glaucocystis geitleri* E.G.Pringsh. *ex* Koch (in Arch. Mikrobiol. 47: 414. 1964) *nom. nud.*
	≡ *Glaucocystis geitleri* E.G.Pringsh. *ex* Komárek & Fott (in Chlorophyceae Grünalgen: 554. 1983) *nom. provis.*
Genus	*Glaucocystopsis* Bourr. (in Bull. Inst. Franç. Afr. Noire, sér.A, 23: 318, 355. 1961)
	≡ *Glaucocystopsis* Bourr. (in Acad. Sci. 251: 416. 1960) *nom. nud.*
	Glaucocystopsis africana Bourr. (in Bull. Inst. Franç. Afr. Noire, sér.A, 23: 318, 355. 1961)
	≡ *Glaucocystopsis africana* Bourr. (in Acad. Sci. 251: 416. 1960) *nom. nud.*
Genus	*Archeopsis* Skuja (in Melchior & Werdermann (eds.), Syllab. Pflanzenfam. 1: 56. 1954) *nom. nud.*
	Archeopsis monococca (Kütz.) Skuja (in Melchior & Werdermann (eds.), Syllab. Pflanzenfam. 1: 56. 1954) *inval.*
	≡ *Palmogloea monococca* (Kütz.) Kütz (in Sp. Alg.: 229. 1849) *nom. inval.*
	≡ *Gloeocapsa monococca* Kütz. (in Phycol. general. oder Anatom., Physiol. Systkde. Tange.: 175. 1843)
Order	Gloeochaetales L.Kies & B.P.Kremer (in Taxon 35(1): 131. 1986)
Family	Gloeochaetaceae Skuja (in Melchior & Werdermann (eds.), Syllab. Pflanzenfam. 1: 56. 1954)
	≡ Gloeochætaceæ Bohlin (in Utkast Grön. Alg.: 25. 1901) *nom. nud.*
	≡ Gloeochaeteae Pascher (in Lotos 54: 175. 1906) *nom. nud.*
Genus	*Gloeochaete* Lagerh. (in Öfversigt Kgl. Vetensk. Akad. Förhandl. 40: 39. 1883, ‘Gloeochæte’)
	Gloeochaete wittrockiana Lagerh. (in Öfversigt Kgl. Vetensk. Akad. Förhandl. 40: 39. 1883)[c]
	≡ *Skujapelta wittrockiana* (Lagerh.) Hall & Claus *ex* Hirose & M.Akiyama (in Illust. Jpn. fresh. Alg.: 155.1977) *inval.*

Table 1.1. Continued.

	Gloeochaete bicornis Kirchn. (in Jahresh. Ver. vaterl. Naturkde. Württ. 44: 165. 1888)[c]
Genus	*Schrammia* P.-A.Dang. (in Le Botaniste 1: 161. 1889)
	Schrammia barbata P.-A.Dang. (in Le Botaniste 1: 158–161. 1889)[c]
Family	Glaucosphaeraceae Skuja (in Melchior & Werdermann (eds.), Syllab. Pflanzenfam. 1: 56. 1954)[d]
Genus	*Cyanoptyche* Pascher (in Jahrb. Wiss. Bot. 71: 459–60. 1929)[d]
	Cyanoptyche gloeocystis Pascher (in Jahrb. Wiss. Bot. 71: 460. 1929)[d]
	Cyanoptyche dispersa Geitler (in Österr. Bot. Z. 106: 469. 1959)[d]
Genus	*Chalarodora* Pascher (in Jahrb. Wiss. Bot. 71: 460. 1929)[d]
	Chalarodora azurea Pascher (in Jahrb. Wiss. Bot. 71: 460. 1929)[d]
Order	Cyanophorales L.Kies & B.P.Kremer (in Taxon 35(1): 131. 1986)
Family	Cyanophoraceae L.Kies & B.P.Kremer (in Taxon 35(1): 131. 1986)
Genus	*Cyanophora* Korshikov (in Russ. Arch. Protistol. 3: 55–64, 71–2. 1924)
	Cyanohora paradoxa Korshikov (in Russ. Arch. Protistol. 3: 55–64, 71–2. 1924)
	Cyanophora tetracyanea Korshikov (in Arch. Protistenkd. 95: 26. 1941)
	Cyanophora biloba Kugrens, B.L.Clay, C.J.Mey. & R.E.Lee (in J. Phycol. 35: 845–6. 1999)
Genus	*Peliaina* Pascher (in Jahrb. Wiss. Bot. 71: 458–9. 1929)[e]
	Peliaina cyanea Pascher (in Jahrb. Wiss. Bot. 71: 459. 1929)[e]
Genus	*Strobilomonas* J.Schiller (in Arch. Protistenkd. 100: 119–20. 1954)[e]
	Strobilomonas cyanea J.Schiller (in Arch. Protistenkd. 100: 120. 1954)[e]

[*]Based on Kies & Kremer (1986) and more recent literatures; not including red or green algae or other bikont lineage.

[a] Descriptive name.

[b] Names or epithets published with an improper Latin termination are to be changed under Article 32.2 of ICN.

[c] Lagerheim (1890) considered that the three species are a same species.

[d] According to Kies & Kremer (1986), *Cyanoptyche* and *Chalarodora* belong to a family Glaucosphaeraceae Skuja (1954) whose type species, however, is *Glaucosphaera vacuolata* Korshikov (1930) that is today considered as a red alga and moved to red algal monotypic order Glaucosphaerales E.C.Yang, Joe Scott, H.S.Yoon & J.A.West (2011) (Scott *et al.*, 2011).

[e] According to Kies & Kremer (1986), *Peliaina* and *Strobilomonas* are indicated not to be glaucophytes.

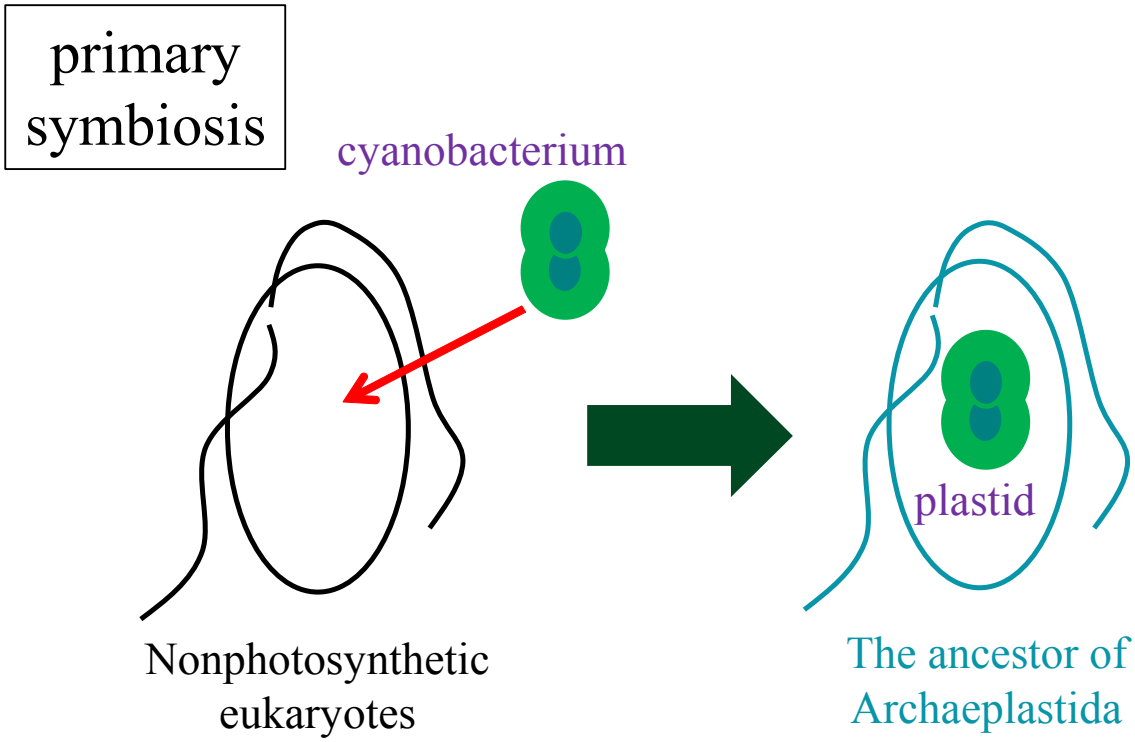

Figure 1.1. Diagrams of primary endosymbiosis.
A heterotrophic eukaryote enslaved a cyanobacterium and become the common ancestor of the primary photosynthetic eukaryotes with photosynthetic organelles or plastids. Based on endosymbiotic theory of Sagan (1967).

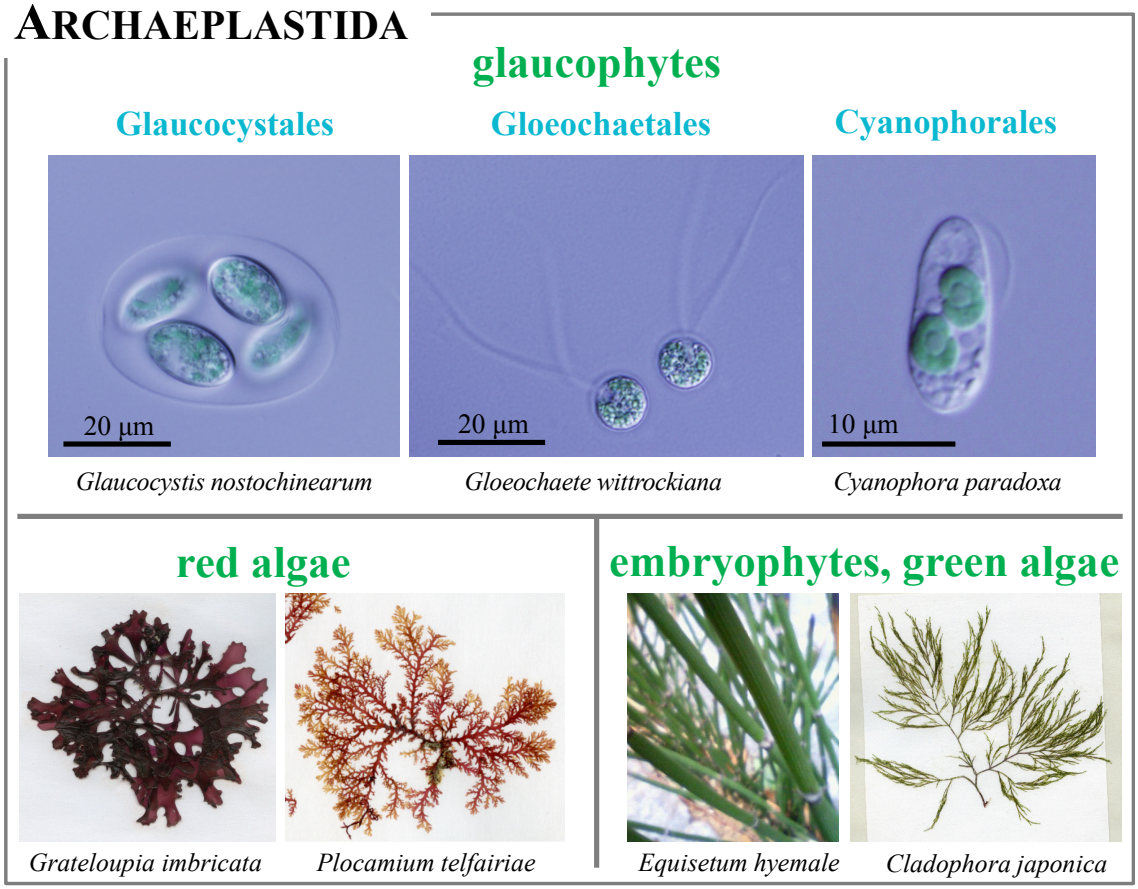

Figure 1.2. Photographs of three major lineages of primary photosynthetic eukaryotes or Archaeplastida including three orders of glaucophytes.

Original photographs. Note that primary photosynthetic eukaryotes are composed of red algae, Chloroplastida (embryophytes and green algae) and glaucophytes. Glaucophytes are composed of three orders: coccoid Glaucocystales, palmelloid Gloeochaetales and flagellate Cyanophorales; they are rare microalgae only from inland freshwater but cultivable as cultured strains in test tube media.

2. TAXONOMIC DELINEATION OF *CYANOPHORA* SPECIES

2.1. INTRODUCTION

Cyanophora is a biflagellate glaucophyte genus belonging to the Cyanophoraceae of the Cyanophorales (Table 1.1) and assumed to have the most primitive features among the photosynthetic eukaryotes (Hall & Claus, 1963; Mignot *et al.*, 1969; Spiegel, 2012). Within Cyanophoraceae, three unicellular biflagellate genera have been described (Kies & Kremer, 1986) (Table 1.1): *Cyanophora* Korshikov (1924), *Peliaina* Pascher (1929) and *Strobilomonas* J.Schiller (1954). While the latter two have not been characterised beyond their original description and are indicated not to be glaucophytes (Kies & Kremer, 1986), *Cyanophora* has been extensively studied and its nuclear genome has been sequenced (Price *et al.*, 2012). This genus includes three species: the type species *C. paradoxa* Korshikov (1924), *C. tetracyanea* Korshikov (1941) and *C. biloba* Kugrens, B.L.Clay, C.J.Mey. & R.E.Lee (1999). Among these, an authentic strain has been maintained for *C. biloba* in the Culture Collection of Algae at the University of Texas at Austin (UTEX, http://web.biosci.utexas.edu/utex/; Starr & Zeikus, 1993; Kugrens *et al.*, 1999) but no authentic strains are available for the remaining two species. After its original description, *C. tetracyanea* was reported from Uppsala County, Sweden (Skuja, 1956) and a strain labelled "*C. tetracyanea*" (Table 2.1) has been maintained but is lacking in morphological data (Kasai *et al.*, 2009). *C. paradoxa* has been collected from England (Whitton, 2002), Italy (Barone *et al.*, 2006) and the USA (Kugrens, 2002). The Pringsheim strain (Pringsheim, 1958), labelled "*C. paradoxa"*, was used in several studies as a model organism (e.g., Sato *et al.*, 2009; Frassanito *et al.*, 2010, 2013; Leblond *et al.*, 2011; Watanabe *et al.*, 2012; Price *et al.*, 2012; Facchinelli *et al.*, 2013; Gross *et al.*, 2013). The Kies strain (Kies, 1979; Kies & Kremer, 1990)

although also known as "*C. paradoxa"*, is thought to belong to a different species than the Pringsheim strain based on molecular data (Löffelhardt *et al.*, 1983; Bohnert *et al.*, 1985; Schenk *et al.*, 1987). Although Kugrens *et al.* (1999) examined the authentic strain of *C. biloba* and a culture (strain unspecified) of "*C. paradoxa*", taxonomic studies of more than two strains have not been undertaken for this genus. Furthermore, molecular data have never been used for taxonomic delineation of *Cyanophora* species.

Ultrastructural features of *C. paradoxa* were examined using transmission and scanning electron microscopy (TEM and SEM, respectively) to demonstrate that the cell periphery lacks a cell wall but consists of plasma membrane and flattened vesicles containing a plate just underneath the membrane (Hall & Claus, 1963; Mignot *et al.*, 1969; Trench & Siebens, 1978; Kies, 1979; Kugrens *et al.*, 1999). When Kugrens *et al.* (1999) examined the two species of *Cyanophora*, they also performed conventional SEM.

Recent advances in ultra-high resolution (UHR) field emission (FE)-SEM revealed a detailed gamete surface in the green alga *Ulva* (Miyamura *et al.*, 2003; Mogi *et al.*, 2008). Sato *et al.* (2009) showed the clear plastid surface of *C. paradoxa* under UHR FE-SEM. However, the surface ornamentations of the vegetative cells of *Cyanophora* have not been examined using UHR FE-SEM.

The present chapter aimed to delimit the species in the genus *Cyanophora* based on light microscopy (LM) as well as combination of several electron microscopy (EM), combined with molecular data, from several globally distributed strains including one newly established. This chapter was also undertaken to reveal detailed surface ornamentation of the vegetative cells of *Cyanophora* using the combination of several EM including UHR FE-SEM. The morphology and taxonomy of five species based on

strains of the genus are described in this study: *C. paradoxa*, *C. biloba*, *C. cuspidata* Tos.Takah. sp. nov., *C. kugrensii* Tos.Takah. sp. nov. and *C. sudae* Tos.Takah. sp. nov.

2.2. MATERIALS AND METHODS

2.2.1. Strains and culture conditions for observation

Seven clonal culture strains of *Cyanophora* and immotile glaucophytes were obtained from public culture collections (Table 2.1) at the National Institute for Environmental Studies (NIES, http://mcc.nies.go.jp/; Kasai *et al.* 2009), Sammlung von Algenkulturen der Universität Göttingen (SAG, http://sagdb.uni-goettingen.de/; Schlösser, 1994), Culture Collection of Algae and Protozoa (CCAP, http://www.sams.ac.uk/ccap) and from UTEX. In addition, I also used a strain of *Cyanophora* newly established by the pipette-washing method (Pringsheim, 1946) from a water-added dried soil sample collected in Japan (strain 101, deposited as NIES-3645 in NIES; Table 2.1). The cultures were maintained in screw-cap tubes with 9–11 mL of AF-6 medium (Kato, 1982; Kasai *et al.*, 2009) under 14 h-light/10 h-dark conditions at 20°C with a photon flux density of *ca*. 100 μmol/m^2/s. Cells of 2–3-week-old cultures were used for LM observations and fixations for EM.

2.2.2. Light microscopy (LM) and scanning electron microscopy (SEM)

LM observations were carried out using living cells with Olympus BX60 and BX53 LMs, equipped with Nomarski interference optics (Olympus, Tokyo, Japan).

UHR FE-SEM was performed as described by Sato *et al.* (2009) with minor modifications. Cells were subjected to double fixation using 2% glutaraldehyde and 1% osmium tetroxide essentially the same as fixation for TEM as described below. The cells were subsequently attached on 0.1%-poly-L-lysine-coated glass SEM plates (Okenshoji, Tokyo, Japan). The samples were dehydrated with an ethanol series, infiltrated with iso-amyl acetate and critical point dried using critical point dryer EM CPD030 (Leica,

Vienna, Austria). After coating with osmium under the osmium coater HPC-1SW (Vacuum Device, Mito, Japan), the cells were observed using SU8020 (Hitachi High-Technologies, Tokyo, Japan) at 1 kV. For comparison, cells were also examined using conventional SEM. Cells for conventional SEM were fixed with 1% osmium tetroxide or double-fixed with 2% glutaraldehyde and 1% osmium tetroxide. The fixed cells were then dehydrated and critical point dried on the glass plates as described above and coated with platinum under the ion sputter coater JFC-1600 (JEOL, Tokyo, Japan). The samples were observed using SU1510 (Hitachi High-Technologies) at an accelerating voltage of 5 or 15 kV.

I statistically analysed cell shape measurements. In SEM photographs, I chose cells that only oriented their longitudinal and right-left axes horizontally. The length (d) of these cells was measured geometrically between anterior and posterior cell poles (OD; Figure 2.1). The upper and lower widths (p and q, respectively) of cells were also measured at trisection points (P'P" at P and Q'Q" at Q, respectively, Figure 2.1). The ratio between the upper and lower widths (ρ) of each cell was defined as p/q and the relative width to length (κ) of each cell was defined as q/d. The population means of ρ and κ were estimated as confidence intervals using the 45 cells of each strain, with a confidence level of 95% using the statistical t-distribution. The two-dimensional scatter diagram of ρ and κ is shown in Figure 2.1.

2.2.3. Transmission electron microscopy (TEM)

The methods for ultrathin section TEM were essentially the same as those of a previous study (Matsuzaki *et al.*, 2010, 2014). Cells were fixed with final concentration of 2% glutaraldehyde and with final concentration of 1% osmium tetroxide and then

dehydrated by ethanol series and propylene oxide and finally embedded in Spurr's resin (Spurr, 1969). Ultrathin sections were cut with a diamond knife (Diatome, Embrach, Switzerland) on an Ultracut UCT (Leica) scooped on cupper meshes and stained with uranyl acetate or samarium chloride and with lead citrate. Sections on the meshes were observed with JEM-1010 (JEOL).

Freeze-fracture electron microscopy was carried out as described previously (Okuda *et al.*, 1994; Sekida *et al.*, 2001). Cells were fixed on the cell paste of yeasts in nitrogen slush. The frozen cells then were fractured and shadowed by evaporated platinum and carbon with Baltec BAF 060 Freeze Etching System (Bal-Tec, Furstentum, Liechtenstein, now: Leica) at −106℃ and 0.1 mPa. The replicas were purified by methanol and cleaned in 2.5% sodium dichromate 50% sulphuric acid mixture overnight, washed with distilled water and then mounted on Formvar-coated grids before observation with JEM-1400 (JEOL).

2.2.4. DNA extraction, PCR and sequencing

DNA was extracted for the molecular phylogeny as described by Nakada and Nozaki (2007) and Hayama *et al.* (2010). Concentrated cells were shaken with ceramic beads in chloroform and cetrimonium bromide (CTAB, hexadecyltrimethylammonium bromide) with Mixer Mill MM 300 (Retsch, Haan, Germany) and the DNA of cells was extracted with illustra Blood genomic Prep Mini Spin Kit (GE Healthcare UK, Little Chalfont, England). Partial photosystem I P700 chlorophyll *a* apoprotein A2 (*psaB*) and photosystem II P680 chlorophyll *a* apoprotein D1 (*psbA*) genes were amplified using polymerase chain reaction (PCR) with degenerate primers (Nozaki *et al.*, 2000; Chong *et al.*, 2014) and the internal transcribed spacer (ITS) regions of nuclear ribosomal DNA

(*r*DNA) (ITS-1, 5.8S *r*DNA and ITS-2) with newly designed primers (Figure 2.2). The PCR product was purified using the Illustra GFX PCR DNA and Gel Band Purification Kit (GE Healthcare UK). The purified DNA fragments were then sequenced directly using an ABI PRISM 3100s Genetic Analyzer (Applied Biosystems, Foster City, CA, USA) with a BigDye Terminator Cycle Sequencing Ready Reaction Kit v. 3.1 (Applied Biosystems).

2.2.5. Construction and comparative analysis of secondary structures of ITS-2 of nuclear ribosomal DNA

After annotating ITS-2 from the ITS regions of nuclear *r*DNA, according to Keller *et al.* (2009), the secondary structure of nuclear *r*DNA ITS-2 was predicted using sequences of strain CCAP 981/1 with DNA mFold RNA Folding Form (http://mfold.rna.albany.edu/) and constructed manually, referring to the consensus secondary structure of nuclear *r*DNA ITS-2 in Chloroplastida (Caisová *et al.*, 2013). Based on this structure, the nuclear *r*DNA ITS-2 sequences of all strains were aligned and structured manually.

2.2.6. Molecular phylogenetic analysis

The *psaB* and *psbA* sequences from 12 glaucophyte strains were aligned using ClustalW (Thompson *et al.*, 1994) in MEGA version 5 (Tamura *et al.*, 2011) and the concatenated 1,461 base pairs of *psaB* and 750 base pairs of *psbA* gene sequences were subjected to phylogenetic analyses. Neighbour-joining (NJ) analysis (Saitou & Nei, 1987) was performed based on maximum-composite-likelihood models, including a 1,000 replication bootstrap analysis (Felsenstein, 1985) with MEGA version 5.

Maximum-likelihood (ML) analysis with 1,000 bootstrap replications was performed by MEGA version 5 based on the general time reversible (GTR) model with invariant sites (GTR+I), determined by a model test with MEGA version 5. Sequences that were identical in the concatenated sequences were treated as the single operational taxonomic unit (OTU). Four strains of three genera of immotile glaucophytes (Table 2.1) were chosen to be the outgroup.

Phylogenetic relationships between species of *Cyanophora* were also examined based on analyses of 614 base pairs of the nuclear *r*DNA ITS regions (with partial LSU *r*DNA) from eight strains of *Cyanophora* representing six OTUs (based on identical sequences). The alignment of the ITS-2 region was carried out based on the secondary structure of ITS-2 (Figure 2.3). The remaining regions were aligned manually because of very small insertions/deletions of nucleotides (5 positions in total, all in ITS-1 region) in these regions. The alignment of the nuclear *r*DNA ITS regions used for the present phylogenetic analyses is available from TreeBASE (http://www.treebase.org/treebase-web/home.html; study ID: S16131). ML and NJ were performed as described above except that one selected model was used: Tamura (1992) 3-parameter method + gamma model (T92+G) for ML. The tree was rooted based on the tree topology of concatenated *psaB* and *psbA* gene phylogeny.

2.3. RESULTS AND DISCUSSION

2.3.1. Surface ornamentations of *Cyanophora paradoxa* cells as revealed by field-emission scanning electron microscopy

Thompson (1973), Trench *et al.* (1978) and Kugrens *et al.* (1999) have examined the cell surface of *Cyanophora* using conventional SEM but the surface ultrastructure was almost ambiguous. In spite of the advancement of UHR FE-SEM, surface ornamentations of the vegetative cells have never been examined using FE-SEM. In the present study, *C. paradoxa* strain NIES-547 vegetative cells were examined using UHR FE-SEM and compared with the data using conventional SEM.

Under high accelerating voltage observation conditions using conventional SEM (15 kV), plastids inside ellipsoidal or ovoid cells were visible (Figure 2.4a), possibly because the electron beam is easily transmitted into cells and generates more signals from the deeper layers in the specimen at an accelerating voltage of 15 kV. Surface ornamentations of the cells were ambiguous as reported by Kugrens *et al.* (1999). Conversely, at a lower accelerating voltage of 5 kV, surface ornamentations of the cells were evident and the plastid was invisible (Figure 2.4b). The entire cell surface was ornamented with angular fenestrations that were attached mutually. The fenestrations were framed by ridges. The cells double-fixed with glutaraldehyde and osmium tetroxide showed less shrinkage on the cell surface than did cells fixed with osmium tetroxide only (Figure 2.4c).

Cells examined using UHR FE-SEM at a low accelerating voltage (LV; 1 kV) had sharper cell surfaces and more delicate fenestrations (Figure 2.4, d–f) than did cells observed using conventional SEM. Furthermore, LV FE-SEM revealed that the cells had

small, protruding structures on the ridges (Figure 2.4, d, e and g). These structures were considered mucocysts (see below). In addition, mucous matter emitted from the mucocysts was observed on the cell surface (Figure 2.4g).

The fenestration ridges were also evident by ultrathin section TEM throughout the cell surface (Figure 2.5a). The ridges were formed by overlapping or attaching outermost plate vesicles just underneath the plasma membrane (Figure 2.5b) while the inner overlapping vesicles were often multi-layered. The protruded structure just outside the mucocyst was also evident by ultrathin section TEM (Figure 2.5c), as reported by Kies (1979) and Kugrens *et al.* (1999).

The present conventional SEM under high accelerating voltage showed almost ambiguous surface ornamentations or fenestrations on the *C. paradoxa* cell surface as in previous observations (Thompson, 1973; Trench *et al.*, 1978; Kugrens *et al.*, 1999) (Figure 2.4a). The present study, however, demonstrated that surface ornamentation was visible at LV even when using conventional SEM (Figure 2.4, b and c). Conventional SEM does not have high resolution especially at LV, for the electron microscopy resolution deteriorates when the electron energy decreases (de Broglie, 1924; Nagatani, 1991). Thus, to investigate the detailed surface ultrastructure of *C. paradoxa*, LV SEM with higher resolution is efficient (Osumi, 1998; Sato *et al.*, 2009). The present LV FE-SEM images provided a similar observation, which clearly demonstrated more detailed and clearer surface ornamentations of *Cyanophora* cells (Figure 2.4, d–g) than did those of previous SEM studies (Trench *et al.*, 1978; Kugrens *et al.*, 1999) (Figure 2.4, a–c). Additionally, the present LV FE-SEM revealed global or popped mucous matter emitted from the mucocysts on the *C. paradoxa* cell surface (Figures 2.4, d, e, g and 2.5c).

The present study demonstrated that LV FE-SEM reveals natural and detailed features of the *C. paradoxa* cell surface. Thus, LV FE-SEM was performed in all of the *Cyanophora* strains (Table 2.1) in this study to compare the ultrastructure as shown in next section.

2.3.2. Light, scanning electron and field-emission scanning electron microscopy of *Cyanophora* species

Using LM, two distinct morphological groups (groups A and B) were recognised in the *Cyanophora* strains (Table 2.2; Figure 2.6, a–e) as reported previously (Takahashi, 2013). Group A had ovoid, obovoid, elongate-ovoid or ellipsoidal vegetative cells without a deep longitudinal furrow on the ventral side (Figure 2.7, a–d). Group B had vegetative cells, dorsoventrally compressed to form a broad, bean-shape, with a deep longitudinal furrow from anterior to posterior ends on the ventral side (Figure 2.7, e–h). The presence or absence of the deep longitudinal furrow can easily be recognised in transverse cell sections with LM (Figure 2.7, d and h). Group B cells generally contained two or four plastids, arranged in two rows of one or two plastids each, respectively, and group A generally had one or two plastids, arranged almost longitudinally or obliquely.

Group A was composed of six strains, classified into three morphological species based on cell shape: *C. paradoxa, C. cuspidata* and *C. kugrensii* (Table 2.2; Figures 2.7, a–d; 2.8, a–c and f–h). *Cyanophora cuspidata* was different than the others, having variable protrusions of posterior ends of the vegetative cells. Its cells were obovoid to ellipsoidal, with a rounded or acute posterior end forming a pointed tail (Figures 2.7b; 2.8, b and g). In contrast, the posterior ends of the other group A species were always

rounded (Figures 2.7, a, c; 2.8, a, c, f and h). Furthermore, *C. paradoxa* and *C. kugrensii* differed in cell shape (Table 2.2). Cells of *C. paradoxa* were ovoid, while those of *C. kugrensii* were elongate-ovoid. Cell shape differences among the three group A species were also evident in my present statistical analysis of vegetative cell measurements in SEM photographs (Figure 2.1).

Using LM, vegetative cells of the six strains of group A, except for those with acute posterior ends found in *C. cuspidata* strains 101 and SAG 45.84, were identified as *C. paradoxa* based on the original description by Korshikov (1924). According to Korshikov (1924), the posterior ends of *C. paradoxa* vegetative cells are not pointed and are similar to those of *C. paradoxa* strains CCAP 981/1, UTEX 555 and NIES-547 and of *C. kugrensii* strain NIES-763 (Table 2.2). The Pringsheim strain (e.g., CCAP 981/1, UTEX 555, NIES-547; Table 2.2) has been widely studied (e.g., Bohnert *et al.*, 1985; Sato *et al.*, 2005, 2007, 2009; Frassanito *et al.*, 2010, 2013; Leblond *et al.*, 2011, 2012; Watanabe *et al.*, 2011, 2012; Baudelet *et al.*, 2013; Facchinelli *et al.*, 2013; Gross *et al.*, 2013) and has an ovoid vegetative cell, which is similar to the original shape of *C. paradoxa* Korshikov (1924). Thus, cells of CCAP 981/1 (the original Pringsheim strain; Day *et al.*, 2004) were selected as the epitype material of *C. paradoxa* (see Section 2.5 Taxonomic accounts). Based on the figures of "*C. paradoxa*" from Italy (Barone *et al.*, 2006), the alga has a pointed posterior end and may be identified as *C. cuspidata.*

Cyanophora biloba strain UTEX 2766 and *C. sudae* strain NIES-764, belonging to group B, differed in the number of plastids and surface ornamentations of cells under LV FE-SEM. Whereas *C. sudae* generally has four plastids, *C. biloba* has generally only two, as reported by Kugrens *et al.* (1999). Furthermore, I demonstrated the fundamental difference between *C. biloba* and *C. sudae* in terms of the surface ornamentation of

vegetative cells, by LV FE-SEM (Figure 2.8; Table 2.2). The present LV FE-SEM observations showed that the fenestrations of *C. sudae* were pentagonal to hexagonal and formed a honeycomb structure on part of the cell surface (Figures 2.8d and 2.9c), while those of *C. biloba* were triangular to pentagonal or often crescent-shaped and did not form a honeycomb structure (Figures 2.8e and 2.9d). Fenestrations of group A species were variable in shape and were not distinguishable between species; shapes were crescent or triangular to hexagonal (Figure 2.8, a–c). Based on LV FE-SEM, the flagella of all strains or species were inserted at the right side of the anterior furrow (Figure 2.8, f–j).

Cyanophora sudae is similar to *C. tetracyanea* in having dorsoventrally compressed cells with four plastids, arranged in two rows of two plastids each (Korshikov, 1941). However, these species can be clearly distinguished by their mode of plastid division. Two plastids in young cells of *C. sudae* were arranged in a transverse pair and the two plastids always divided transversely as in *C. biloba* (Figure 2.7, f and g). According to Korshikov (1941), however, young cells of *C. tetracyanea* have two plastids that are arranged in a longitudinal pair along the longitudinal central line (along the furrow); the two plastids divide longitudinally (see fig. 4d of Korshikov 1941; Figure 2.10). Skuja (1956) reported "*C. tetracyanea*" from Uppsala County, Sweden, but it is not certain whether this species was *C. tetracyanea* or *C. sudae* because plastid division was not described.

2.3.3. Ultrathin section and freeze-fracture transmission electron microscopy

According to previous studies (Mignot *et al.*, 1969; Kies, 1979; Kugrens *et al.*, 1999;

Kugrens, 2002), the cell coverings of *Cyanophora* species consist of the cell membrane and underlying flattened vesicles (plate vesicles) each of which includes a plate. The surfaces of plates and vesicles are observable by TEM as replicas, using the freeze-fracture method by which the cell coverings are scratched at random depths to peel the cell membrane, vesicles and plates, so that vesicles and plates are exposed (Kugrens *et al.*, 1999; Kugrens, 2002).

Cell surfaces of all strains observed by LV FE-SEM were ornamented with fenestrations framed by ridges (Figures 2.8, a–e; 2.9, c and d), as *C. paradoxa* strain NIES-547 described above (Figure 2.4). Based on ultrathin section TEM, cells in all study strains showed that flattened vesicles enclose the whole protoplast just underneath the cell membrane and that each contains a single plate layer between the upper and lower membranes of the vesicle (Figures 2.5 and 2.11). The ridges framing fenestrations shown by LV FE-SEM were the margins of the outermost plate vesicles, based on the ridges in ultrathin section TEM (Figure 2.11).

The present study investigated freeze-fractured cell replicas of *C. biloba* and *C. sudae* and found plate- or vesicle-like structures, similar to the fenestrations of each species shown by LV FE-SEM (Figure 2.9, a–d). Thus, the fenestrations found in the present LV FE-SEM observations may reflect the form of the outermost layer of the plate vesicles that are in contact or overlapping at the cell periphery (Figure 2.11).

2.3.4. Molecular phylogenetic analyses

The concatenated *psaB* and *psbA* trees showed that seven *Cyanophora* strains were subdivided into two monophyletic groups, consistent with the two groups (A and B) determined in the present comparative morphology (Figure 2.12). This suggests that the

two morphology types, determined using LM or SEM, reflect the basal phylogeny of the genus *Cyanophora*. Within group A, *C. cuspidata* strains 101 and SAG 45.84 formed a small clade that was sister to *C. kugrensii* strain NIES-763, whereas *C. paradoxa* strains CCAP 981/1, UTEX 555 and NIES-547 were in the most basal position.

Based on the nuclear *r*DNA ITS sequences, the relationships between species of *Cyanophora* were resolved as in the present concatenated gene tree although the sister relationship between *C. cuspidata* and *C. kugrensii* was weakly resolved (with only 54–73% bootstrap values in ML and NJ) (Figure 2.13).

2.3.5. Secondary structures of nuclear *r*DNA ITS-2

Taxonomic studies at species level using molecular data have not previously been reported and sexual reproduction is unknown in the Glaucophyta (Kies, 1992). Thus, it seems difficult to discuss delimitation of the *Cyanophora* species based on molecular data or intercrossing experiments (Mayr, 1942). However, such a discussion may be possible when using data from other groups of eukaryotes based on the DNA region or gene that is also applicable for glaucophytes. Recent studies suggest that presence of at least one compensatory base change (CBC) in the secondary structures of nuclear *r*DNA ITS-2 between two organisms (especially in its conserved region) may represent a genetic distance at or above the biological species level in various eukaryotes such as Archaeplastida (green algae) and Opisthokonta (e.g., fungi, metazoans) (Coleman, 2000, 2009; Müller *et al.*, 2007). Thus, I examined CBC in the secondary structures of nuclear *r*DNA ITS-2.

Although secondary structures of nuclear *r*DNA ITS-2 have not previously been studied in glaucophyte species, the *Cyanophora* ITS-2 secondary structures were

constructed here for eight strains of the five species based on those of Chloroplastida (Coleman, 2003; Caisová *et al.*, 2013). The structures in the *Cyanophora* species were highly conserved in having four helices, similar to those of other studied eukaryotic species (Coleman, 2003; Koetschan *et al.*, 2010; Caisová *et al.*, 2013). Helix III was the longest, helix II had U-U mismatches with an AAA motif between helix II and III, and helix III had UGGU motif near its 5' site apex (Figure 2.3).

Within group A, no CBC was identified between *C. cuspidata* strains 101 and SAG 45.84 but a single CBC was detected in helix I between the sister species *C. cuspidata* and *C. kugrensii* (Figure 2.14a). Therefore, given that the CBC species concept (*sensu* Müller *et al.* 2007) is applicable for *Cyanophora*, these sister species would have sufficient genetic distance to be separated into distinct species (Coleman, 2000, 2009; Smith *et al.*, 2011; Wełnicz *et al.*, 2011; Xu *et al.*, 2012; Caisová *et al.*, 2013; Rybalka *et al.*, 2013; Wolf *et al.*, 2013). Likewise, in group B, the ITS-2 secondary structures of *C. biloba* and *C. sudae* revealed a single CBC in helix II (Figure 2.14b). However, delimitation of species based on only a single DNA region is very speculative and Caisová *et al.* (2013) pointed out problems for species recognition using CBC in the secondary structures of nuclear *r*DNA ITS-2 in some lineages of Chloroplastida. Thus, I also examined genetic distances between the *Cyanophora* species using another DNA region (see below).

2.3.6. Genetic distance based on plastid *psaB* genes

In order to discuss the genetic distance for supporting separation of species, *p*-distances of *psaB* genes between sister species of *Cyanophora* (Figures 2.12 and 2.13) were calculated and compared with those between green algal sister species that are

delineated based on both molecular and morphological data (Nakada & Nozaki, 2007; Nakada *et al.*, 2008; Matsuzaki *et al.*, 2014)(Figure 2.15). The *p*-distance between the sister species in *Cyanophora* group A (*C. cuspidata* and *C. kugrensii*) is 3.6% whereas that of the sister species in *Cyanophora* group B (*C. sudae* and *C. biloba*) is 6.2%. These values fall within the ranges of the *psaB p*-distances (1.0–7.3%) between the sister species in the unicellular green algae *Chloromonas*, *Hafniomonas* and *Chlorogonium*. Therefore, five *Cyanophora* species that were delineated based on the present morphological data (Table 2.2) may have sufficient genetic distances to be recognised as different species.

2.4. CONCLUSIONS

Based on comparative morphological and molecular examinations, cultured material of the genus *Cyanophora* was classified into five species: *C. paradoxa*, *C. cuspidata, C. kugrensii*, *C. biloba* and *C. sudae* (Table 2.2; Figure 2.6, a–e). The Kies strain (SAG 45.84) belongs to *C. cuspidata* whereas the Pringsheim strain (CCAP 981/1, UTEX 555 and NIES-547) belongs to *C. paradoxa,* as previously suggested by genome sequence differences (Löffelhardt *et al.*, 1983; Löffelhardt, 1987; Bohnert *et al.*, 1985). *Cyanophora tetracyanea* is similar to two species in group B, as it has dorsoventrally compressed, bean-shaped vegetative cells with a deep longitudinal furrow on the ventral side and plastids arranged in two longitudinal rows (Korshikov, 1941). However, *C. tetracyanea* can be clearly distinguished from group B species based on its mode of plastid division. Within group B, *C. biloba* and *C. sudae* differed in terms of plastid number and surface ornamentation of cells concatenated LV FE-SEM (Table 2.2). The other three species belong to group A and differ in cell shape (Table 2.2).

The present classification of the five morphological species of *Cyanophora* is consistent with results of the molecular phylogenetic analyses of concatenated *psaB* and *psbA* genes and nuclear *r*DNA ITS sequences, in independency of each species. Based on presence of CBC in the secondary structure of the nuclear *r*DNA ITS-2 and *p*-distances of *psaB* genes, genetic distances between the sister species may be sufficient to support separation of the five *Cyanophora* species. Thus, it is clear that comparative morphological observations, combined with molecular data, can facilitate identification of species taxonomy in the genus *Cyanophora*. My distinction of five *Cyanophora* species (Table 2.2) suggests that the species diversity of Glaucophyta may be

significantly higher than previously believed. Glaucophytes were previously considered a small group based on LM observations but they may contain many undescribed species that can be delineated using morphological and molecular data. Several glaucophyte species have been discovered or recorded only once to few times because glaucophytes occur rarely. Thus, establishing glaucophyte culture strains using field-collected samples is also important for future studies. Novel isolates of glaucophytes collected in the field and their ultrastructural and molecular data may reveal the true biodiversity of the division Glaucophyta.

In delineating *Cyanophora* species, LV FE-SEM was very efficient to reveal the essential difference between species. Furthermore combination of EM unveils the peripheral ultrastructure of *Cyanophora* and LV FE-SEM can observe the surface ornamentations of whole *Cyanophora* cells. Thus, LV FE-SEM is a useful tool to examine the peripheral ultrastructures of cells without a wall or extracellular matrix. Peripheral ultrastructures of vegetative cells with a wall or extracellular matrix in another glaucophyte genus *Glaucocystis* are taken up in the next Chapter.

2.5. TAXONOMIC ACCOUNTS[3]

Cyanophora paradoxa Korshikov (in Russ. Arch. Protistol. 3: 55–64, 71–2, pl. III, fig. 1–7. 1924) (Figures 2.6a; 2.7a; 2.8, a and f).

Diagnosis:

Unicellular motile biflagellates, *ca*. 7–15 µm long × *ca*. 3–6 µm wide. Cells typically ovoid with a rounded posterior end, without deep longitudinal furrow in the ventral side. Two flagella unequal, inserted in the right side of subapical portion. Contractile vacuoles two to four in number, positioned near the base of the flagella. Nucleus single, with a nucleolus, located in the posterior half of the cell. Plastids (cyanoplasts) spherical in shape with a central body, generally one to two in number, arranged longitudinally or obliquely. Fenestrations in cell surface ornamentations angular or often crescent-shaped.

Lectotype (here designated): Korshikov 1924. Russ. Arch. Protistol. 3, pl. III, fig. 1.

Lectotype locality: Belopolye, Russian Empire (now Bilopillia, Ukraine) or near Kharkov Oblast, Russian Empire or USRR (now Kharkiv Oblast, Ukraine).

Lectotypic authentic strain: Not available.

Epitype (here designated): Resin-embedded cells of the new authentic strain CCAP 981/1, deposited as TNS-AL-57397 in Department of Botany, National Museum of Nature and Science (TNS).

Epitype locality: Near Cambridge, England (Pringsheim 1958).

Epitypic authentic strain (here designated): CCAP 981/1.

---

[3]New names and new typifications proposed or designated here in this thesis are *not* intended to be *effectively published* under the Article 30.8 of International Code of Nomenclature for algae, fungi, and plants (ICN).

Cyanophora cuspidata Tos.Takah. **sp. nov.** (Figures 2.6b; 2.7b; 2.8, b and g).

Diagnosis:

Unicellular motile biflagellates, *ca*. 5–12 µm long × *ca*. 2–5 µm wide. Cells typically obovoid to ellipsoidal with a rounded or pointed posterior end forming a tail, without deep longitudinal furrow in the ventral side. Two flagella unequal, inserted in the right side of subapical portion. Contractile vacuoles two to four in number, positioned near the base of the flagella. Nucleus single, with a nucleolus, located in the posterior half of the cell. Plastids (cyanoplasts) spherical in shape with a central body, generally one to two in number, arranged longitudinally or obliquely. Fenestrations in cell surface ornamentations angular or often crescent-shaped.

Holotype: Resin-embedded vegetative cells of the authentic strain 101, deposited as TNS-AL-57398 in TNS.

Type locality: Ikoma-shi, Nara, Japan (34.731949° N and 135.731168° E).

Holotypic authentic strain (here designated): Isolate 101, also available as NIES-3645 from NIES (Table 2.1).

Etymology: From Latin adjective "*cuspidatus, -a, -um*" meaning "tipped", since cells of this species often develop an acute posterior end.

Cyanophora kugrensii Tos.Takah. **sp. nov.** (Figures 2.6c; 2.7c; 2.8, c and h).

Diagnosis:

Unicellular motile biflagellates, *ca*. 5–15 µm long × *ca*. 2–6 µm wide. Cells typically elongate-ovoid with a rounded posterior end, without deep longitudinal furrow in the ventral side. Two flagella unequal, inserted in the right side of subapical portion. Contractile vacuoles two to four in number, positioned near the base of the flagella.

Nucleus single, with a nucleolus, located in the posterior half of the cell. Plastids (cyanoplasts) spherical in shape with a central body, generally one to two in number, arranged longitudinally or obliquely. Fenestrations in cell surface ornamentations angular or often crescent-shaped.

Holotype: Resin-embedded vegetative cells of the authentic strain NIES-763 (TNS-AL-57399), deposited in TNS.

Type locality: Mitsukaido-shi, Ibaraki, Japan (now Joso-shi).

Holotypic authentic strain (here designated): NIES-763.

Etymology: Named after the late Prof. Paul Kugrens, who contributed much to morphology and taxonomy of flagellates.

Cyanophora sudae Tos.Takah. **sp. nov.** (Figures 2.6d; 2.7, e, f; 2.8, d, i; 2.9, a and c).

Diagnosis:

Unicellular motile biflagellates, *ca*. 9–12 μm long × *ca*. 4–9 μm wide. Cells broad, bean-shaped with a deep longitudinal furrow in the centre of ventral side. Two flagella unequal, subapically inserted in the right side of the furrow. Contractile vacuoles two to four in number, positioned near the base of the flagella. The nucleus located in the posterior half of the cell with a nucleolus. Plastids (cyanoplasts) spherical in shape with a central body, generally in dividing stage, four in number and arranged in two longitudinal rows of two plastids each. Plastid divisions always transverse in two plastids arranged transversely in a cell. Fenestrations in cell surface ornamentations pentagonal to hexagonal, often forming a honeycomb structure.

Holotype: Resin-embedded cells of the authentic strain NIES-764, deposited as TNS-AL-57400 in TNS.

Type locality: Mitsukaido-shi, Ibaraki, Japan (now Joso-shi).

Holotypic authentic strain (here designated): NIES-764.

Etymology: Named after Prof. Shoichiro Suda (University of the Ryukyus), who collected the sample and established strain NIES-764.

Cyanophora biloba Kugrens, B.L.Clay, C.J.Mey. & R.E.Lee (in J. Phycol. 35: 845–6. 1999) (Figures 2.6e; 2.7g; 2.8, e, j; 2.9, b and d).

Diagnosis:

Unicellular motile biflagellates, *ca*. 9–12 μm long × *ca*. 4–9 μm wide. Cells broad, bean-shaped with a deep longitudinal furrow in the centre of ventral side. Two flagella unequal, subapically inserted in the right side of the furrow. Contractile vacuoles two to four in number, positioned near the base of the flagella. The nucleus located in the posterior half of the cell with a nucleolus. Plastids (cyanoplasts) spherical in shape with a central body, generally in dividing stage, two in number and arranged in one longitudinal row of two plastids each. Plastid divisions always transverse in two plastids arranged transversely in a cell. Fenestrations in cell surface ornamentations triangular to pentagonal or often crescent-shaped.

Holotype (designated by Kugrens et al., 1999): Kugrens *et al.* 1999. J. Phycol. 35: 847. Fig.4, a scanning electron micrograph of isotype.

Isotype: Resin-embedded cells of the same strain to UTEX 2766.

Type locality: Near Fort Collins City, Colorado, USA.

Holotypic authentic strain: UTEX 2766.

2.6. KEY TO SPECIES OF *CYANOPHORA*[4]

A. Cells dorsoventrally compressed, with a deep longitudinal furrow in ventral side; plastids arranged in two longitudinal rows in a cell ---------- B.

A. Cells ovoid, obovoid, ellipsoidal or elongate-ovoid, without a deep longitudinal furrow in ventral side; plastids arranged longitudinally or obliquely in a cell ---------- D.

B. Plastid division longitudinal in the centre of the cell under the furrow ---------- *C. tetracyanea* Korshikov (1941)[5]

B. Plastid division transverse ---------- C.

C. Fenestrations in the cell surface ornamentation triangular to pentagonal or often crescent-shaped, lacking honeycomb structure; plastids generally two ---------- *C. biloba* Kugrens, B.L.Clay, C.J.Mey. & R.E.Lee (1999)

C. Fenestrations on the cell surface ornamentation pentagonal to hexagonal, forming honeycomb structure; plastids generally four ---------- *C. sudae* Tos.Takah. sp. nov.

D. Production of cells with an acute posterior end present ---------- *C. cuspidata* Tos.Takah. sp. nov.

D. Production of cells with an acute posterior end absent ---------- E.

---

[4] Based on the present study and Kugrens *et al.* (1999).
[5] According to Korshikov (1941).

E. Cells ovoid ---------- *C. paradoxa* Korshikov (1924)

E. Cells elongate-ovoid ---------- *C. kugrensii* Tos.Takah. sp. nov.

2.7. ADDENDUM

After the submission of the contents on the Chapter 2 to Journal of Phycology (21 February 2014), Chong *et al.* (available online 28 March 2014, Mol. Phylog. Evol., DOI: 10.1016/j.ympev.2014.03.019) reported the cryptic diversity within glaucophyte species using plastidial, mitochondrial and nuclear DNA markers. The phylogenetic results within the genus *Cyanophora* in their study were consistent with those of the present study in recognition of possible multiple species and two divergent lineages or groups A and B (Figure 2.12) within *Cyanophora*. However, Chong *et al.* (2014) did not delimit the species of *Cyanophora* using morphological data within each of groups A and B.

2.8. TABLES AND FIGURES

Table 2.1. Species and strains of *Cyanophora* and other glaucophytes used in this study.

Species	Strain designation	Origin of strain	Locality	GenBank accession number		
				psaB	*psbA*	ITS1-5.8S *r*DNA-ITS2
Cyanophora paradoxa	CCAP[a] 981/1[b] (new epitypic authentic strain) *"Cyanophora paradoxa"* (= CCMP[c] 329[b])	Green and slightly alkaline pond[a,c,d,e]	Cambridge, England, UK[a,c,d,e]	*AB973446*	*LC120678*	*AB973918*
				AB973445	*LC120679*	*AB973917*
	NIES[d]-547[b] *"Cyanophora paradoxa"*			*AB973447*	*LC120680*	*AB973919*
	UTEX[e] 555[b] *"Cyanophora paradoxa"*			*AB973448*	NP_043238	*AB973920*
Cyanophora kugrensii	NIES-763 (new holotypic authentic strain) *"Cyanophora paradoxa"*	Lotus field soil[d]	Yoshino Park, Mitsukaido-shi[f], Ibaraki, Japan[d]	*AB973449*	KF631322	*AB973921*
Cyanophora cuspidata	101[g] (new holotypic authentic strain) (= NIES-3645)	Paddy dried soil samples[h]	Takayama-cho, Ikoma-shi, Nara, Japan, in 15 March 2012 (34°43'55.0"N, 135°43'52.2"E)	*AB973450*	*LC120681*	*AB973922*
	SAG[i] 45.84[j] *"Cyanophora paradoxa"* (= SAG 45.84M[j])	Soil sample[i]	Free State of Bavaria, Germany (49°38'14.2"N, 10°59'02.5"E)[i]	*AB973451*	*LC120682*	*AB973923*
				AB973444	KF631323	*AB973916*
Cyanophora biloba	UTEX 2766 (holotypic authentic strain of *Cyanophora biloba*)[e,k]	Ephemeral alpine pond[k]	Colorado, USA (40°37'72"N, 105°40'41"W)[e,k]	*AB973452*	KF631324	*AB973924*
Cyanophora sudae	NIES-764 (new holotypic authentic strain) *"Cyanophora tetracyanea"*	Lotus field soil[d]	Yoshino Park, Mitsukaido-shi[f], Ibaraki, Japan[d]	*AB973453*	KF631321	*AB973925*
"Gloeochaete wittrockiana"	SAG 46.84			*AB973454*	KF631340	*LC120715*
"Cyanoptyche gloeocystis"	SAG 4.97			*AB973455*	KF631338	*LC120716*
Glaucocystis nostochinearum[l]	SAG 16.98[l]			*AB973457*	KF631337	*LC120721*
Glaucocystis geitleri[l]	SAG 229-1[l]			*AB973458*	*LC120685*	*LC120728*

Table 2.1. Continued.

Accession numbers in italics type indicate sequences determined by this work.

[a] Culture Collection of Algae and Protozoa (CCAP, http://www.ccap.ac.uk/).

[b] Although UTEX 555 originates from the same Pringsheim strain as NIES-547 and CCMP 329 (= CCAP 981/1), sequences from the UTEX 555 were slightly different from the others (Watanabe *et al.* 2012). Thus, these four Pringsheim strains were all sequenced but no difference was found in analysed *psaB* region though the *psaB* sequence of UTEX 555 from National Centre for Biotechnology Information (NCBI, http://www.ncbi.nlm.nih.gov/) had a two-base difference in the analysed region from my present sequences of the four strains including UTEX 555. There was also no difference among my present nuclear ITS1-5.8S *r*DNA-ITS2 sequences of four Pringsheim strains and CCAP 981/1 sequences obtained from NCBI and CCMP 329 sequences from the *Cyanophora* genome project (http://cyanophora.rutgers.edu/cyanophora/). LM, TEM and FE-SEM were also performed using CCMP 329 cells in this thesis and no essential difference was found among the four Pringsheim strains.

[c] National Center for Marine Algae and Microbiota (NCMA, formerly CCMP, the Provasoli-Guillard National Center for Culture of Marine Phytoplankton, https://ncma.bigelow.org/).

[d] National Institute for Environmental Studies (NIES, http://mcc.nies.go.jp/; Kasai *et al.* 2009).

[e] Culture Collection of Algae at the University of Texas at Austin (UTEX, http://web.biosci.utexas.edu/utex/default.aspx; Starr & Zeikus, 1993).

[f] Now Joso-shi.

[g] Newly isolated in this study.

[h] From this sample, seven clonal isolates 101, 102, 107, 1037-21, 1037-22, Ax10 and Ax12 were established using the pipette-washing method. Since the *psaB* and nuclear ITS1-5.8S *r*DNA-ITS2 sequences of these new cultures were identical in the analysed regions, only isolate 101 was used for this study.

[i] Sammlung von Algenkulturen der Universität Göttingen (SAG, http://sagdb.uni-goettingen.de/; Schlösser, 1994).

[j] SAG 45.84M was also sequenced but the *psaB* and nuclear ITS1-5.8S *r*DNA-ITS2 sequences of this culture were identical to those of SAG 45.84 in the analysed regions and only SAG 45.84 was used for this study. These strains originated from the Kies strain.

[k] Based on Kugrens *et al.*, (1999).

[l] For details of the strains and species information, see Chapter 3; Table 3.1.

Table 2.2. Comparison of the morphological characteristics of *Cyanophora* species examined in cultures of the present study.

Species	*C. paradoxa* Korshikov	*C. cuspidata* sp. nov.	*C. kugrensii* sp. nov.	*C. sudae* sp. nov.	*C. biloba* Kugrens *et al.*	*C. tetracyanea* Korshikov
Cell shape	ovoid without a deep longitudinal furrow	obovoid to ellipsoidal without a deep longitudinal furrow	elongate-ovoid without a deep longitudinal furrow	dorsoventrally compressed to form a broad, bean-shape	dorsoventrally compressed to form a broad, bean-shape	dorsoventrally compressed to form a broad, bean-shape
Cell size	*ca*. 7–15 µm long × *ca*. 3–6 µm wide	*ca*. 5–12 µm long × *ca*. 2–5 µm wide	*ca*. 5–15 µm long × *ca*. 2–6 µm wide	*ca*. 9–12 µm long × *ca*. 4–9 µm wide	*ca*. 9–12 µm long × *ca*. 4–9 µm wide	*ca*. 10 µm long × *ca*. 7 µm wide
Formation of posterior pointed end (tail)	absent	present	absent	absent	absent	absent
Plastid number	generally 1–2	generally 1–2	generally 1–2	2–8, generally 4	2–4, generally 2	2–4, generally 4
Plastid division	oblique or longitudinal	oblique or longitudinal	oblique or longitudinal	transverse	transverse	longitudinal
Fenestrations in cell surface ornamentation	angular or often crescent-shaped	angular or often crescent-shaped	angular or often crescent-shaped	pentagonal to hexagonal	triangular to pentagonal or often crescent-shaped	ND
Strains examined	CCAP 981/1, UTEX 555, NIES-547	101 (= NIES-3645), SAG 45.84	NIES-763	NIES-764	UTEX 2766	ND
Morphological group	group A	group A	group A	group B	group B	ND
Based on	present study	present study	present study	present study	present study	original description

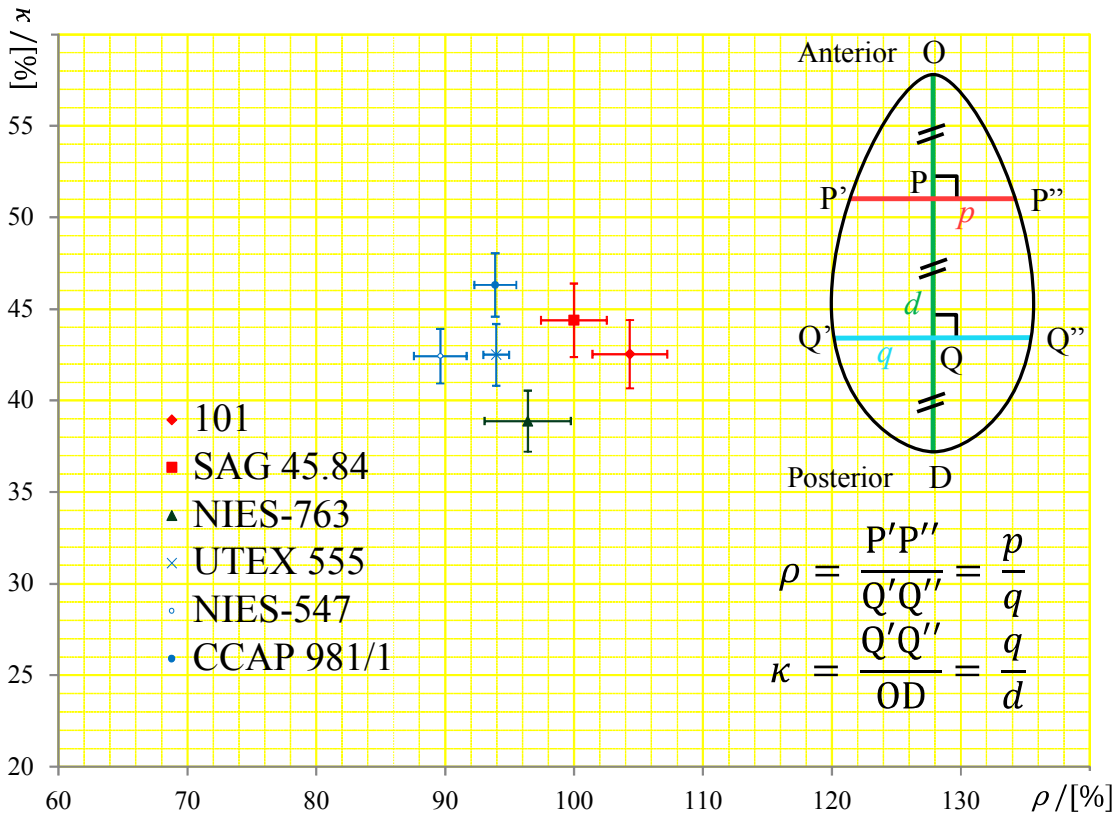

Figure 2.1. Statistical analysis of the cell shape measurements of six strains in group A of *Cyanophora* species (Table 2.2).

The horizontal and vertical axes signify the estimated population means of the ratio between upper and lower width (ρ/[%]) of the cells and the relative width to the length (κ/[%]) of the cells, respectively. The error bars of ρ and κ represent 95% confidence intervals of the population means of ρ and κ measuring based on 45 cells for each strain. For details of the definitions and measurements of the measuring quantities, see Section 2.2. Materials and Methods.

Primer designation	Sequence (5'–3')
ITS_Fa_Cyanophorae	GTAGGTGAACCTGCGGAAGGATCA
ITS_Fc_Cyanophorae	GCAACGATGAAGAACGCAGC
ITS_Rb2_Cyanophorae	CGCTTCACTCGCCGTTACTAGG
ITS_Rd_Cyanophorae	GCTGCGTTCTTCATCGTTGC

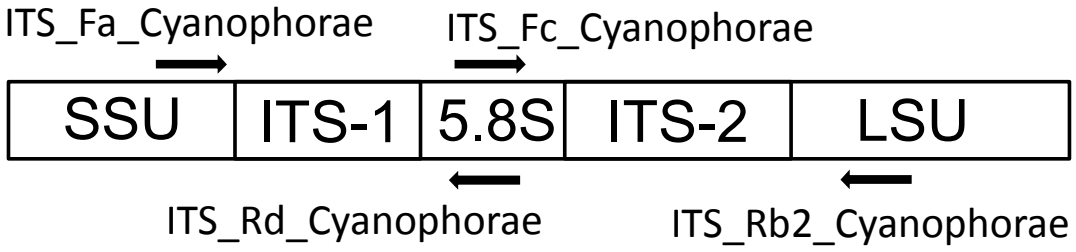

Figure 2.2. Newly designed primers used for amplifications and sequencing of the internal transcribed spacer (ITS) regions of nuclear ribosomal DNA of *Cyanophora.*

a

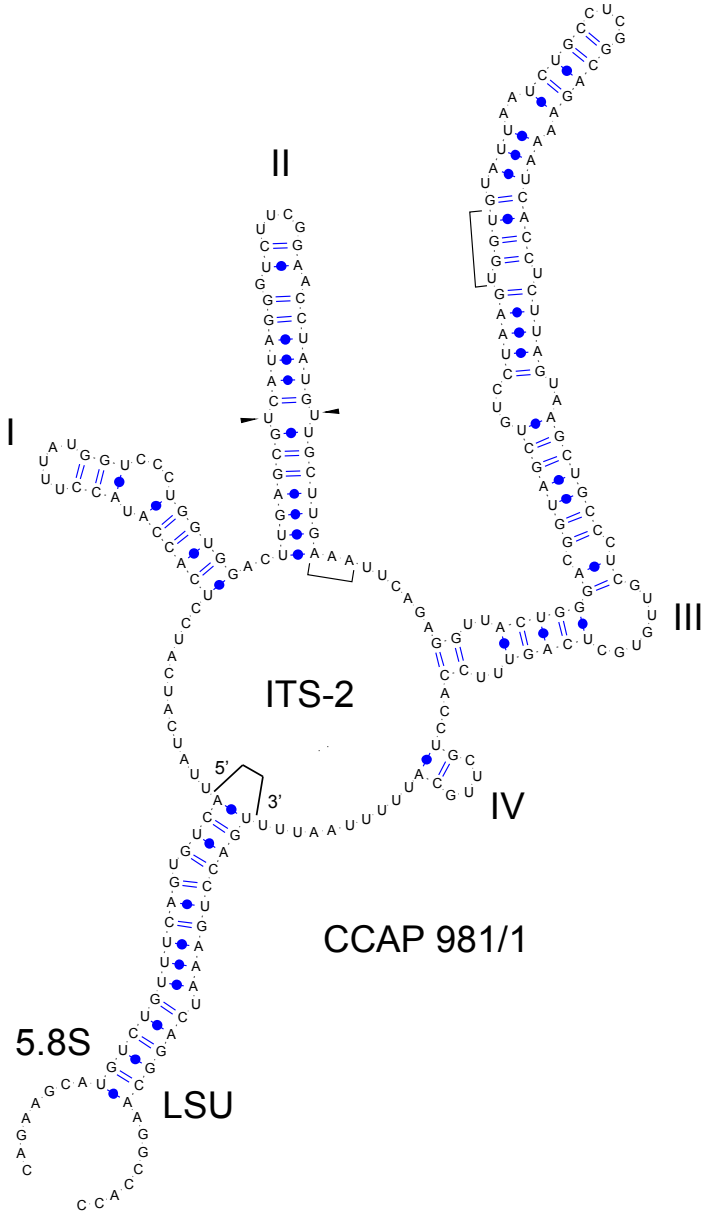

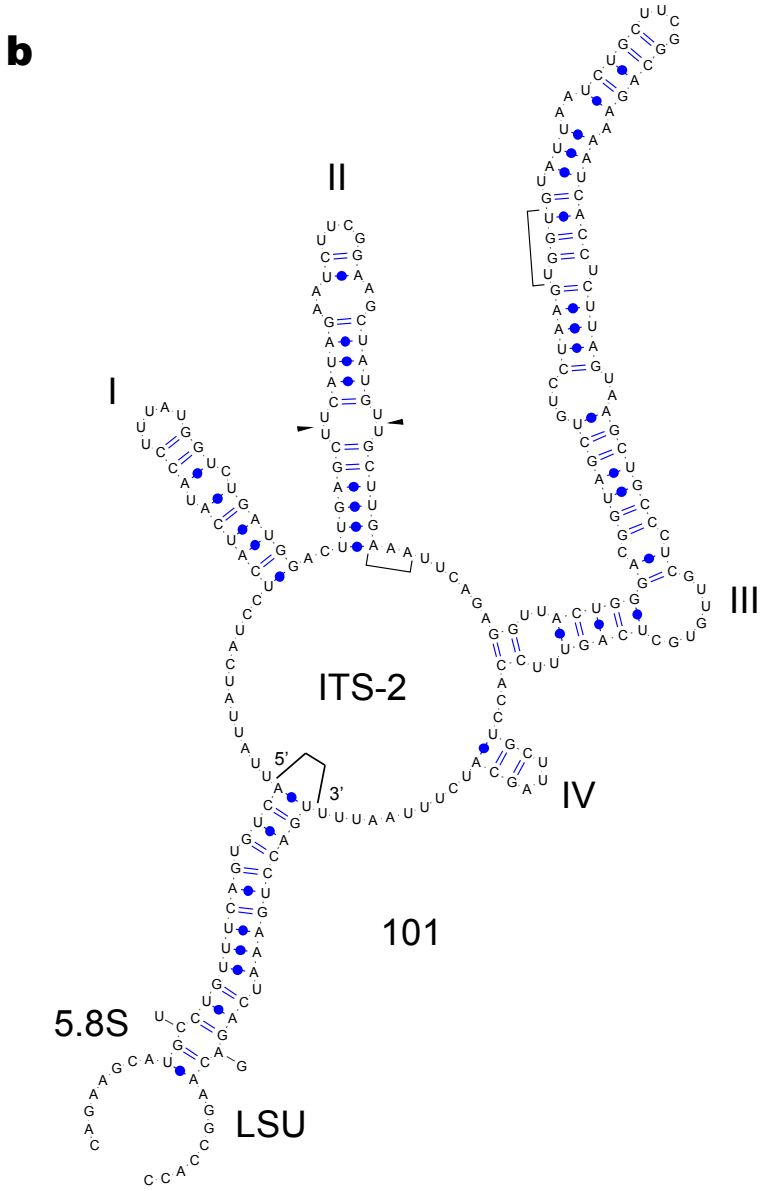
b
II
I
III
ITS-2
5'
3'
IV
101
5.8S
LSU

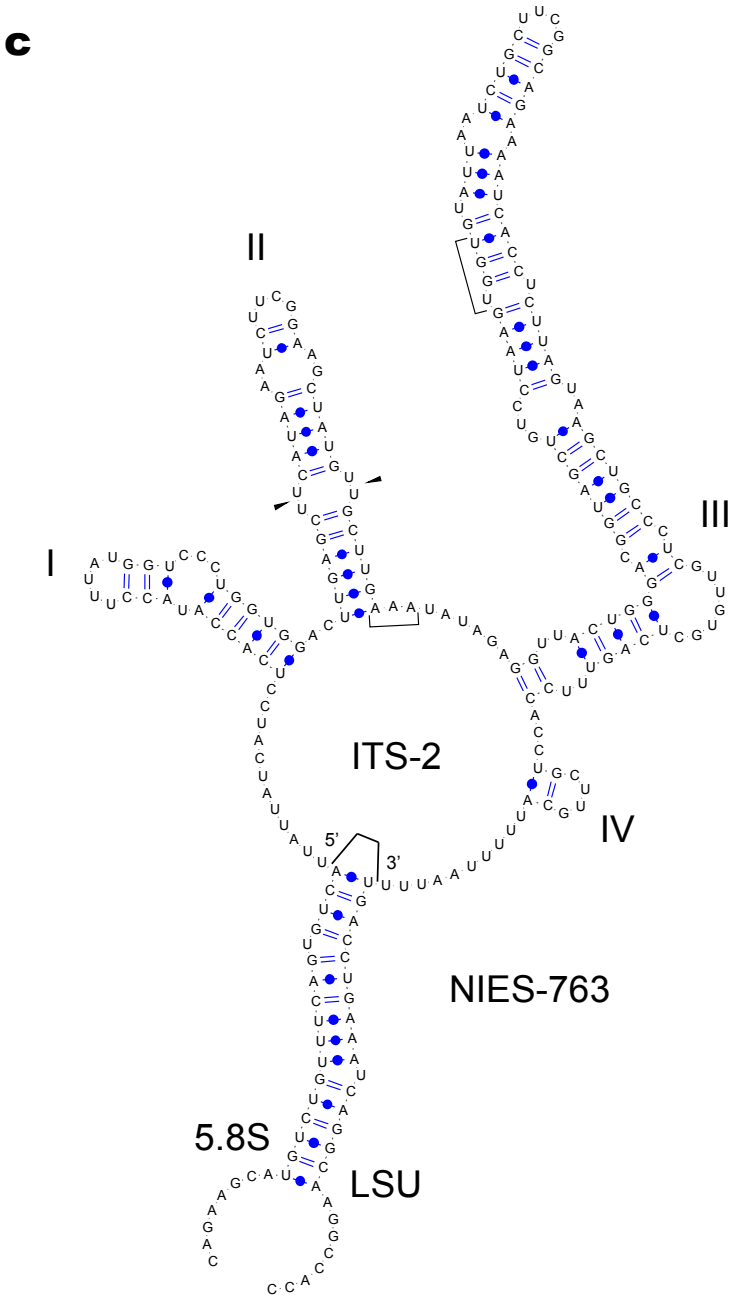
c
II
III
I
ITS-2
IV
5'
3'
NIES-763
5.8S
LSU

d

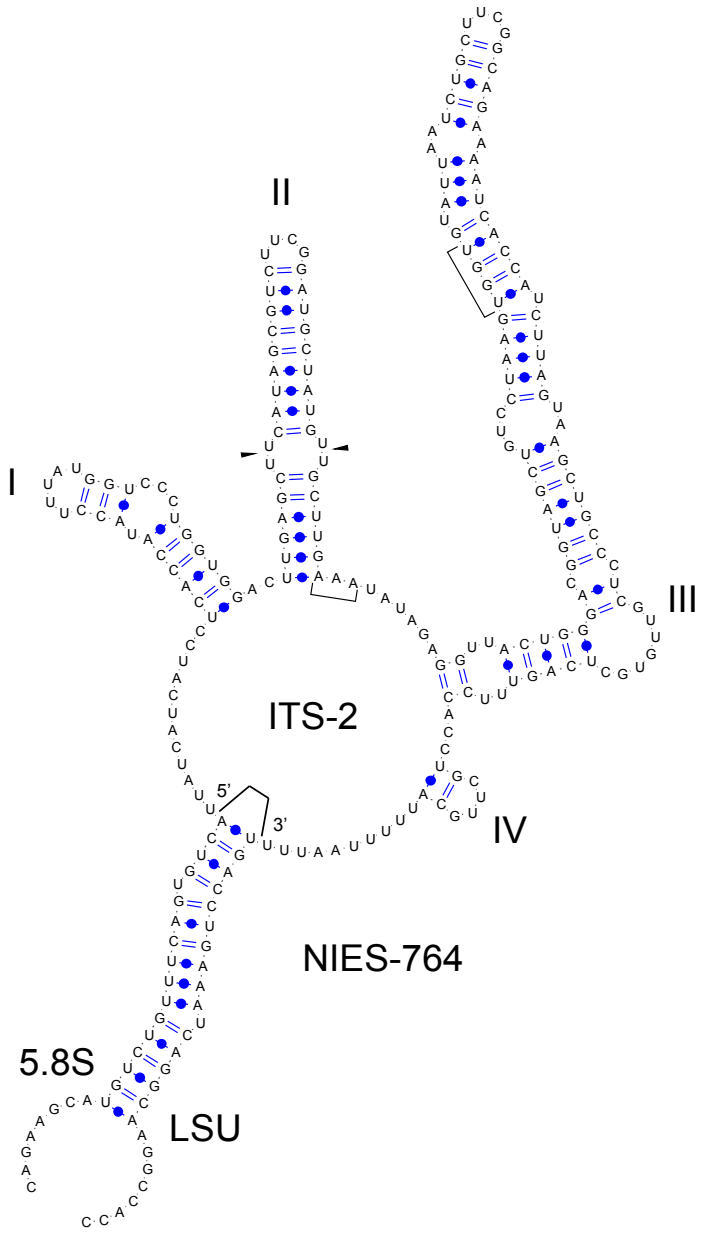

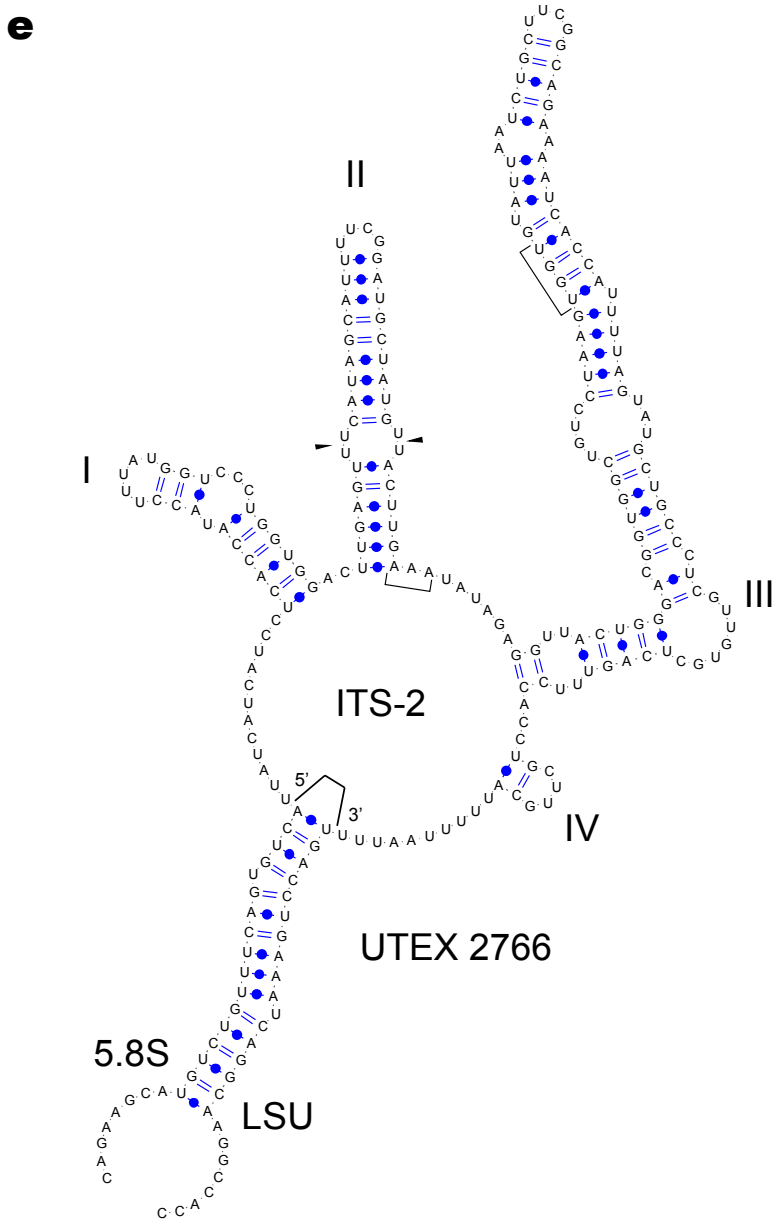

Figure 2.3. Secondary structures of nuclear *r*DNA ITS-2 of five species of *Cyanophora.*

(a) *C. paradoxa* Korshikov strains CCAP 981/1, UTEX 555 and NIES-547. (b) *C. cuspidata* Tos.Takah. sp. nov. strain 101 with structural variation found in strain SAG 45.84 indicated by outside line. (c) *C. kugrensii* Tos.Takah. sp. nov. strain NIES-763. (d) *C. sudae* Tos.Takah. sp. nov. strain NIES-764. (e) *C. biloba* Kugrens, B.L.Clay, C.J.Mey. & R.E.Lee strain UTEX 2766. Note that ITS-2 secondary structures were highly conserved within the genus *Cyanophora* and that they had four helices with helix III as the longest, U-U mismatches (arrowheads) in the helix II with AAA motif (bracket) between the helix II and III and UGGU motif (bracket) near the 5' site apex of helix III.

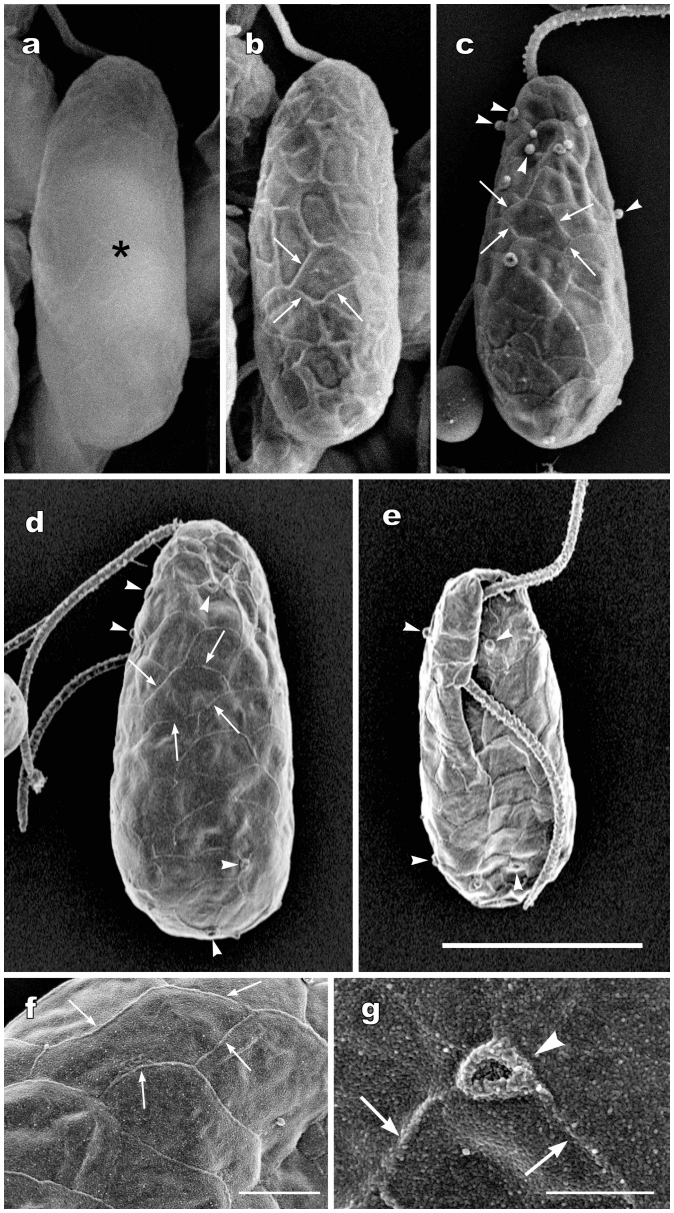

Figure 2.4. Scanning electron microscopy (SEM) of *Cyanophora paradoxa* NIES-547 vegetative cells.

(a–e) Scale bar, 5 µm. The same magnification was used throughout. (f) Scale bar, 1 µm. (g) Scale bar, 500 nm. (a, b) Cells treated with single fixation (1% osmium tetroxide) and (c–g) with double fixation (2% glutaraldehyde and 1% osmium tetroxide). Note the surface mucous matter (arrowheads) emitted from the mucocysts. (a) Dorsal side examined using conventional SEM at an accelerating voltage of 15 kV. Note that the plastid (asterisk) inside the cell is visible. (b, c) Dorsal sides using conventional SEM at an accelerating voltage of 5 kV. Note that the plastid is invisible but that the surface ornamentations or fenestrations framed by ridges (arrows) are visible. (d–g) UHR FE-SEM at an accelerating voltage of 1 kV. (d) Dorsal side and (e) ventral side. (f) An area of the cell surface showing fenestrations surrounded by ridges (arrows). (g) Possible mucocysts (arrowheads) along the ridges (arrows). Note the mucous matter already emitted and possibly popped.

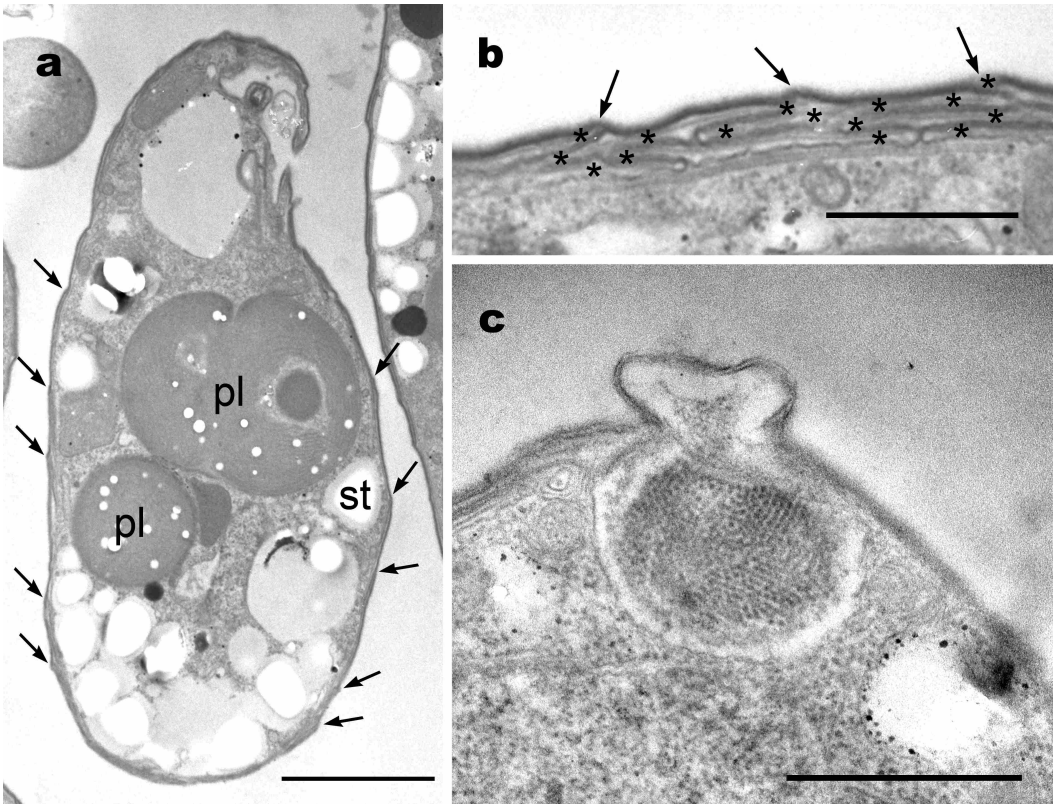

Figure 2.5. Transmission electron microscopy (TEM) of *Cyanophora paradoxa* NIES-547 vegetative cells.

pl, plastid; st, starch grain. Note that the cell covering is composed of overlapping plates (asterisks) within flattened vesicles beneath the plasma membrane. (a) Longitudinal section of the cell showing ridges (arrows) throughout the cell surface. Scale bar, 2 μm. (b) Plate vesicles that deeply overlapped. Note the uppermost vesicles forming ridges (arrows) on the cell surface. Scale bar, 500 nm. (c) Longitudinal section of the mucocyst with a protruded structure at the cell periphery. Scale bar, 500 nm.

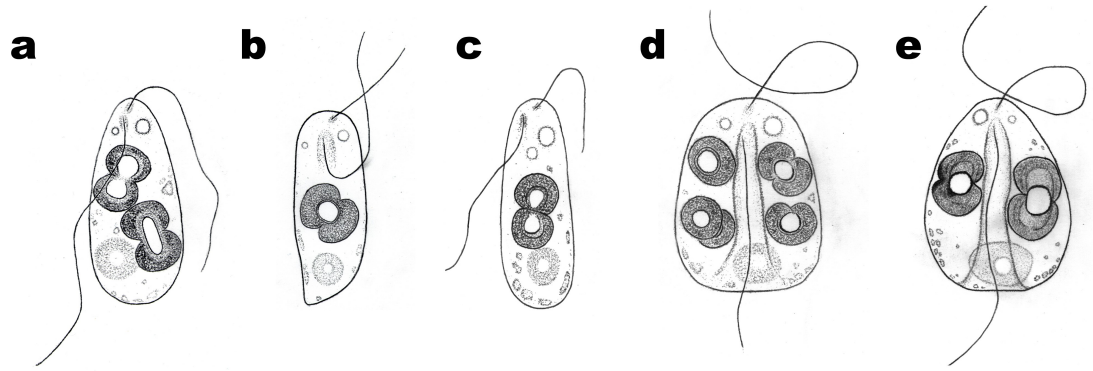

Figure 2.6. Light microscopic drawings of the vegetative cells of five *Cyanophora* species.

(a) *C. paradoxa* Korshikov. (b) *C. cuspidata* Tos.Takah. sp. nov. (c) *C. kugrensii* Tos.Takah. sp. nov. (d) *C. sudae* Tos.Takah. sp. nov. (e) *C. biloba* Kugrens, B.L.Clay, C.J.Mey. & R.E.Lee. Drawings are not to scale.

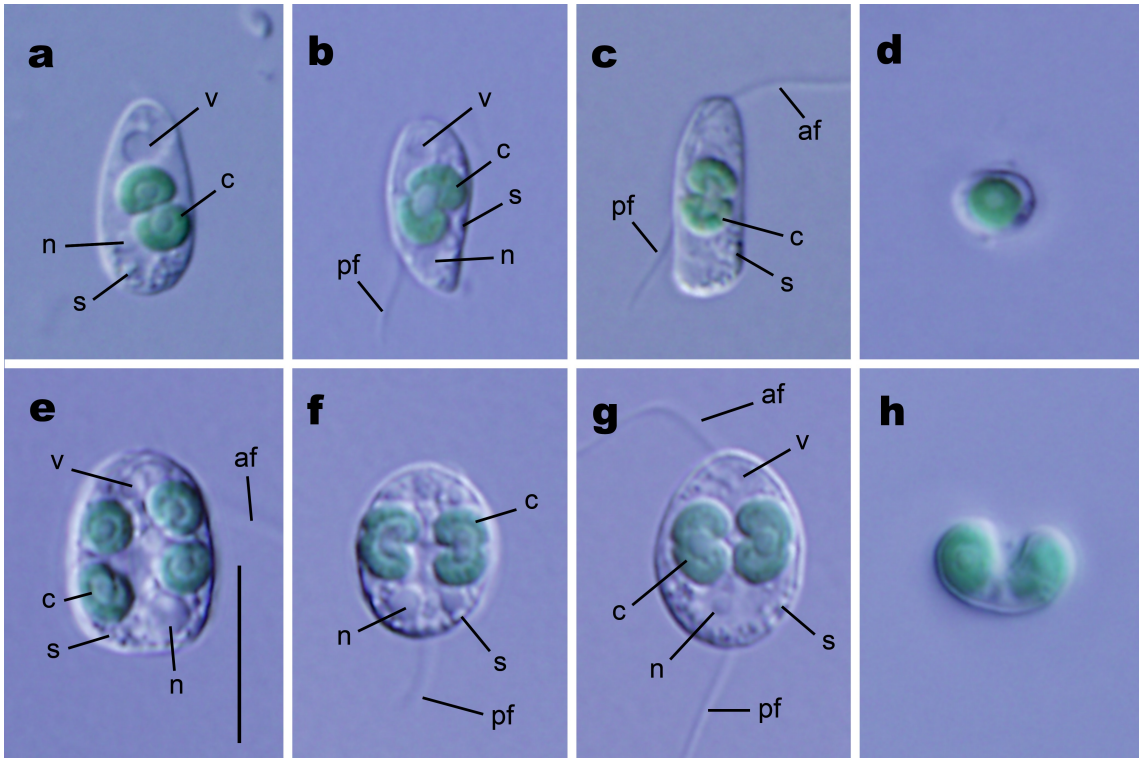

Figure 2.7. Differential interference contrast microscopy of vegetative cells of five *Cyanophora* species, shown at the same magnification throughout.

Scale bar, 10 µm. af, anterior flagellum; pf, posterior flagellum; c, plastid; n, nucleus; s, starch grain; v, contractile vacuoles. (a) Side view of a cell of *C. paradoxa* Korshikov strain CCAP 981/1. (b) Side view of a cell of *C. cuspidata* Tos.Takah. sp. nov. strain 101. (c) Side view of a cell of *C. kugrensii* Tos.Takah. sp. nov. strain NIES-763. (d) Optical section of antapical view of a cell without a deep furrow in *C. cuspidata* strain 101. (e, f) *C. sudae* Tos.Takah. sp. nov. strain NIES-764. (e) Front view showing four plastids. (f) Front view with two dividing plastids. Note that plastid divisions are transverse. (g) Front view with two dividing plastids in *C. biloba* Kugrens, B.L.Clay, C.J.Mey. & R.E.Lee strain UTEX 2766. Note that plastid divisions are transverse. (h) Optical section of antapical view of a cell with a deep furrow in *C. sudae* strain NIES-764.

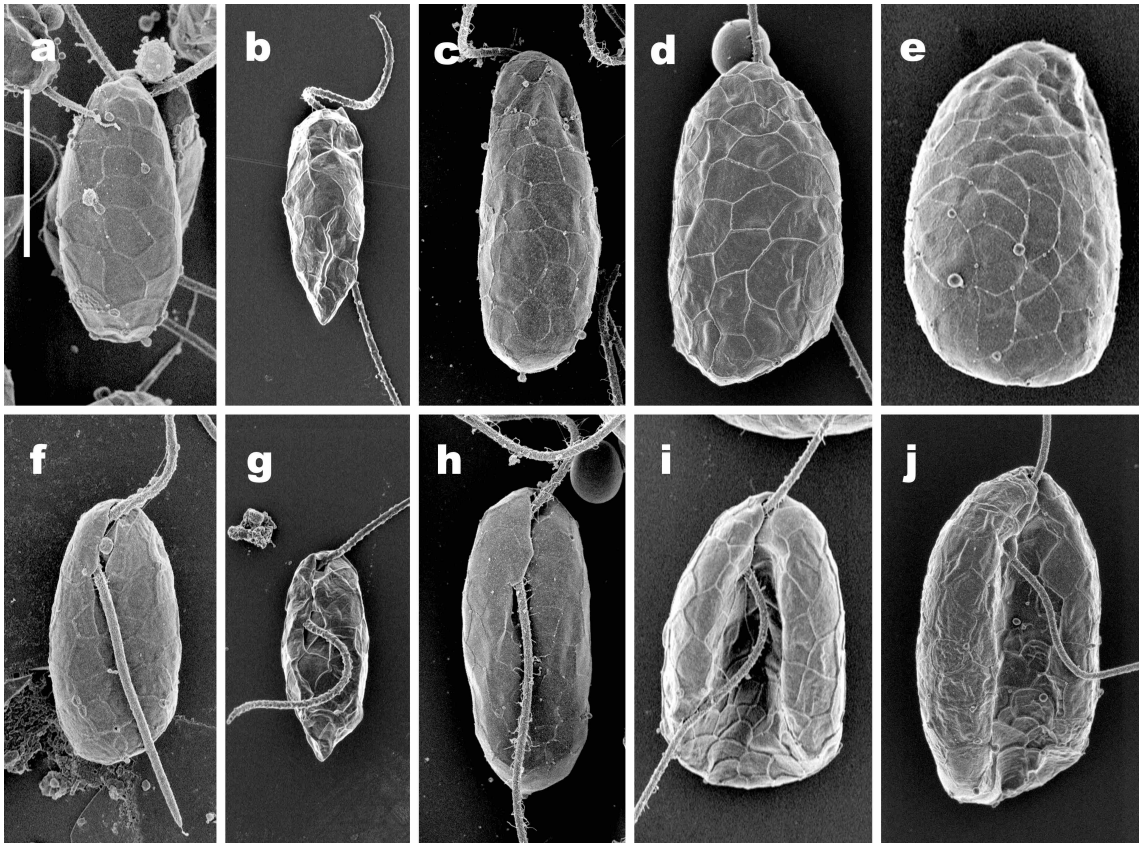

Figure 2.8. Field-emission scanning electron microscopy of the dorsal and ventral sides of vegetative cells of five *Cyanophora* species.

All images are at the same magnification. Scale bar, 5 μm. Upper and lower panels show dorsal sides, showing fenestrations aligned by ridges, and ventral sides, showing anterior folds with flagella, respectively. Note the flagella attached to the right part of the anterior fold. (a, f) *C. paradoxa* Korshikov strain CCAP 981/1, with a rounded posterior end. (b, g) *C. cuspidata* Tos.Takah. sp. nov. strain 101, showing a pointed posterior end. (c, h) *C. kugrensii* Tos.Takah. sp. nov. strain NIES-763, with a rounded posterior end. (d, i) *C. sudae* Tos.Takah. sp. nov. strain NIES-764, showing a deep furrow (i). (e, j) *C. biloba* Kugrens, B.L.Clay, C.J.Mey. & R.E.Lee strain UTEX 2766, showing a deep furrow (j).

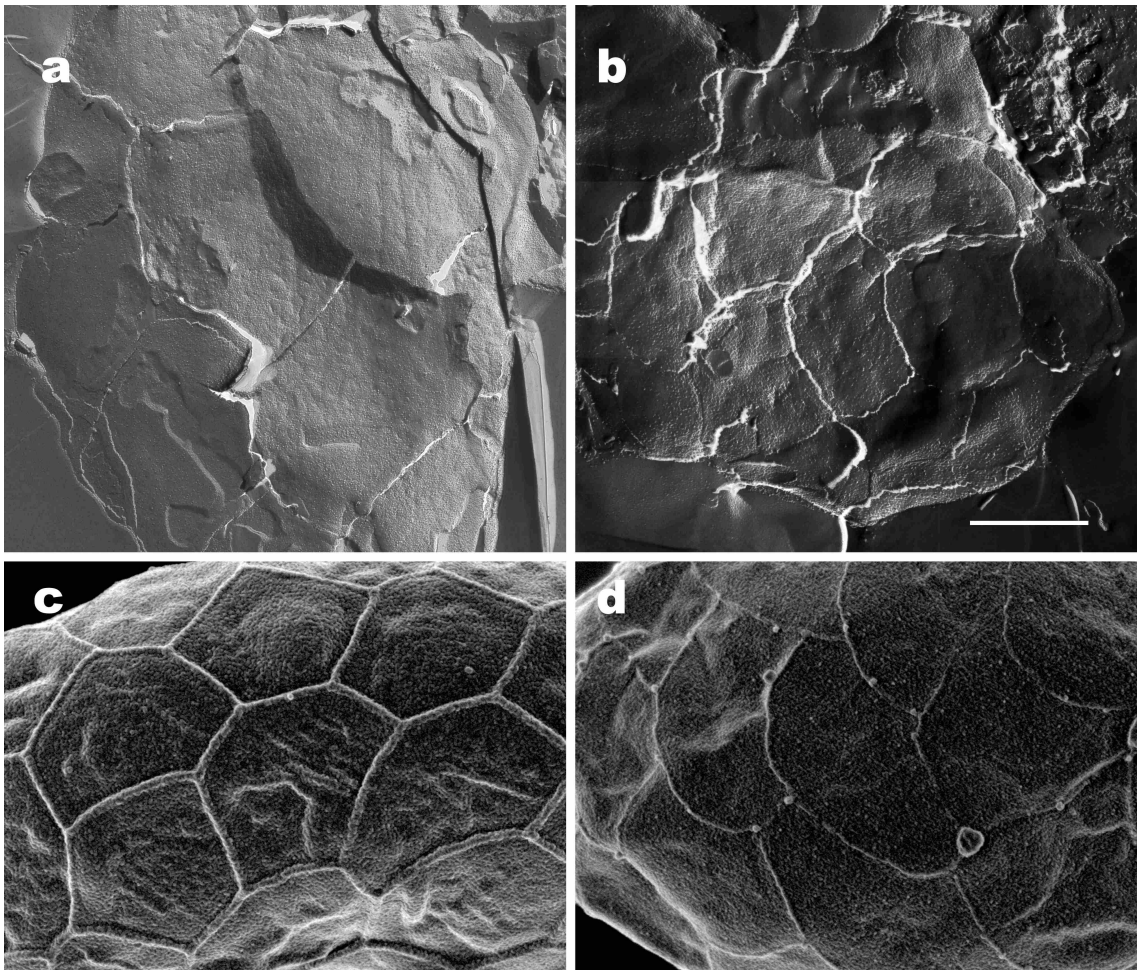

Figure 2.9. Cell coverings of two *Cyanophora* species in group B (Table 2.2), shown at the same magnification throughout.

All images are at the same magnification. Scale bar, 1 μm. (a, b) The peripheral fenestrations of plate vesicles behind the cell covering, revealed via the freeze-fracture replica method under transmission electron microscopy. (a) *C. sudae* Tos.Takah. sp. nov. strain NIES-764. (b) *C. biloba* Kugrens, B.L.Clay, C.J.Mey. & R.E.Lee strain UTEX 2766. (c, d) The cell surface under field-emission scanning electron microscopy, showing fenestrations aligned by ridges. (c) *C. sudae* strain NIES-764. (d) *C. biloba* strain UTEX 2766.

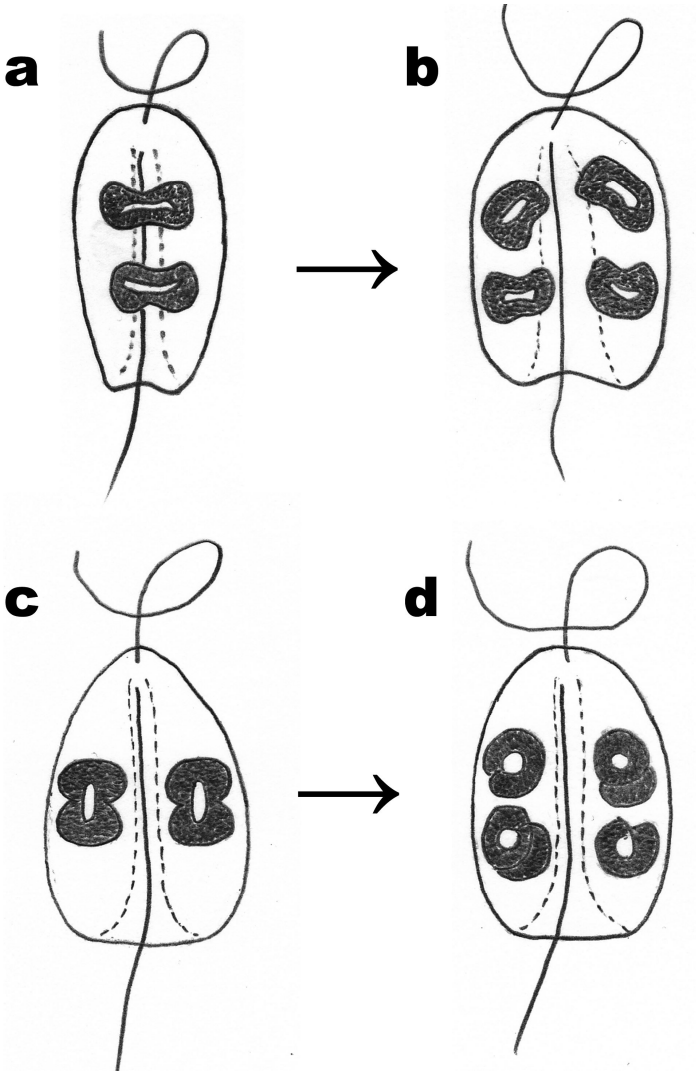

Figure 2.10. Diagram showing difference in plastid division between *Cyanophora tetracyanea* Korshikov (a, b) and *Cyanophora sudae* Tos.Takah. sp. nov. **(c, d)**.

Based on the present study and Korshikov (1941). Young cell of *C. tetracyanea* (a) has two plastids arranged in a longitudinal pair along the longitudinal central line and the plastids divide longitudinally to form two plastids positioned in each lobe of the adult cell (b). In contrast, two plastids in young cell of *C. sudae* are arranged in a transverse pair across the longitudinal central line of the cell (c) and the plastids divide transversely to form two plastids in each lobe of the adult cell (d).

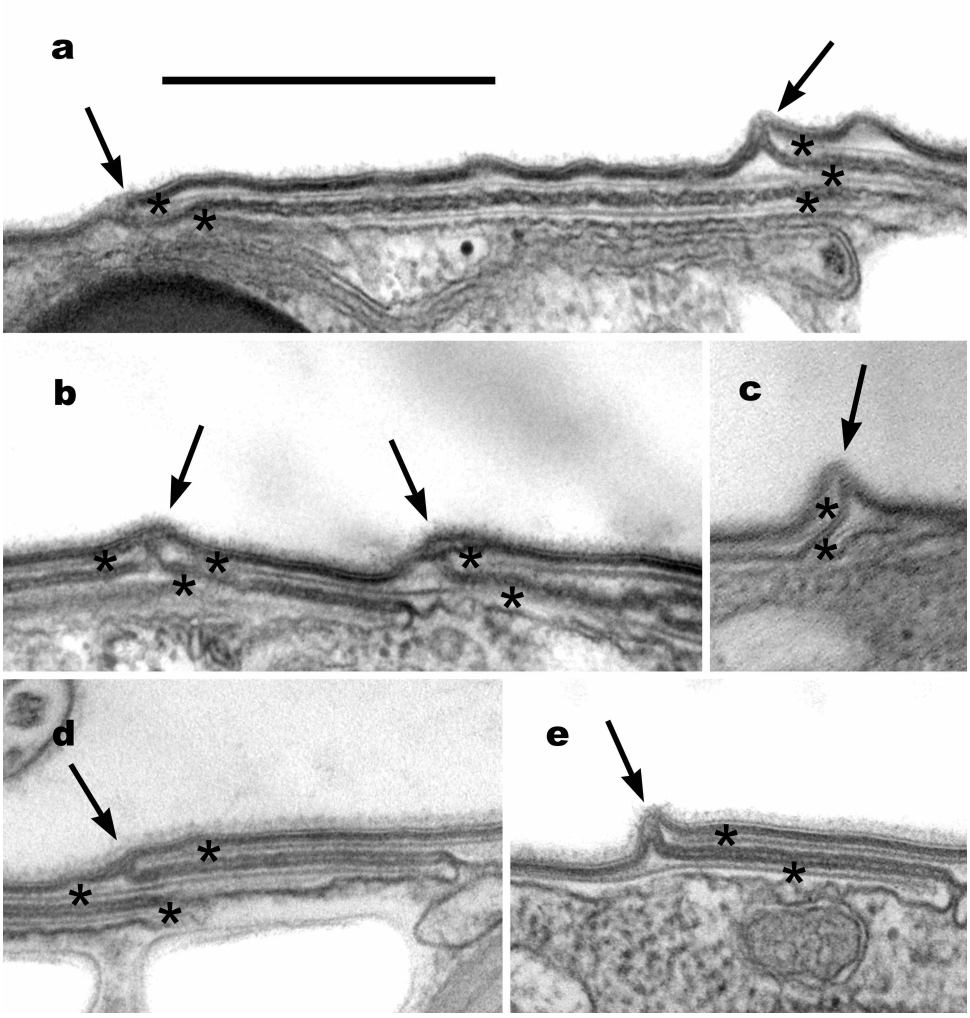

Figure 2.11. Transmission electron microscopy of vegetative cells of *Cyanophora* species.

All at the same magnification throughout. Scale bar, 1 μm. Note that the cell covering is composed of overlapping plates (asterisks) within flattened vesicles beneath the plasma membrane. Arrows indicate ridges formed by the margins of the outermost plate vesicles. (a) *C. cuspidata* Tos.Takah. sp. nov. strain SAG 45.84. (b, c) *C. kugrensii* Tos.Takah. sp. nov. strain NIES-763. (d, e) *C. sudae* Tos.Takah. sp. nov. strain NIES-764.

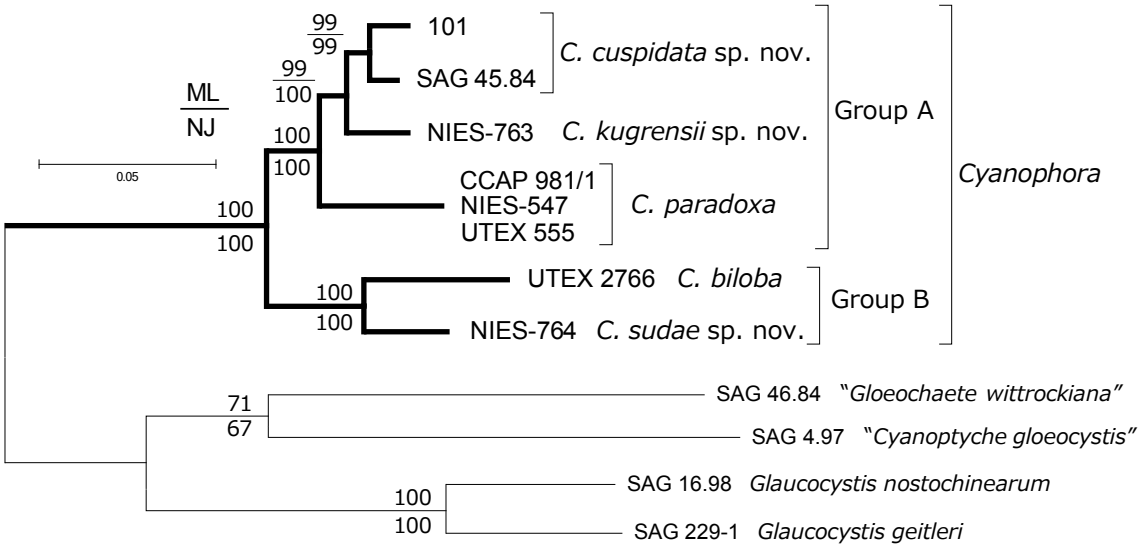

Figure 2.12. Maximum likelihood (ML) tree based on concatenated analyses of 1,461 and 750 base pairs of the coding regions of the plastid *psaB* and *psbA* genes, respectively, from eight strains of five *Cyanophora* species and four strains of other glaucophyte genera (Table 2.1).

Branch lengths are proportional to the genetic distances, which are indicated by the scale bar above the tree. Groups A and B represent morphologically distinct groups (Table 2.2). Numbers above branches represent ≥50% bootstrap values (based on 1,000 replications) of the ML analyses and below branches are ≥50% bootstrap values (based on 1,000 replications) of neighbour-joining (NJ). For details of the phylogenetic methods, see Subsection 2.2.6.

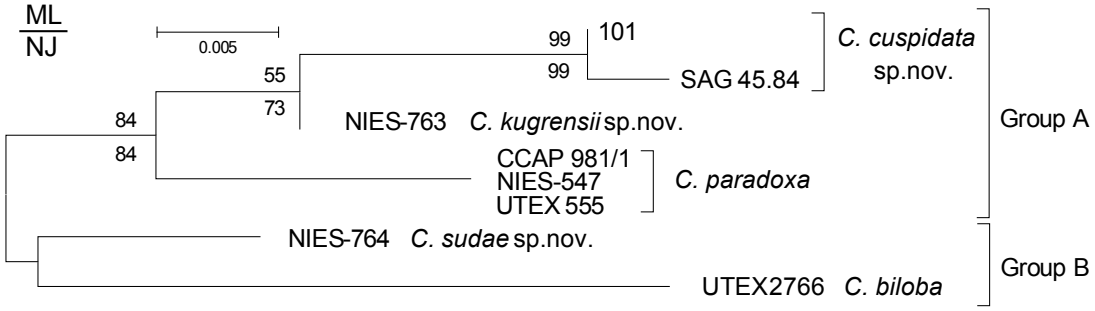

Figure 2.13. Maximum likelihood (ML) tree based on analyses of 614 base pairs of internal transcribed spacer (ITS) regions of nuclear ribosomal DNA (ITS-1, 5.8S *r*DNA, ITS-2) and partial LSU *r*DNA, from eight strains of five *Cyanophora* species (Table 2.1).

Branch lengths are proportional to the genetic distances, which are indicated by the scale bar above the tree. Groups A and B represent morphologically distinct groups (Table 2.2). Numbers above branches represent ≥50% bootstrap values (based on 1000 replications) of the ML analyses and below branches are ≥50% bootstrap values (based on 1,000 replications) of neighbour-joining (NJ). For details of the phylogenetic methods, see Subsection 2.2.6.

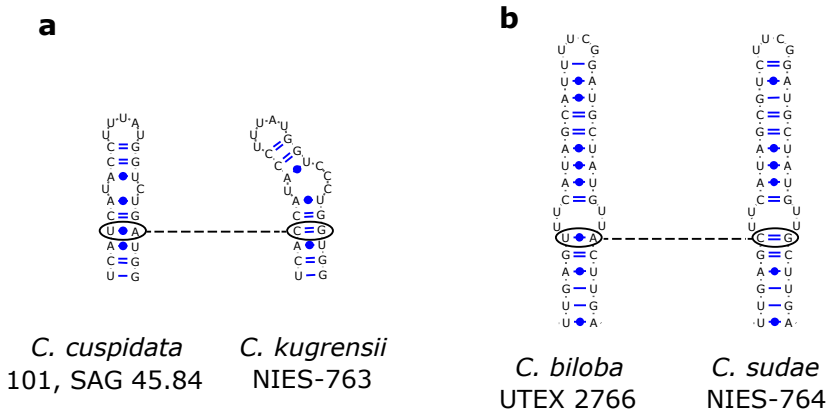

Figure 2.14. Comparison of the secondary structures of nuclear *r*DNA ITS-2 between sister species of *Cyanophora* resolved in the present molecular phylogeny (Figure 2.12).

Dotted lines indicate compensatory base changes between the helices. For complete secondary structures, see Figure 2.3. (a) Helix I between *C. cuspidata* Tos.Takah. sp. nov. strains 101 and SAG 45.84 and *C. kugrensii* Tos.Takah. sp. nov. strain NIES-763. (b) Helix II between *C. biloba* Kugrens, B.L.Clay, C.J.Mey. & R.E.Lee strain UTEX 2766 and *C. sudae* Tos.Takah. sp. nov. strain NIES-764.

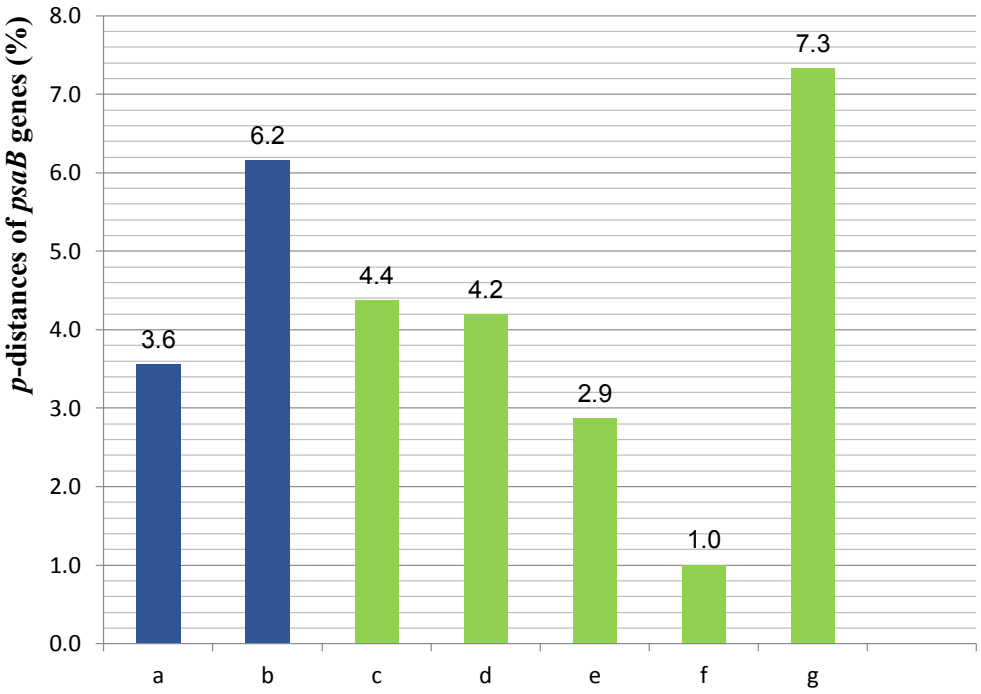

Figure 2.15. Nucleotide differences (%) or *p*-distances of *psaB* genes between sister species in *Cyanophora* and unicellular green algal genera.

The smallest difference is shown when multiple combinations of strains are present between sister species. For details of phylogenetic relationships and *psaB* gene sequence data of the green algal genera, see Subsection 2.3.6. (a) *C. cuspidata* sp. nov. and *C. kugrensii* sp. nov. (group A), (b) *C. biloba* and *C. sudae* sp. nov. (group B), (c) *Chloromonas chlorococcoides* and *Ch. reticulata*, (d) *Ch. hohamii* and *Ch. tenuis,* (e) *Hafniomonas laevis* and *H. montana*, (f) *H. conica* and *H. turbinea* and (g) *Chlorogonium capillatum* and *Ch. euchlorum*.

3. TAXONOMIC DELINEATION OF *GLAUCOCYSTIS* SPECIES

3.1. INTRODUCTION

The coccoid glaucophyte family Glaucocystaceae (Glaucocystales) (Table 1.1) are characterised by having a thick, cellulosic cell wall wherein they reproduce themselves (Komárek & Fott, 1983; Kies & Kremer, 1986). This family includes two genera, *Glaucocystis* Itzigs. *ex* Rabenh. (1866) and *Glaucocystopsis* Bourr. (1961) (Skuja, 1954; Komárek & Fott, 1983; Kies & Kremer, 1986) (Table 1.1); whereas monotypic genus *Glaucocystopsis* has just four plastids in a cell, the other genus *Glaucocystis* has more than four plastids (Bourrelly, 1960, 1961, 1985; Komárek & Fott, 1983). Early investigation of the genus *Glaucocystis* was performed using field-collected materials (Lagerheim, 1884; Hieronymus, 1892; Griffiths, 1915; Chodat, 1919; Geitler, 1923), establishing the genus concept. To date, seven species have been described within the genus, based upon the cell wall character or cell shape under light microscope (LM) (Geitler, 1923; Prescott, 1962; Starmach, 1966; Patel & Isabella George, 1979; Patel, 1981; Komárek & Fott, 1983; Prasad *et al.*, 1984; Kies & Kremer, 1986): *G. bullosa* (Kütz. 1836) Wille (1919), *G. nostochinearum* Itzigs. *ex* Rabenh. (1866), *G. cingulata* Bohlin (1897), *G. duplex* Prescott (1944), *G. oocystiformis* Prescott (1944), *G. indica* R.J.Patel (1981), *G. reniformis* B.N.Prasad, R.K.Mehrotra & P.K.Misra (1984) (Table 1.1). There remains no authentic strain in each species. Although strains identified as the type species *G. nostochinearum* are available from worldwide culture collections, but they lack morphological data for species identification (Schlösser, 1994; Kasai, 2009) (Table 3.1). No other species of *Glaucocystis* have been maintained in culture collections. Among the seven species, only *G. nostochinearum* has been considered as a cosmopolitan species (Prasad, 1961; Prescott, 1962; Starmach, 1966; Compère, 1976;

Hirose & Yamagishi, 1977); based only upon LM information, coccoid glaucophyte algae have been identified as *G. nostochinearum* from all over the world [e.g., South Africa, Mali, Tanzania (Compère, 1976), Côte d'Ivoire (Bourrelly, 1960, 1961; Compère, 1976), Malawi (Schmidle, 1902; Compère, 1976), Portugal (Vasconcelos & Morais, 2009), Spain (Caballero, 1945; Alvarez Cobelas & Gallardo, 1986), France (Bourrelly, 1957), Britain (West, 1904; Whitton, 2002), Belgium (Schouteden-Wéry, 1911; Van Meel, 1939, 1944; Hoffmann & Kostikov, 2004; Van Wichelen *et al.*, 2008), Netherland (Simons, 2010), Germany (Rabenhorst, 1866, 1868; Kühn & Schnepf, 2002), Sweden (Borge, 1906), Austria (Kies, 1989; Gärtner & Ingolić, 2001), Czech (Hansgirg, 1892), Poland (Gutwiński, 1909), Ukraine (Korshikov, 1953; Hu *et al.*, 1996; Kapustin, 2014), Romania (Cărăuş, 2002, 2012), Bulgaria (Belkinova *et al.*, 2002), India (Prasad, 1961; Patel & Isabella George, 1979; Chatterjee & Keshri, 2005), Bangladesh (Islam, 1998), Burma (Skuja, 1949), Thailand (Ariyadej *et al.*, 2004), Indonesia (Gutwiński, 1901), China (Hu *et al.*, 1996; Hu & Wei, 2006), Korea (Kim & Chung, 1994), Japan (Hirose & Yamagishi, 1977), New Zealand (Gordon, 2013), Canada (Fenwick, 1966), U.S.A. (Smith, 1933; Prescott, 1962), Cuba (Lagerheim, 1886b), Brazil (de Azevedo Barros, 2010)]. *G. nostochinearum*, however, has been described as having different morphological characteristics depending upon given authors or identifiers (Prasad, 1961; Prescott, 1962; Komárek & Fott, 1983). Therefore, taxonomic studies based upon molecular methods and comparative ultrastructure as in *Cyanophora* (see Chapter 2) are also required in this genus, using various clonal strains. Recently, Chong *et al.* (2014) performed molecular phylogenetic analyses using worldwide strains available and showed that the cryptic, genetic diversity exists within *Glaucocystis* but did not report morphological diversity nor delimit the species within the genus.

Pringsheim (1958) identified an original isolate (SAG 229-2) as *G. nostochinearum* var. *incrassata* Lemmerm. (1908); he also provided a provisional name *G. geitleri* E.G.Pringsh. (1958) *nom. provis.* for another original isolate (SAG 229-1). However, he did not compare these two strains with other strains identified as *G. nostochinearum* var. *nostochinearum*. Schnepf *et al.* (1966) observed three strains of *Glaucocystis* (SAG 229-1, SAG 229-2 and SAG 229-3) by ultrathin section transmission electron microscopy (TEM) and reported that there is no ultrastructural difference between the three. After their observations, no comparative morphology has been performed using several strains in the genus *Glaucocystis*.

Two glaucophyte genera, the flagellate *Cyanophora* and coccoid *Glaucocystis*, are genetically diverse and each includes multiple possible cryptic species (Chong *et al.* 2014). In the genus *Cyanophora* (Chapter 2), the combination of ultrathin section and freeze-fracture TEM and low accelerating voltage (LV) field emission scanning electron microscopy (FE-SEM) could elucidate the three-dimensional (3D) ultrastructural features of the protoplast periphery of the naked vegetative cells of various *Cyanophora* strains and demonstrated that ultrastructural differences are useful for delineating *Cyanophora* species. Similar ultrastructural diversity is expected in *Glaucocystis* but the cell wall of this genus would prohibit visualisation of the native ultrastructural features of the protoplast periphery by FE-SEM. Although freeze-fracture TEM revealed leaflet-like surface appearances of flattened vesicles in the coccoid glaucophyte genus *Glaucocystis* (Robinson & Preston, 1971a; Willison & Brown Jr., 1978a), the 3D ultrastructural features of the *Glaucocystis* protoplast periphery are unclear, especially regarding the spatial relationship between the plasma membrane and flattened vesicles (Schnepf *et al.*, 1966; Robinson & Preston, 1971a; Willison & Brown Jr., 1978a; Kies,

1979).

Recent advancements in ultra-high voltage electron microscopy (UHVEM) have enabled thick-section micrographs in biological samples (Cyranoski, 2009). Based on 3D UHVEM tomography, the *in situ* peripheral ultrastructure of protoplasts can be observed, even when enclosed by extracellular structures (Nishida *et al.*, 2013). However, 3D UHVEM has not previously been applied to algae or protozoa.

The present chapter aimed to delimit the species in the genus *Glaucocystis* based on combination of several microscopy including 3D UHVEM, combined with molecular data, from several globally distributed strains including three newly established. To examine ultrastructural diversity in the genus *Glaucocystis*, the present study performed the UHVEM tomography using high-pressure freezing (HPF) and freeze-substitution (FS) fixation of *Glaucocystis* species. Three types of 3D ultrastructure of the protoplast periphery of *Glaucocystis* cells were revealed by 3D-modelling based on UHVEM tomography as well as by ultrathin section TEM using HPF-FS. On the basis of the three peripheral types and of other characters under LM and LV FE-SEM, the morphology and taxonomy of six species based on strains of the genus are described in this chapter: *G. nostochinearum*, *G. oocystiformis*, *G. incrassata* (Lemmerm.) Tos.Takah. comb. & stat. nov., *G. geitleri* E.G.Pringsh. *ex* Tos.Takah. sp. nov., *G. miyajii* Tos.Takah. sp. nov. and *G. bhattacharyae* Tos.Takah. sp. nov.

3.2. MATERIALS AND METHODS

3.2.1. Strains and culture conditions for observation

10 culture strains of *Glaucocystis* were obtained from public culture collections (Table 3.1) at the National Institute for Environmental Studies (NIES, http://mcc.nies.go.jp/; Kasai *et al.* 2009) and the Sammlung von Algenkulturen der Universität Göttingen (SAG, http://sagdb.uni-goettingen.de/)(Schlösser, 1994). SAG 229-1 is one of the most widely used *Glaucocystis* strains and originates from Pringsheim's "authentic" strain of "*Glaucocystis geitleri* nom. provis." (Koch, 1964; Schnepf *et al.*, 1966) (Tables 1.1 and 3.1). SAG 16.98 is labelled as the type species "*G. nostochinearum*" and was collected in Germany (Schlösser, 1994) (http://sagdb.uni-goettingen.de/) where the type locality of *G. nostochinearum* is located (Rabenhorst, 1866). "*Glaucocystis incrassata*" SAG 229-2 was identified as "*G. nostochinearum* var. *incrassata* Lemmerm. (1908)" by Pringsheim (1958) and previously labelled as "*G. incrassata*" (Koch, 1964; Schnepf *et al.*, 1966) (Table 3.1). In addition, I also used three strains of *Glaucocystis* newly established by the pipette-washing method (Pringsheim, 1946) from water samples collected in Japan (strain 118, 126 and Thu10; Table 3.1). The cultures were maintained in screw-cap tubes with 9–11 mL AAF-6 medium (Kato, 1982; Kasai *et al.*, 2009) under 14 h-light/10 h-dark conditions at 20°C with a photon flux density of *ca*. 50–60 μmol/m^2/s.

3.2.2. Light microscopy (LM) and field-emission scanning electron microscopy (FE-SEM)

LM observations were carried out as described in Chapter 2. LV FE-SEM was

performed as described in Chapter 2 but cells were harvested directly and critical point dried using critical point dryer JCPD-5 (JEOL, Tokyo, Japan) and were observed using an ultra-high resolution (UHR) FE-SEM SU8220 (Hitachi High-Technologies, Tokyo, Japan).

3.2.3. High-pressure freezing (HPF) and freeze-substitution (FS) fixation

Previous reports have performed ultrathin section TEM of *Glaucocystis* using chemical fixation (Ueda, 1961; Lefort, 1965; Schnepf, 1965; Schnepf & Koch, 1966; Schnepf *et al.*, 1966; Bourdu & Lefort, 1967; Echlin, 1967; Hall & Claus, 1967; Lefort & Pouphile, 1967; Robinson & Preston, 1971a, 1971b; Schnepf & Brown Jr., 1971; Willison & Brown Jr., 1978a, 1978b; Kies, 1979) but *Glaucocystis* ultrastructure is reported to be affected by fixation artefacts (Lefort & Pouphile, 1967; Willison & Brown Jr., 1978a).

Since the HPF-FS fixation method is generally expected to be superior to chemical fixation in preserving the integrity of cellular ultrastructure (Osumi, 1998; Sato *et al.*, 2009; Saito, 2013), this method was performed for TEM and UHVEM as described previously (Sato *et al.*, 2009; Saito, 2013) with minor modifications. Briefly, cells were harvested directly from the cultures using a pipette and frozen under high pressure using a high-pressure freezing machine (HPM010; Bal-Tec, Furstentum, Liechtenstein, now: Leica). The samples were placed onto frozen 4% osmium tetroxide anhydrous acetone at liquid-nitrogen temperature and post-fixed in the solution incubated at −80°C for 5 days before warming gradually to −20°C for 2 h, then to 4°C for 1 h and finally to room temperature. The samples were washed three times with anhydrous acetone and infiltrated with increasing concentrations of Spurr's resin (Spurr, 1969) in anhydrous acetone, and finally embedded in Spurr's resin.

3.2.4. Transmission electron microscopy (TEM) and ultra-high-voltage electron microscopy (UHVEM)

Ultrathin section TEM was performed as described in Chapter 2 except for the HPF-FS fixation method. Prior to UHVEM observation, thick sections (1 or 2 μm) were cut using an ultramicrotome (Ultracut E; Reichert-Jung, Vienna, Austria, now: Leica) and mounted on formvar-coated copper grids. The thick sections were stained in 10% uranyl acetate in 70% methanol with 150 W microwave for 30 s and then incubated for 20 min. After washing and drying, the sections were stained in lead citrate with 150 W microwave for 30 s and then incubated for 10 min. Colloidal gold particles (20 or 60 nm in diameter) were deposited on both sides of each section, and the samples were observed using UHVEM (H-3000; Hitachi, Tokyo, Japan) at an accelerating voltage of 2 MV. Tomographic image series were recorded using a 4096 × 4096 pixel slow scan CCD camera (TVIPS, Gauting, Germany). Single axis tilt series were obtained from ± 60° with 2° increments. Reconstruction of the tomographic images and 3D-modelling was performed as described previously (Nishida *et al.*, 2013).

3.2.5. Molecular phylogenetic analyses and comparative analysis of secondary structures of ITS-2 of nuclear ribosomal DNA

DNA extraction, polymerase chain reaction (PCR) and direct sequencing of the PCR products were performed as described in Chapter 2 using primers designed for previous or present study (Nozaki *et al.*, 2000; Chong *et al.*, 2014; Figure 2.2). The secondary structure of nuclear ribosomal DNA (*r*DNA) internal transcribed spacer (ITS)-2 was constructed as described in Chapter 2, also referring to the secondary structure of

Cyanophora strains (Figure 2.3).

Phylogenetic relationships between species of *Glaucocystis* were examined based on analyses of the concatenated 1,461 base pairs of partial photosystem I P700 chlorophyll *a* apoprotein A2 (*psaB*) and 750 base pairs of photosystem II P680 chlorophyll *a* apoprotein D1 (*psbA*) gene sequences from 13 strains of *Glaucocystis* representing 10 operational taxonomic units (OTUs) (based on identical sequences) and three strains of three glaucophyte genera as outgroup. The alignment was carried out as described in Chapter 2 and subjected to phylogenetic analyses. Maximum-likelihood (ML) and neighbour-joining (NJ) analyses were performed as described in Chapter 2 except that one selected model was used: the general time reversible (GTR) + gamma model with invariant sites for ML.

3.3. RESULTS AND DISCUSSION

3.3.1. Light microscopy

By LM, vegetative cells in all of the strains exhibited ellipsoidal shape lacking any equatorial ring as observed in *Glaucocystis cingulata* (Bohlin, 1897; Skuja, 1949; Philipose, 1967; Patel & Isabella George, 1979; Komárek & Fott, 1983). However, the cell wall at the cell poles showed differences between strains (Figure 3.1). Within the 13 strains examined, strains 126, NIES-1369 and NIES-966 were different from the others, having variable protrusions of polar cell wall or polar nodules (Figure 3.1d) as described in original description of *G. oocystiformis* (Prescott, 1944). In addition, the present strains were broadly ellipsoidal in shape and measured to be 25–35μm long and 15–25 μm wide in cell size and resembled holotype illustration in original description of this species (Prescott, 1944, 1962; Komárek & Fott, 1983) (Table 3.2; Figure 3.1). The autospores in a colony were generally four (Table 3.2; Figure 3.2). Thus, these three strains were clearly identified as *G. oocystiformis* by LM. This species exhibited another diagnostic character by UHVEM and ultrathin section TEM (described below).

In the other species (lacking such polar nodules), the shape of cell pole was distinguishable by having or lacking thickenings of the cell wall at cell poles (Figure 3.1). Three species lacked such polar thickenings (Figure 3.1, b, e and f): *G. nostochinearum* strains SAG 16.98 and SAG 45.88, *G. miyajii* strains Thu10 and NIES-1961 and *G. bhattacharyae* strains 118 and SAG 27.80. *G. bhattacharyae* strains 118 and SAG 27.80 were measured to be 17–27 μm long and 12–22 μm wide in cell size; *G. nostochinearum* strains SAG 16.98 and SAG 45.88 or *G. miyajii* strains Thu10 and NIES-1961 were measured to be 18–23 μm or 19–24 μm long and 10–15 μm wide,

respectively (Table 3.2; Figure 3.1). The autospores in a colony were generally four in the three species (Table 3.2; Figure 3.2). Among the three species, cell shape of *G. bhattacharyae* strains 118 and SAG 27.80 were truncate (Figure 3.1f) and differed from the other two species that had ellipsoidal, not truncate vegetative cells without any other distinctive characters at the cell poles (Figure 3.1, b and e). On the other hand, *G. nostochinearum* strains SAG 16.98 and SAG 45.88 and *G. miyajii* strains Thu10 and NIES-1961 were difficult to be distinguished from each other by LM. By UHVEM and ultrathin section TEM, however, I clearly distinguished the two species (see Subsection 3.3.3). According to Rabenhorst (1866, 1868), cell shape of *G. nostochinearum* was ellipsoidal without distinctive characters in the cell wall and/or cell poles. Strain SAG 16.98 had an ellipsoidal vegetative cell and lacked such characters (Figure 3.1b), similar to the original shape of *G. nostochinearum* (Rabenhorst, 1866, 1868). This strain originates from Germany (Schlösser, 1994; http://sagdb.uni-goettingen.de/) (Table 3.1) where the type locality of *G. nostochinearum* is located (Rabenhorst, 1866). Thus, cells of SAG 16.98 were selected as the epitype material of *G. nostochinearum* (see Section 3.5 Taxonomic accounts).

Four strains of two species had vegetative cells with polar cell wall thickenings (but without polar nodules) (Figure 3.1, a and c): *G. geitleri* strains SAG 229-1, SAG 229-3 and SAG 28.80 and *G. incrassata* strain SAG 229-2. Within the four strains, the strain SAG 229-2 was clearly identified as *G. nostochinearum* var. *incrassata* by LM, comparing original description of the variety as did Pringsheim (1958) using the original Christensen isolate (SAG 229-2). This strain was broadly truncate-ellipsoidal often with polar thickenings in shape and measured to be 20–30 μm long and 13–23 μm wide in cell size (Table 3.2; Figure 3.1). The autospores in a colony were generally four

or eight (Table 3.2; Figure 3.2). Since this strain exhibited several characters based on LM and EM distinguishing it than the other species as well as it was diverged genetically (discussed below), I raised var. *incrassata* to *G. incrassata* (Lemmerm.) Tos.Takah. comb. & stat. nov. On the other hand, *G. geitleri* strains SAG 229-1, SAG 229-3 and SAG 28.80 were broadly truncate-ellipsoidal, sometimes with polar thickenings in shape, and measured to be 30–40 μm long and 20–30 μm wide in cell size (Table 3.2; Figure 3.1). The autospores in a colony were generally two (Table 3.2; Figure 3.2). This species, thus, clearly differed from *G. incrassata* strain SAG 229-2, on the basis of their large cell size and their autospore numbers within a colony (Table 3.2; Figure 3.2), as already pointed by Pringsheim (1958) using an original George isolate (SAG 229-1). He, however, did not validly publish but merely provided a provisional name *G. geitleri* E.G.Pringsh. (1958) *nom. provis.* for the species. Now that his results reappeared in my observation, I accepted his proposal and gave it *G. geitleri* E.G.Pringsh. *ex* Tos.Takah. sp. nov. Besides, both species also exhibit 3D ultrastructural difference by UHVEM and ultrathin section TEM (described below).

Autospores (daughter cells) of *Glaucocystis* species were surrounded by mother cell wall to form colony. In terms of colony, mother cell wall lacked any attaching stalk as observed in *G. indica* (Patel, 1981) and *G. reniformis* (Prasad *et al.*, 1984; Chatterjee & Keshri, 2005). However, the extension of mother cell wall was distinctive into two types (Figure 3.2): the colony extension was prominent in *G. geitleri* strains SAG 229-1, SAG 229-3 and SAG 28.80, *G. nostochinearum* strains SAG 16.98 and SAG 45.88, *G. oocystiformis* strains 126, NIES-1369 and NIES-966 and *G. miyajii* strains Thu10 and NIES-1961; each individual was arranged separately to form spaces between each other (Figure 3.2, a, b, d and e). On the other hand, the mother cell wall of *G. incrassata*

strain SAG 229-2 and *G. bhattacharyae* strains 118 and SAG 27.80 enclosed the inside cell tightly and was less extended (Figure 3.2, c and f). The surface of the mother cell wall observed by LV FE-SEM is described below.

3.3.2. Field-emission scanning electron microscopy

Cell wall of *Glaucocystis* is composed of cellulose filaments and several observation has revealed the highest cellulose I_{α} crystallite contents throughout organisms as well as the *ex situ* cellulose filament structure derived from this alga by TEM and several spectroscopy (Schnepf, 1965; Robinson & Preston, 1971b; Willison & Brown Jr., 1978a, 1978b; Sugiyama *et al.*, 1991; Imai *et al.*, 1999; Briois *et al.*, 2013; Lee *et al.*, 2014). To date, however, FE-SEM has not been performed to show the *in situ* colony surface or to compare the ultrastructural feature between strains.

Here, by LV FE-SEM, the cellulose filaments of mother cell wall were unveiled on the surface of the *Glaucocystis* colonies (Figure 3.3). The fibrils on the surface of the mother cell wall were essentially identical in shape among the strains examined but two types of the filament arrangements were recognised. The whole mother cell wall surface generally exhibited gauze fabric-like appearance, with small spaces between fibrils, in *Glaucocystis geitleri* strains SAG 229-1, SAG 229-3 and SAG 28.80, *G. nostochinearum* strains SAG 16.98 and SAG 45.88, *G. oocystiformis* strains 126, NIES-1369 and NIES-966 and *G. miyajii* strains Thu10 and NIES-1961 (Figure 3.3, a, b, d and e). On the other hand, the fibrils were tightly arranged and did not show small spaces between them on almost all of the surface of the mother cell wall in *G. incrassata* strain SAG 229-2 and *G. bhattacharyae* strains 118 and SAG 27.80 (Figure 3.3, c and f).

The ultrastructural difference in mother cell wall observed by LV FE-SEM (Figure 3.3; Table 3.2) is considered to reflect the difference in expansion of the mother cell wall observed by LM (described above; Figure 3.2; Table 3.2).

3.3.3. Ultra-high voltage electron microscopy and 3D-modelling

In order to compare the peripheral 3D ultrastructure of protoplasts enclosed by a cell wall between *Glaucocystis* species, I observed one strain (designated here as the authentic strain) for each of the six *Glaucocystis* species by UHVEM.

Using UHVEM tomography, the 3D ultrastructural features of the plasma membrane and the flattened vesicles at the protoplast periphery of the *Glaucocystis* species examined here were visualised with high contrast (Figures 3.4–3.8). In all of the species, the flattened vesicles were leaflet-like in shape, lacked a plate-like interior structure, and were distributed throughout the entire protoplast periphery just underneath the single-layered plasma membrane (except for the region near basal bodies; see below; Figure 3.8), but did not completely enclose the protoplast periphery to form small spaces between the vesicles at the protoplast periphery.

The present comparative peripheral tomography clearly showed essential differences in the protoplast periphery between species (Figures 3.4–3.7). I observed various regions of matured vegetative cells by UHVEM and tomography, as well as ultrathin section TEM (described below; Figure 3.9); the peripheral 3D structures were essentially consistent within each species. Based on the results obtained by UHVEM tomography, within *Glaucocystis*, three periphery types were distinguished: A, B and C. Based on the native 3D ultrastructural features of the protoplast periphery in *Glaucocystis* species established by UHVEM tomography, each type of peripheral 3D

ultrastructure was also evident and distinguishable from the other two types, even by ultrathin section TEM (described below; Figure 3.9). In order to show the 3D arrangements and relationship between plasma membrane and flattened vesicles at protoplast periphery visually, 3D-modelling was reconstructed based upon a chosen UHVEM tomography from each periphery type.

The periphery type A was observed in *G. geitleri* cells (Figure 3.4) and in *G. oocystiformis* cells (Figure 3.7, a and b) by UHVEM tomography. The plasma membrane exhibited bar-like grooves when viewed from the outside (or bar-like ridges when viewed from the inside) (Figure 3.4, b–d and g). These grooves were measured to be 500–1,500 nm long, 60–90 nm wide and 100–150 nm deep; they were arranged almost in parallel at regular intervals of 500–800 nm. The flattened vesicles just below the plasma membrane were 30–70 nm thick and almost ellipsoidal or ovoid in front view (700–2,000 nm long and 300–600 nm wide) with a bar-like invagination in the centre when viewed from the outside (Figure 3.4, b, c and e). The invagination of the flattened vesicle was measured to be 500–1,500 nm long, 80–110 nm wide and 100–150 nm deep. Each groove on the plasma membrane was backed almost entirely with the invagination of the flattened vesicle just underneath the plasma membrane; the backing was often associated with microtubules arranged in parallel (Figure 3.4f). The flattened vesicles were almost separated from one another at the protoplast periphery of this type of cells. Many elongated mitochondria were observed below the flattened vesicles at the protoplast periphery (Figure 3.4b).

The periphery type B was observed in *G. nostochinearum* cells (Figure 3.5) by UHVEM tomography. The plasma membrane was almost flat in surface view (Figure 3.5, b–d and g), lacking the depression or invagination that was observed in *G. geitleri*.

The flattened vesicles just underneath the plasma membrane neighboured the inner surface of the plasma membrane at regular patterns in *G. nostochinearum* (Figure 3.5, b, c, e and f). The vesicles were 30–70 nm thick and elongate-cylindrical in front view (1,500–2,000 nm long and 500–1,000 nm wide); they were almost smooth from a surface view (Figure 3.5e). Their marginal regions were often slightly overlapped with one another (Figure 3.5f).

The periphery type C was observed in *G. incrassata* cells (Figure 3.6), in *G. miyajii* cells (Figure 3.7, c and d) and in *G. bhattacharyae* cells (Figure 3.7, e and f) by UHVEM tomography. The plasma membrane exhibited bar-like grooves when viewed from the outside (or bar-like ridges when viewed from the inside) (Figure 3.6, b–d and g). The grooves were generally arranged in parallel at regular intervals of 200–600 nm but sometimes the arrangement was oblique (Figure 3.6, b–d and g). These grooves measured 500–1,500 nm long, 60–90 nm wide and 100–150 nm deep. Flattened vesicles were positioned immediately below the plasma membrane and measured 30–70 nm thick and appeared almost ellipsoidal or ovoid in front view (600–2,000 nm long and 300–600 nm wide), with a bar-like invagination in the centre when viewed from the outside (Figure 3.6, b, c and e). Each groove on the plasma membrane was backed almost entirely by invagination of the flattened vesicle, and associated with microtubules that were arranged almost in parallel (Figure 3.6f). The marginal regions of the flattened vesicles often slightly overlapped one another (Figure 3.6, b, e and f).

Although vestigial flagella in *Glaucocystis* cells have previously been observed by ultrathin section TEM (Schnepf & Koch, 1966; Schnepf *et al.*,1966; Willison & Brown Jr., 1978a; Kies, 1979), the present UHVEM tomography of all six species clearly showed the 3D ultrastructure of the protoplast periphery surrounding basal bodies and

neighbouring vestigial flagella. The 3D structure of the protoplast periphery surrounding basal bodies and neighbouring vestigial flagella was essentially identical in the six species. Two vestigial flagella were situated between the cell wall and protoplast periphery at the cell equator, were positioned within the furrow of the protoplast surface, and were connected to the basal bodies within the cytoplasm. Flattened vesicles were absent near the basal bodies as observed previously but the present UHVEM clearly revealed ovoid-to-spherical vesicles that were distributed below the plasma membrane near the basal bodies and vestigial flagella (Figure 3.8).

In the present study, the 3D ultrastructural arrangement of the plasma membrane and the underlying leaflet-like flattened vesicles in the coccoid glaucophyte genus *Glaucocystis* were clearly observed by UHVEM tomography and 3D-modelling using HPF-FS method. Moreover, within *Glaucocystis,* three periphery types were clearly distinguished from each other based on the 3D UHVEM tomographic comparison of peripheral ultrastructures just inside the wall. Hence, UHVEM tomography can be used to explore the 3D ultrastructural arrangement of the periphery, even in the presence of a wall or extracellular matrix, and can be used to compare the subcellular ultrastructure or 3D arrangement of organisms.

3.3.4. Ultrathin section transmission electron microscopy

In each species of *Glaucocystis*, a single, continuous plasma membrane enclosed the protoplast, and numerous flattened vesicles closely neighboured the inner surface of the plasma membrane and were distributed throughout the whole protoplast periphery (Figure 3.9). These flattened vesicles consisted of two neighbouring membranes in section but no plate-like structure was found within the vesicles. Golgi bodies were

distributed within the cytoplasm, and frequently found near the basal bodies of vestigial flagella.

Based on the ultrathin section TEM comparison using HPF-FS of all of the *Glaucocystis* strains, the species exhibited differences in form and arrangement of the flattened vesicles just underneath the plasma membrane (Figure 3.9). The three periphery types revealed by UHVEM tomography and 3D-modelling were also distinguishable by the present ultrathin section TEM.

G. geitleri strains SAG 229-1, SAG 229-3 and SAG 28.80 and *G. oocystiformis* strains 126, NIES-1369 and NIES-966 exhibited the periphery type A. The protoplast showed numerous small depressions at the periphery in section (Figure 3.9, a and d). Such a depression was at intervals of 500–800 nm and shared by the plasma membrane and the centre of the underlying flattened vesicle. At the depression, both plasma membrane and the two neighbouring membranes of the underlying flattened vesicles were depressed acutely to become an arch-shaped protrusion. The flattened vesicles did not overlap with each other at the protoplast periphery.

G. nostochinearum strains SAG 16.98 and SAG 45.88 cells, however, exhibited the periphery type B (Figure 3.9b). The plasma membrane and the underlying flattened vesicles at the protoplast periphery did not show depressions in section (Figure 3.9b). The neighbouring flattened vesicles slightly overlapped with one another at the protoplast periphery.

G. incrassata strain SAG 229-2, *G. miyajii* strains Thu10 and NIES-1961 and *G. bhattacharyae* strains 118 and SAG 27.80 exhibited the periphery type C. The protoplast showed numerous small depressions at intervals of 200–600 nm in section, shared by the plasma membrane and the centre of the underlying flattened vesicle

(Figure 3.9, c, e and f). The neighbouring flattened vesicles slightly overlapped with one another at the protoplast periphery.

By these periphery types (Figure 3.10) recognised by UHVEM and ultrathin section TEM, *G. nostochinearum* (periphery type B) and *G. miyajii* (periphery type C) were distinguished from each other clearly although they were undistinguishable by LM.

The fact that previous studies of *Glaucocystis* did not reveal the ultrastructural diversity of this genus (Schnepf *et al.*, 1966; Schnepf & Brown Jr., 1971) may result from the difference in fixation of cells. In the previous studies, the cells were fixed by chemical fixation that altered ultrastructure by artefacts (Willison & Brown Jr., 1978a) whereas I used HPF-FS fixation for all of the samples of *Glaucocystis*.

3.3.5. Molecular phylogenetic analyses

The phylogenetic tree of the concatenated *psaB* and *psbA* sequences (Figure 3.11) showed that 13 *Glaucocystis* strains were subdivided into six phylogenetic groups (monophyletic groups when more than one OTU), equivalent to G1–G6 groups recognised by Chong *et al.*, (2014). Each species recognised by morphology discussed above corresponded to a single lineage in the tree. Unlike the phylogenetic analyses of Chong *et al.* (2014), based on my phylogenetic tree, each group was discrete and each monophyletic group was resolved with ≥99% bootstrap values in ML and NJ; the basal relationships were also resolved and stem group and crown group were recognised. The crown group was discrete from the stem group with 100% bootstrap values in ML and NJ and composed of four species (*G. nostochinearum* strains SAG 16.98 and SAG 45.88, *G. oocystiformis* strains 126, NIES-1369 and NIES-966 and *G. miyajii* strains Thu10 and NIES-1961 and *G. bhattacharyae* strains 118 and SAG 27.80). *G.*

nostochinearum strains SAG 16.98 and SAG 45.88 and *G. oocystiformis* strains 126, NIES-1369 and NIES-966 exhibited nearest phylogenetic groups among those within the crown group although the relationship within the crown group was weakly resolved. The stem group was composed of two species (*G. incrassata* strain SAG 229-2 and *G. geitleri* strains SAG 229-1, SAG 229-3 and SAG 28.80). *G. geitleri* strains SAG 229-1, SAG 229-3 and SAG 28.80 were in the most basal position.

3.3.6. Evaluation of species based on secondary structures of nuclear *r*DNA ITS-2 and genetic distances of *psaB* genes

As discussed in Chapter 2 for species of *Cyanophora*, species of *Glaucocystis* delineated here based on morphological differences (Table 3.2) and phylogeny (Figure 3.11) were evaluated by the secondary structure of nuclear *r*DNA ITS-2 (Figures 3.12 and 3.13) and genetic distance of *psaB* genes (Figure 3.14). Within each *Glaucocystis* species or the phylogenetic group, no compensatory base change (CBC) was identified between strains. Within the crown group (Figure 3.11), however, at least one CBC was detected between any two species except between *G. miyajii* and *G. bhattacharyae* (for example in helix II, Figure 3.13). Between the crown group species and *G. incrassata*, at least one CBC was also detected whereas between the most basal *G. geitleri* and any other species were detected at least five CBCs. Therefore, *Glaucocystis* species would have sufficient genetic distance to be separated into distinct species.

On the other hand, *p*-distances of *psaB* genes between species of *Glaucocystis* were calculated (Figure 3.14) within the crown group (Figure 3.11) and compared with the ranges exhibited between green algal and *Cyanophora* species (discussed above; Subsection 2.3.6; Figure 2.15). Within the genus *Glaucocystis*, the crown group species

G. oocystiformis and *G. nostochinearum* exhibited the smallest difference of *psaB* *p*-distance (5.2%) whereas the other *psaB p*-distance between each of the two species within the crown group was the ranges of 6.3–8.1% (Figure 3.14). These values did not exceed the ranges of the *psaB p*-distances (1.0–7.3%) between the sister species in the unicellular green algae as well as glaucophyte genus *Cyanophora* (Figure 2.15). Thus, compared with other several genera, the six *Glaucocystis* species examined here would have sufficient genetic distance to be separated into distinct species.

3.4. CONCLUSIONS

Although glaucophyte strains have been considered to include multiple possible cryptic species based on several DNA markers (Chong *et al.* 2014), no species delineation has been established. No ultrastructural difference has been reported within *Glaucocystis*, possibly because conventional EM methods have provided only local information of cells. Alternatively, I performed UHR FE-SEM surface observations, providing global and ultrafine information because it was efficient to unveil peripheral ultrastructure and detailed cell shape to delineate glaucophyte *Cyanophora* species (Chapter 2). Indeed, the present global and ultrafine information by present UHR FE-SEM revealed the two types of cellulose filament arrangements in mother cell wall. UHR FE-SEM, however, was not expected to elucidate the peripheral ultrastructure in *Glaucocystis* as in *Cyanophora* because it do not provide inside information. In this study, I applied comparative 3D UHVEM tomography to taxonomic study of microscopic organisms for the first time. The present 3D UHVEM tomography resolved the native *in situ* peripheral ultrastructures of the protoplasts, even in the presence of a cell wall; besides, it also showed ultrastructural differences between the *Glaucocystis* species (Figures 3.4–3.7). As supported by ultrathin section TEM (Figure 3.9), periphery types of six species were classified into type A, B and C (Figure 3.10).

Based on comparative morphological and molecular examinations, cultured material of the genus *Glaucocystis* was classified into six species: *G. nostochinearum*, *G. oocystiformis G. incrassata, G. geitleri*, *G. miyajii* and *G. bhattacharyae* (Table 3.2). In contrast to previous reports (Schnepf *et al.*, 1966; Schnepf & Brown Jr., 1971), ultrastructural diversity of the protoplast periphery is apparent within the genus

Glaucocystis. Each phylogenetic group (G1–G6), recognised by phylogenetic analyses of Chong *et al.* (2014), corresponded a single species of the present classification (Figure 3.11). Although *G. oocystiformis* has not been reported after its original description, this species exhibited a phylogenetic group in the crown group (Figure 3.11) and was clearly identified by its original description and differed from the other species examined based on the essential differences by LM and EM. By comparative LM of strains, *G. geitleri* and *G. incrassata* were clearly distinguished from *G. nostochinearum* on the basis of their polar cell wall thickenings, their cell size and their autospore numbers within a colony (Table 3.2; Figure 3.2), as previously suggested by Pringsheim (1958) using the original isolates of the new authentic strains of them. Although *G. miyajii* is similar to the type species *G. nostochinearum* by LM, 3D ultrastructural differences clearly distinguished each other (Table 3.2).

The novel strains established by a single field sample were classified into three species within the six species (Table 3.1). Although the type species *G. nostochinearum* has been considered as a cosmopolitan species so far (Prasad, 1961; Prescott, 1962; Starmach, 1966; Compère, 1976; Gordon, 2013), the records may consist of several species that might include more than one species recognised here. The reason why the type species has been described somewhat diverse or confused (Prasad, 1961; Prescott, 1962; Komárek & Fott, 1983) might be ascribable to the mixture of two or more *Glaucocystis* species in a single sample. Establishment, utilisation and maintenance of clonal strains enable comparison by molecular analyses and several microscopy methods between them as in this study.

Since global and ultrafine observations such as 3D UHVEM tomography and UHR FE-SEM surface observations can provide the global information of characters entirely,

these global and ultrafine microscopy will become the mainstream methods to reconstruct the microbial taxonomy unveiling native ultrastructures.

3.5. TAXONOMIC ACCOUNTS[6]

Glaucocystis nostochinearum Itzigs. *ex* Rabenh. (in Alg. Eur. 94–5: no. 1935. 1866).

＝***Glaucocystis nostochinearum*** Itzigs. (1854) *ined., inval.*

＝***Oocystis cyanea*** Nägeli *in litt., inval.*

＝***Cyanocystis itzigsohniana*** Rabenh. *in litt. inval.*

＝***Glaucocystis molochinearum*** Geitler (in Arch. Hydrobiol. 15: 280. 1924) *nom. nud., orth. err.*

Diagnosis:

Coccoid, enclosed by cellulosic cell wall; solitary or colonial generally with four cells. Cells *ca*. 18–23 μm long × 10–15 μm wide, ellipsoidal, lacking polar thickening, polar nodule and equatorial ring in shape. Two vestigial flagella between cell wall and protoplast periphery, positioned at equator of cells. Protoplast periphery, without numerous small depressions arranged regularly. Flattened vesicles leaflet-like, lacking regular bar-like depressions, slightly overlapping one another. Colony, lacking attaching stalk, extended prominently; mother cell wall surface generally with a loose open weave.

Syntypes: Rabenhorst's exsiccate, *Die Algen Europa's* packet no. 1935.

Lectotype (here designated): the permanent slide R1935J! prepared from a syntype of Farlow Herbarium, University of Harvard (FH), deposited in FH.

Syntypic authentic strain: not available.

---

[6]New name, rank, combination and typification proposed or designated here in this thesis are *not* intended to be *effectively published* under the Article 30.8 of International Code of Nomenclature for algae, fungi, and plants (ICN).

Type locality: Berlin, Prussia (now, Germany).

Epitypic authentic strain (here designated): SAG 16.98.

Epitype locality: Lower Saxony, pond in quarry at Walkenried/Harz, surface of *Myriophyllum* sp., Germany.

Glaucocystis oocystiformis Prescott (in Farlowia 1(3): 372. 1944).

= *Glaucocystis caucasica* Tarnogr. (1957; *not seen original*).

Diagnosis:

Coccoid, enclosed by cellulosic cell wall; solitary or colonial generally with four cells. Cells *ca*. 30–40 μm long × 20–30 μm wide, ellipsoidal, sometimes with clear polar nodule, lacking equatorial ring in shape. Two vestigial flagella between cell wall and protoplast periphery, positioned at equator of cells. Protoplast periphery, with numerous small depressions arranged regularly. Depression at intervals of *ca*. 500–800 nm, shared by plasma membrane and centre of underlying flattened vesicle. Flattened vesicles leaflet-like, not overlapping one another. Colony, lacking attaching stalk, extended prominently; mother cell wall surface often with a loose open weave.

Holotype (here designated): Prescott 1944. Farlowia. pl. 4, fig. 20.

Holotypic authentic strain: not available.

Type locality: Trout Lake, Vilas County, Wisconsin, USA.

Type locality of G. caucasica: Caucasus, USSR.

Epitypic authentic strain (here designated): Isolate 126.

Epitype locality: Funabashi-shi, Chiba, Japan (35.694283°N, 140.048166°E).

Glaucocystis incrassata (Lemmerm.) Tos.Takah. **comb. & stat. nov.**

≡***Glaucocystis nostochinearum* var. *incrassata*** Lemmerm. (in Arch. Hydrobiol. Planktonkd. 4: 178. 1908).

≡***Glaucocystis nostochinearum* f. *incrassata*** (Lemmerm.) Starmach (in Fl. Słodw. Pol.: 760. 1966) *nom. nud.*

=***Glaucocystis incrassata*** (Lemmerm.) Lemmerm. *ex* Koch (in Arch. Mikrobiol. 47: 414. 1964) *nom. nud.*

Basionym: ***Glaucocystis nostochinearum* var. *incrassata*** Lemmerm. (in Arch. Hydrobiol. Planktonkd. 4: 178. 1908).

Diagnosis:

Coccoid, enclosed by cellulosic cell wall; solitary or colonial often with four or eight cells. Cells *ca*. 20–30 μm long × 13–23 μm wide, truncate-ellipsoidal, generally with clear polar thickening, lacking polar nodule and equatorial ring in shape. Two vestigial flagella between cell wall and protoplast periphery, positioned at equator of cells. Protoplast periphery, with numerous small depressions arranged regularly. Depression at intervals of *ca*. 200–600 nm, shared by plasma membrane and centre of underlying flattened vesicle. Flattened vesicles leaflet-like, slightly overlapping one another. Colony, lacking attaching stalk, enclosing tightly; mother cell wall fibrils tightly arranged.

Holotype (here designated): Lemmermann, Arch. Hydrobiol. Planktonkd. 4: 178. 1908, Taf. V., fig. 4

Holotypic authentic strain: not available.

Type locality: Lentini, Sicilia, Italia.

Epitypic authentic strain: SAG 229-2.

Epitype locality: Denmark.

Glaucocystis geitleri E.G.Pringsh. *ex* Tos.Takah. **sp. nov.**

≡***Glaucocystis geitleri*** E.G.Pringsh. (in Prad, Stud. Pl. Physiol.: 177–8. 1958) *nom. provis., inval.*

≡***Glaucocystis geitleri*** E.G.Pringsh. *ex* Koch (in Arch. Mikrobiol. 47: 414. 1964) *nom. nud.*

≡***Glaucocystis geitleri*** E.G.Pringsh. *ex* Komárek & Fott (in Chlorophyceae Grünalgen: 554. 1983) *nom. provis., inval.*

=***Glaucocystis nostochinearum*** var. ***geitleri*** Schenk (in ELS: 2, 3, 6. 2001) *nom. nud.*

Diagnosis:

Coccoid, enclosed by cellulosic cell wall; solitary or colonial generally with two cells. Cells *ca*. 30–40 μm long × 20–30 μm wide, truncate-ellipsoidal, sometimes with clear polar thickening, lacking polar nodule and equatorial ring in shape. Two vestigial flagella between cell wall and protoplast periphery, positioned at equator of cells. Protoplast periphery, with numerous small depressions arranged regularly. Depression at intervals of *ca*. 500–800 nm, shared by plasma membrane and centre of underlying flattened vesicle. Flattened vesicles leaflet-like, not overlapping one another. Colony, lacking attaching stalk, extended prominently; mother cell wall surface generally with a loose open weave.

Type locality: Cambridge, England, UK.

Holotypic authentic strain: SAG 229-1.

Glaucocystis miyajii Tos.Takah. **sp. nov.**

Diagnosis:

Coccoid, enclosed by cellulosic cell wall; solitary or colonial generally with four cells. Cells *ca*. 19–24 μm long × 10–15 μm wide, ellipsoidal, lacking polar thickening, polar nodule and equatorial ring in shape. Two vestigial flagella between cell wall and protoplast periphery, positioned at equator of cells. Protoplast periphery, with numerous small depressions arranged regularly. Depression at intervals of *ca*. 200–600 nm, shared by plasma membrane and centre of underlying flattened vesicle. Flattened vesicles leaflet-like, slightly overlapping one another. Colony, lacking attaching stalk, extended prominently; mother cell wall surface often with a loose open weave.

Type locality: Funabashi-shi, Chiba, Japan (35.694283°N, 140.048166°E).

Holotypic authentic strain: Isolate Thu10.

Etymology: Named after Prof. Kazuyuki Miyaji (University of Toho), who contributed much to phycology.

Glaucocystis bhattacharyae Tos.Takah. **sp. nov.**

Diagnosis:

Coccoid, enclosed by cellulosic cell wall; solitary or colonial generally with four cells. Cells *ca*. 17–27 μm long × 12–22 μm wide, truncate-ellipsoidal, lacking polar thickening, polar nodule and equatorial ring in shape. Two vestigial flagella between cell wall and protoplast periphery, positioned at equator of cells. Protoplast periphery, with numerous small depressions arranged regularly. Depression at intervals of *ca*. 200–600 nm, shared by plasma membrane and centre of underlying flattened vesicle. Flattened vesicles leaflet-like, slightly overlapping one another. Colony, lacking attaching stalk, enclosing tightly; mother cell wall fibrils tightly arranged.

Type locality: Funabashi-shi, Chiba, Japan (35.694283°N, 140.048166°E).

Holotypic authentic strain: Isolate 118.

Etymology: Named after Prof. Debashish Bhattacharya (Rutgers University), who contributed much to phycology.

3.6. KEY TO SPECIES OF *GLAUCOCYSTIS*[7]

A. Colony with stalks ----------B.

A. Colony without stalks ----------C.

B. Cell shape ellipsoidal ---------- *G. indica* R.J.Patel (1981)[8]

B. Cell shape kidney-shaped ----------

---------- *G. reniformis* B.N.Prasad, R.K.Mehrotra & P.K.Misra (1984)[9]

C. Cell wall with equatorial ring---------- *G. cingulata* Bohlin (1897)[10]

C. Cell wall without equatorial ring----------D.

D. Cell shape spherical----------*G. duplex* Prescott (1944)[11]

D. Cell shape ellipsoidal ----------E.

E. Cell wall with polar nodules ----------*G. oocystiformis* Prescott (1944)

E. Cell wall without polar nodules ---------- F.

---

[7] Based on the present study, Komárek & Fott (1983), Starmach (1966) and Prescott (1962). Although "*Glaucocystis simplex* Tarnogr. (1959 with Russian description and an illustration)" (Table 1.1) has been treated as a validly published name for a doubtful *Glaucocystis* species by Komárek & Fott (1983) and Kies & Kremer (1986), the name was not validly published under Article 44. 1 of ICN because of lack of Latin description. Thus, I did not include the alga here.

[8] According to Patel (1981).

[9] According to Prasad *et al.* (1984) and Chatterjee & Keshri (2005).

[10] According to Bohlin (1897), Skuja (1949), Philipose (1967) and Patel & Isabella George (1979).

[11] According to Prescott (1944, 1962), Patel & Isabella George (1979) and Chatterjee & Keshri (2005).

F. Cell wall with polar thickenings ----------G.

F. Cell wall without polar thickenings ----------H.

G. Mother cell wall extended, cell size 30–50 × 19–30 μm, grooves at intervals of 500–800 nm, vesicles not overlapping ---------- *G. geitleri* E.G.Pringsh. *ex* Tos.Takah. sp. nov.

G. Mother cell wall not extended, cell size 22–32 × 15–24 μm, grooves at intervals of 200–600 nm, vesicles frequently overlapping ---------- *G. incrassata* (Lemmerm.) Tos.Takah. comb. & stat. nov.

H. Cell size small (10–18 × 6–10 μm) ---------- *G. bullosa* (1836) Wille (1919)[12]

H. Cell size not small (18–27 × 10–22 μm) ----------I.

I. Polar shape truncate, mother cell wall enclosing tightly ---------- *G. bhattacharyae* Tos.Takah. sp. nov.

I. Polar shape not truncate, mother cell wall extended----------J.

J. Grooves at cell periphery present, vesicles frequently overlapping ---------- *G. miyajii* Tos.Takah. sp. nov.

J. Grooves at cell periphery absent, vesicles frequently overlapping ---------- *G. nostochinearum* Itzigs. *ex* Rabenh. (1866)

[12] According to Kützing (1836), Hansgirg (1892) and Wille (1919).

3.7. TABLES AND FIGURES

Table 3.1. Species and strains of *Glaucocystis* and other glaucophytes used in this study.

Species	Strain designation	Origin of strain	Locality	GenBank accession number		
				psaB	*psbA*	ITS1-5.8S *r*DNA-ITS2
Glaucocystis nostochinearum	SAG[a] 16.98 (new epitypic authentic strain)	Pond in quarry at surface of *Myriophyllum* sp.[a]	Walkenried/Harz, Lower Saxony, Germany (51°35'33.5"N 10°36'10.0"E)[a]	*AB973457*	KF631337	*LC120721*
	SAG 45.88	Pool at Voslapp, desalted sand from Jade River[a]	Voslapp, Wilhelmshaven, Germany (53°35'24.6"N 8°06'29.0"E)[a]	*LC120666*	KF631335	*LC120722*
Glaucocystis miyajii	Thu10[b] (new holotypic authentic strain)	Freshwater sample from a pond[c]	Miyama, Funabashi-shi, Chiba, Japan, in 3 July 2012 (35°41'43.3"N 140°02'53.8"E)	*LC120667*	*LC120683*	*LC120723*
	NIES[d]-1961	Freshwater[d]	Kofutamata-machi, Kanazawa-shi, Ishikawa, Japan[d]	*LC120668*	KF631333	*LC120724*
Glaucocystis bhattacharyae	118[b] (new holotypic authentic strain)	Freshwater sample from a pond[c]	Miyama, Funabashi-shi, Chiba, Japan, in 3 July 2012 (35°41'43.3"N 140°02'53.8"E)	*LC120669*	*LC120684*	*LC120725*
	SAG 27.80	Freshwater[a]	France[a]	*LC120670*	KF631328	*LC120726*
Glaucocystis incrassata	SAG 229-2 (new epitypic authentic strain)	Freshwater[a]	Denmark[a]	*LC120671*	KF631325	*LC120727*
Glaucocystis geitleri	SAG 229-1 (new holotypic authentic strain) (=NIES-2141)	Freshwater[a]	Cambridge, England, UK (52°11'32.5"N 0°09'48.2"E)[a,d]	*AB973458*	*LC120685*	*LC120728*
				LC120672		*LC120731*
	SAG 229-3	Freshwater[a]	ND[a]	*LC120673*	KF631327	*LC120729*
	SAG 28.80	Freshwater[a]	ND[a]	*LC120674*	KF631326	*LC120730*

Table 3.1. Continued.

Glaucocystis oocystiformis	126[b] (new epitypic authentic strain)	Freshwater sample from a pond[c]	Miyama, Funabashi-shi, Chiba, Japan, in 3 July 2012 (35°41'43.3"N 140°02'53.8"E)	*LC120675*	*LC120686*	*LC120718*
	NIES-1369	Freshwater[d]	Kakuma-machi, Kanazawa-shi, Ishikawa, Japan[d]	*LC120676*	KF631330	*LC120719*
	NIES-966	Freshwater from Renge-numa[d]	Kitashiobara-mura, Yama-gun, Fukushima, Japan[d]	*LC120677*	KF631329	*LC120720*
Cyanophora paradoxa[f]	CCAP[e] 981/1[f] (authentic strain)			*AB973446*	*LC120678*	*AB973918*
Cyanophora sudae[f]	NIES-764[f] (authentic strain)			*AB973453*	KF631321	*AB973925*
"Gloeochaete wittrockiana"	SAG 46.84			*AB973454*	KF631340	*LC120715*
"Cyanoptyche gloeocystis"	SAG 34.90			*AB973456*	KF631339	*LC120717*

Accession numbers in italics type indicate sequences determined by this work.

[a] Sammlung von Algenkulturen der Universität Göttingen (SAG, http://sagdb.uni-goettingen.de/; Schlösser, 1994).

[b] Newly isolated in this study.

[c] From this sample, 16 clonal isolates were established using the pipette-washing method. Based on the *psaB* and nuclear ITS1-5.8S *r*DNA-ITS2 sequences, these new cultures were divided into three genetic groups: 118 group (118, 115, 116, 119, 123, 131); 126 group (126, 134, 121, 124, 125, 128, 127, 130, Thu9) and Thu10 group (Thu10). Therefore, from each group, only a single isolate was chosen and used for this study.

[d] National Institute for Environmental Studies (NIES, http://mcc.nies.go.jp/; Kasai *et al.* 2009).

[e] Culture Collection of Algae and Protozoa (CCAP, http://www.ccap.ac.uk/).

[f] For details of the strains and species information, see Chapter 2; Table 2.1.

Table 3.2. Comparison of the morphological characteristics of *Glaucocystis* species.

Species	*G. oocystiformis* Prescott	*G. geitleri* sp. nov.	*G. incrassata* comb. & stat. nov.	*G. bhattacharyae* sp. nov.	*G. miyajii* sp. nov.	*G. nostochinearum* Rabenh.
Mother cell wall extension	prominent	prominent	not prominent	not prominent	not prominent	not prominent
Gauze fabric-like appearance of mother cell wall	present	present	absent	absent	present	present
Formation of colony stalks	absent	absent	absent	absent	absent	absent
Cell numbers within a colony	2–4, generally 4	2–4, generally 2	4–8, generally 4	1–4, generally 4	2–4, generally 4	2–4, generally 4
Cell size	*ca*. 15–25 µm wide × *ca*. 25–35 µm long	*ca*. 20–30 µm wide × *ca*. 30–40 µm long	*ca*. 13–23 µm wide × *ca*. 20–30 µm long	*ca*. 12–22 µm wide × *ca*. 17–27 µm long	*ca*. 10–15 µm wide × *ca*. 19–24 µm long	*ca*. 10–15 µm wide × *ca*. 18–23 µm long
Cell and polar shape	ellipsoidal sometimes with polar nodules	truncate-ellipsoidal sometimes with polar thickenings	truncate-ellipsoidal often with polar thickenings	truncate-ellipsoidal without polar thickenings	ellipsoidal	ellipsoidal
Equatorial ring	absent	absent	absent	absent	absent	absent
Cell wall thickness	*ca*. 150–350 nm	*ca*. 300–500 nm	*ca*. 100–300 nm	*ca*. 150–350 nm	*ca*. 150–350 nm	*ca*. 100–300 nm
Regular groove	present	present	present	present	present	absent
Groove interval	*ca*. 500–800 nm	*ca*. 500–800 nm	*ca*. 200–600 nm	*ca*. 200–600 nm	*ca*. 200–600 nm	ND
Vesicle frequent overlapping	present	present	absent	absent	absent	present
Authentic strains	126	SAG 229-1	SAG 229-2	118	Thu10	SAG 16.98
Other strains examined	NIES-1369, NIES-966	SAG 229-3, SAG 28.80		SAG 27.80	NIES-1961	SAG 45.88
Based on	present study	present study	present study	present study	present study	present study

Table 3.2. Extended.

Species	*G. bullosa* Wille	*G. indica* R.J.Patel	*G. reniformis* B.N.Prasad *et al.*	*G. cingulata* Bohlin	*G. duplex* Prescott
Mother cell wall extension	ND	prominent	prominent	prominent	prominent
Gauze fabric-like appearance of mother cell wall	ND	ND	ND	ND	ND
Formation of colony stalks	absent	present	present	absent	absent
Cell numbers within a colony	3–8	2–8	2–4, generally 2	2–8	8–16
Cell size	*ca*. 6–10 µm wide × *ca*. 10–18 µm long	*ca*. 9–18 µm wide × *ca*. 18–31 µm long	*ca*. 15–18 µm wide × *ca*. 24–29 µm long	*ca*. 12–68 µm wide × *ca*. 16–68 µm long	*ca*. 40–44 µm wide × *ca*. 40–44 µm long
Cell and polar shape	ellipsoidal	ellipsoidal	kidney-shaped	ellipsoidal to spherical	spherical
Equatorial ring	absent	absent	absent	present	absent
Cell wall thickness	ND	ND	ND	ND	ND
Regular groove	ND	ND	ND	ND	ND
Groove interval	ND	ND	ND	ND	ND
Vesicle frequent overlapping	ND	ND	ND	ND	ND
Authentic strains	not available	not available	not available	not available	not available
Other strains examined	not available	not available	not available	not available	not available
Based on	original description	original description	original description	original description, Komárek & Fott (1983)	original description, Komárek & Fott (1983)

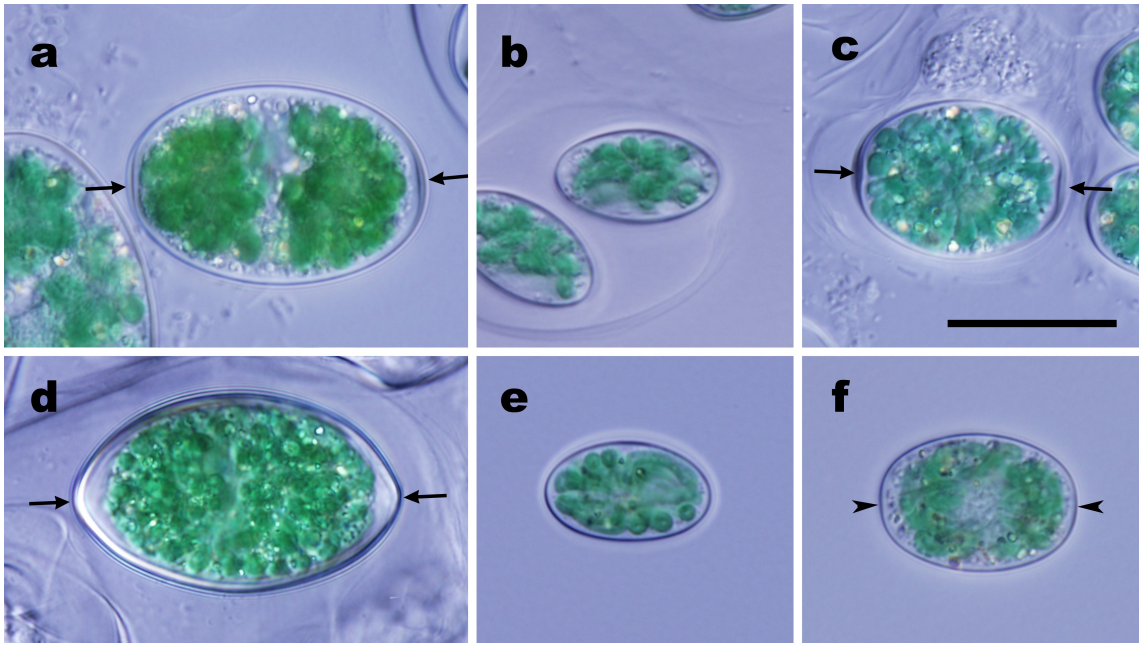

Figure 3.1. Differential interference contrast microscopy of vegetative cells of six species of the *Glaucocystis*.

Shown at the same magnification. Scale bar, 20 µm. Note that immobile vegetative cells are enclosed by a cell wall. (a) *G. geitleri* E.G.Pringsh. *ex* Tos.Takah. sp. nov. strain SAG 229-1, showing polar thickenings (arrows). (b) *G. nostochinearum* Itzigs. *ex* Rabenh. strain SAG 16.98. (c) *G. incrassata* (Lemmerm.) Tos.Takah. comb. & stat. nov. strain SAG 229-2, showing polar thickenings (arrows). (d) *G. oocystiformis* Prescott strain 126, showing polar nodules (arrows). (e) *G. miyajii* Tos.Takah. sp. nov. strain Thu10. (f) *G. bhattacharyae* Tos.Takah. sp. nov. strain 118, showing truncate cell shape (arrowheads).

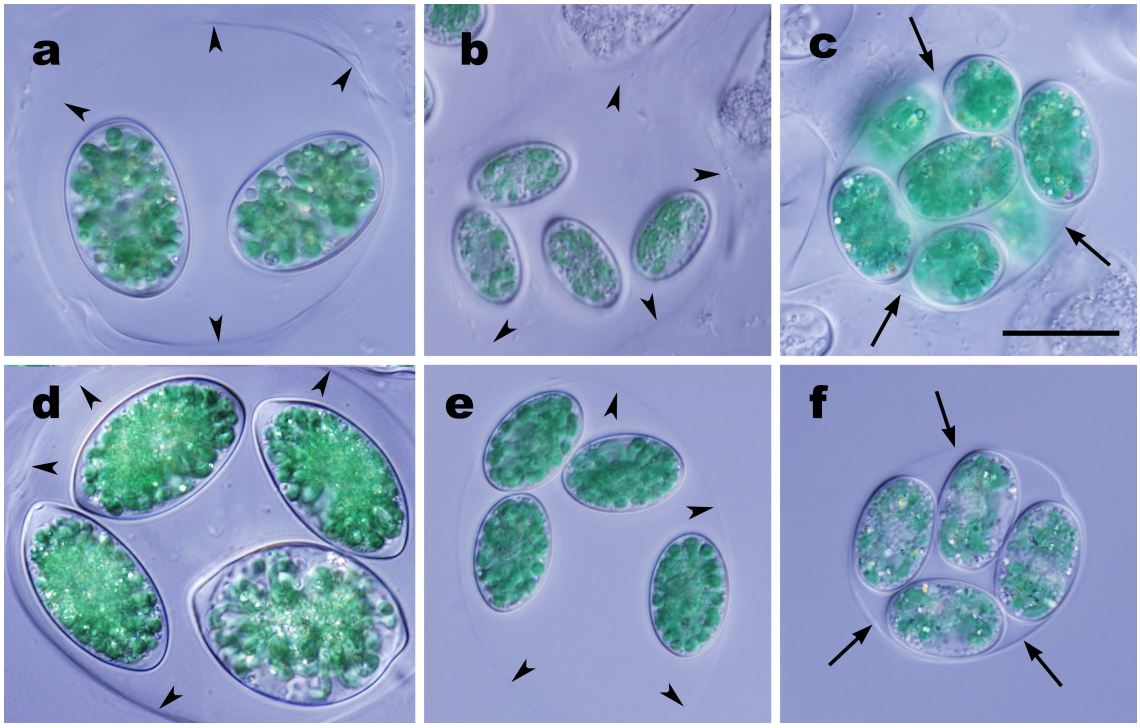

Figure 3.2. Differential interference contrast microscopy of colony of six species of the *Glaucocystis*.

Shown at the same magnification. Scale bar, 20 µm. Note that the each colony is enclosed by mother cell wall (arrows) tightly (c, f) or arranged separately to form spaces between each other within extended mother cell wall (arrowheads) (a, b, d and e). (a) *G. geitleri* E.G.Pringsh. *ex* Tos.Takah. sp. nov. strain SAG 229-1. (b) *G. nostochinearum* Itzigs. *ex* Rabenh. strain SAG 16.98. (c) *G. incrassata* (Lemmerm.) Tos.Takah. comb. & stat. nov. strain SAG 229-2. (d) *G. oocystiformis* Prescott strain 126. (e) *G. miyajii* Tos.Takah. sp. nov. strain Thu10. (f) *G. bhattacharyae* Tos.Takah. sp. nov. strain 118.

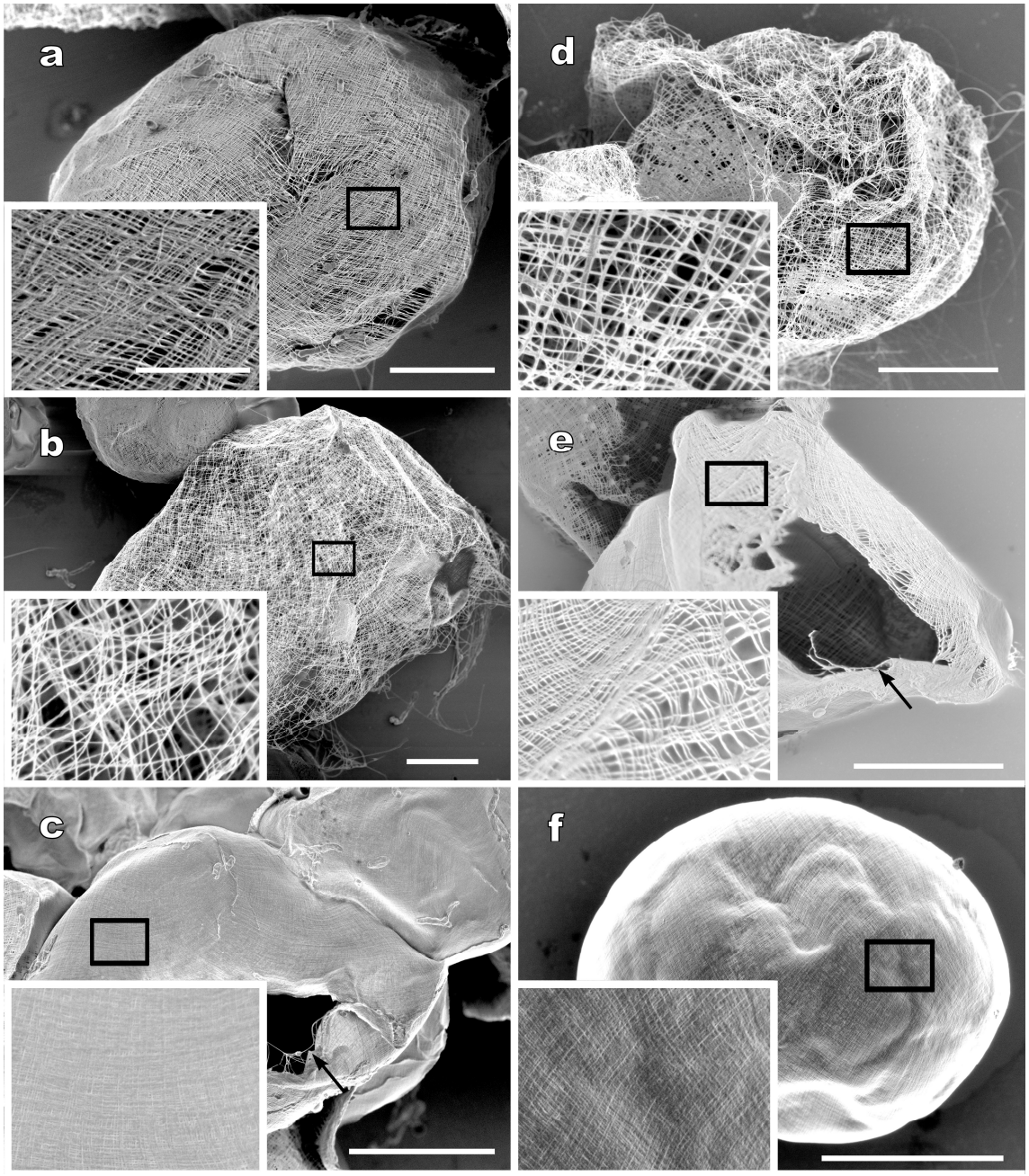

Figure 3.3. Field-emission scanning electron microscopy of colony of six species of the *Glaucocystis.*

Insets show higher magnification image of the a mother cell wall surface (boxed area) at the same magnification. Scale bar, 10 μm and 2 μm (insets). Note that the each colony is enclosed by a mother cell wall, showing gauze fabric-like fibrils globally with a loose open weave (a, b, d and e) or tightly arranged fabric-like fibrils (c, f). (a) *G. geitleri* E.G.Pringsh. *ex* Tos.Takah. sp. nov. strain SAG 229-1. (b) *G. nostochinearum* Itzigs. *ex* Rabenh. strain SAG 16.98. (c) *G. incrassata* (Lemmerm.) Tos.Takah. comb. & stat. nov. strain SAG 229-2, showing inside daughter cell at partly pierced mother cell wall (arrow). (d) *G. oocystiformis* Prescott strain 126. (e) *G. miyajii* Tos.Takah. sp. nov. strain Thu10. (f) *G. bhattacharyae* Tos.Takah. sp. nov. strain 118.

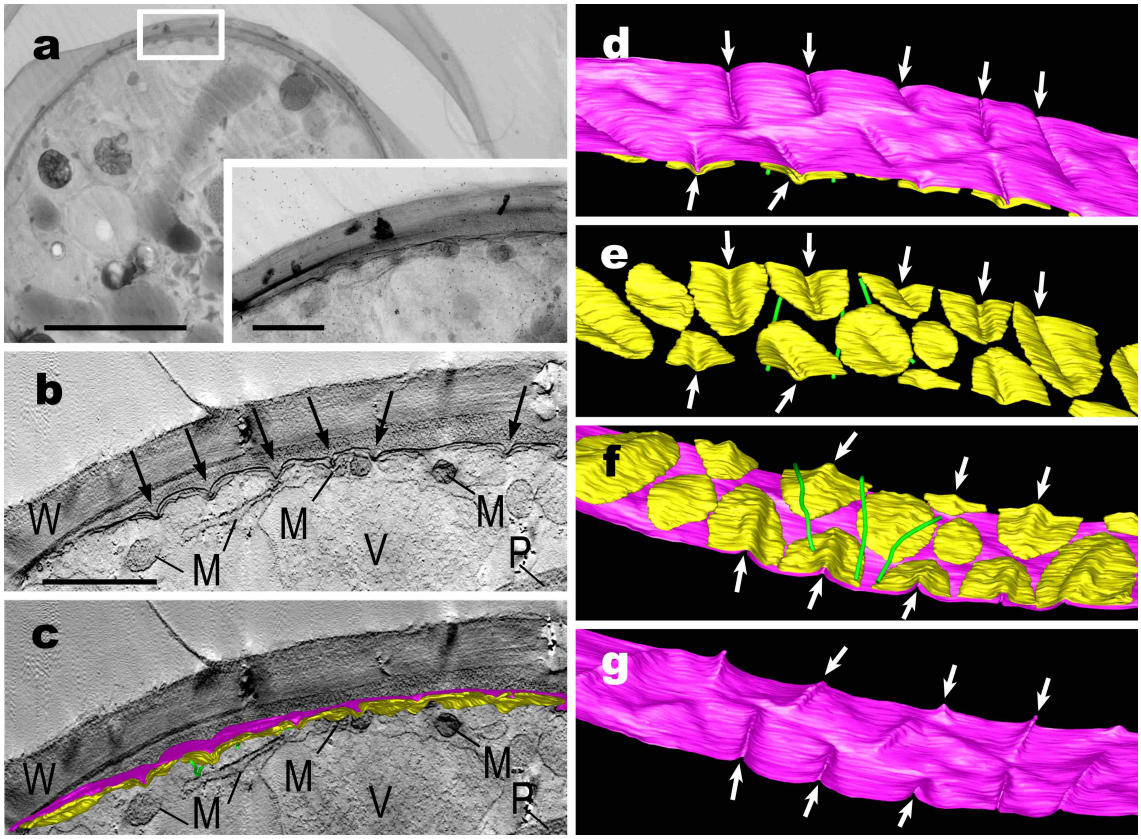

Figure 3.4. Electron tomography and 3D-modelling of protoplast periphery of *Glaucocystis geitleri* sp. nov. SAG 229-1 vegetative cell.

Note that this species exhibits periphery type A (Figure 3.10). (a) Ultra-high voltage electron microscopic image. Inset shows higher magnification image of the cell periphery (boxed area). Scale bar, 5 μm and 1 μm (inset). (b) Tomographic image of boxed area in (a). Note that plasma membrane is grooved deeply at regular intervals (arrows). Scale bar, 1 μm. M, mitochondrion; P, plastid; V, vacuole; W, cell wall. (c–g) 3D images showing distribution of plasma membrane (magenta), and underlying flattened vesicles (yellow) associated with microtubules (green) on cytoplasmic side. Not to scale. Arrows indicate that each bar-like groove of plasma membrane is covered by invagination of flattened vesicle. (c) View with a tomographic image. For abbreviations of organelles, see (b). (d, e) View from cell wall side. (f, g) View from cytoplasmic side.

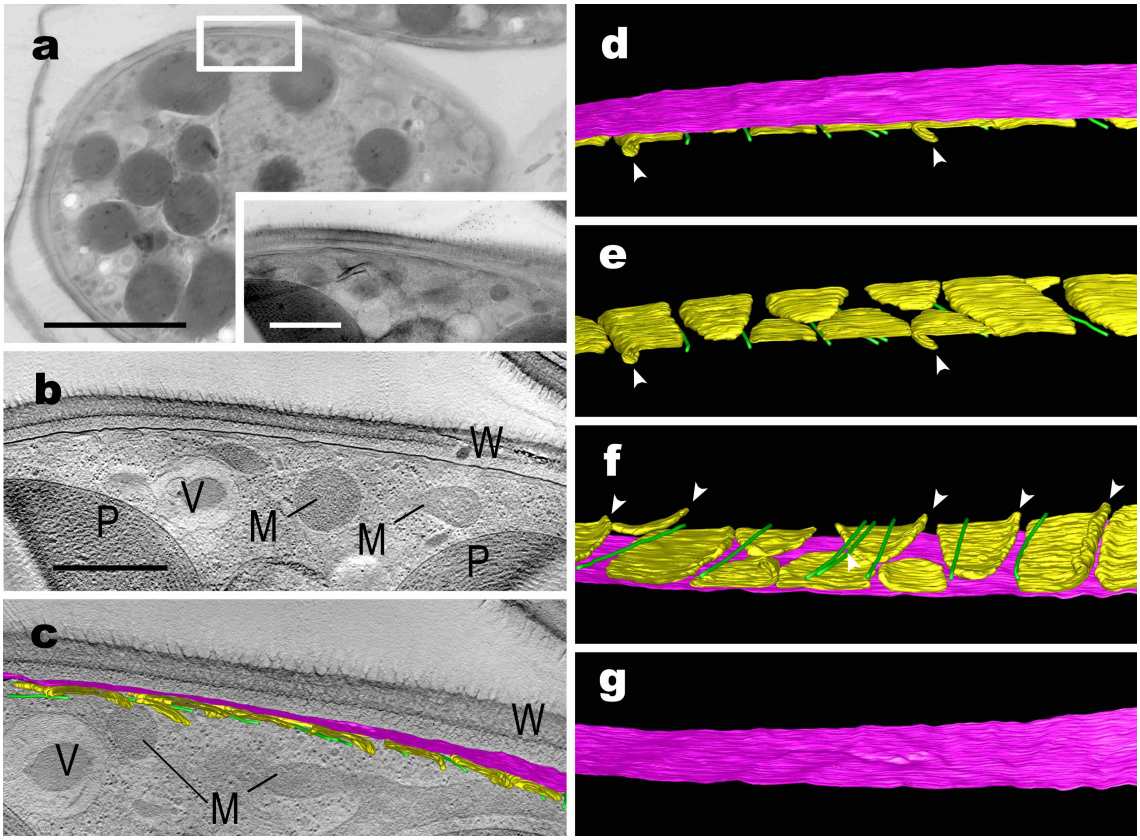

Figure 3.5. Electron tomography and 3D-modelling of protoplast periphery of *Glaucocystis nostochinearum* SAG 16.98 vegetative cell.

Note that this species exhibits periphery type B (Figure 3.10). (a) Ultra-high voltage electron microscopic image. Inset shows higher magnification image of the cell periphery (boxed area). Scale bar, 5 μm and 1 μm (inset). (b) Tomographic image of boxed area in (a). Note that the plasma membrane lacks deep grooves at section. Scale bar, 1 μm. M, mitochondrion; P, plastid; V, vacuole; W, cell wall. (c–g) 3D images showing distribution of plasma membrane (magenta), and underlying flattened vesicles (yellow) associated with microtubules (green) on cytoplasmic side. Not to scale. Note that plasma membrane and flattened vesicles exhibit almost smooth surfaces. Arrowheads indicate slight overlapping of neighbouring flattened vesicles. (c) View with a tomographic image. (d, e) View from the cell wall side. (f, g) View from the cytoplasmic side.

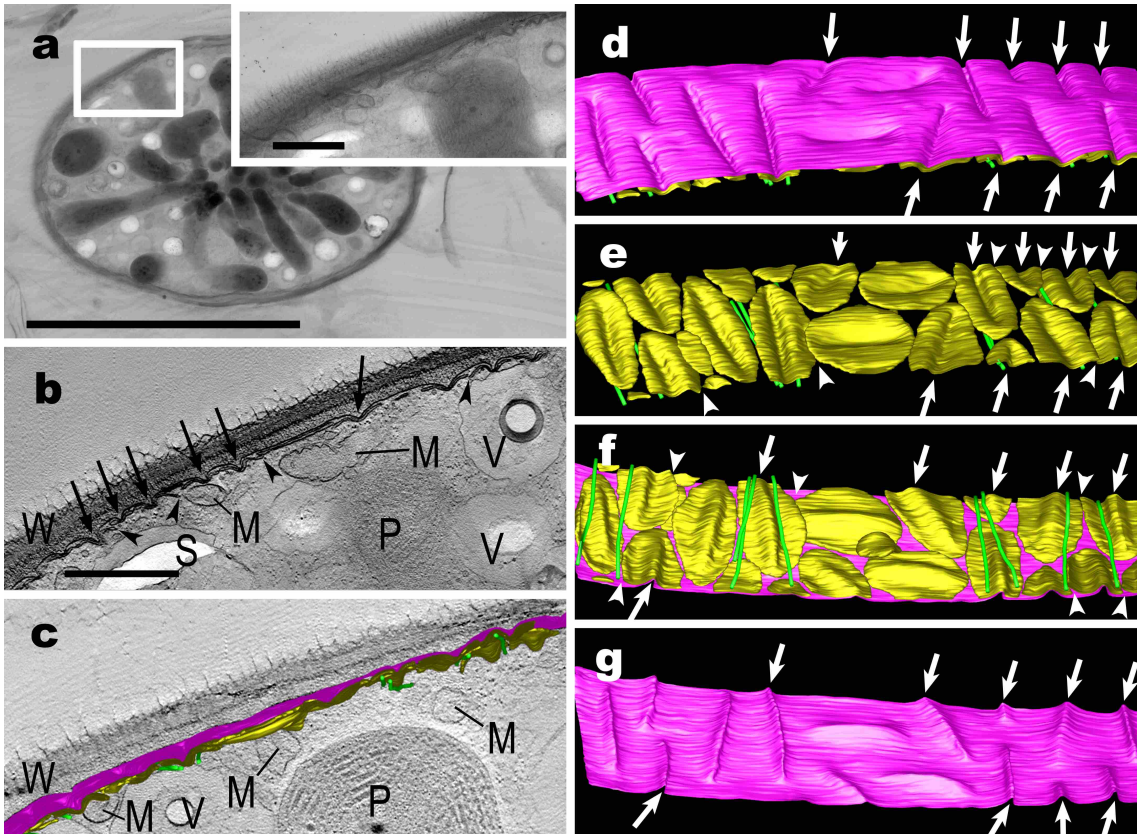

Figure 3.6. Electron tomography and 3D-modelling of protoplast periphery of *Glaucocystis incrassata* comb. & stat. nov. SAG 229-2 vegetative cell.

Note that this species exhibits periphery type C (Figure 3.10). (a) Ultra-high voltage electron microscopic image. Inset shows higher magnification image of the cell periphery (boxed area). Scale bar, 5 µm and 1 µm (inset). (b) Tomographic image of boxed area in (a). Note that plasma membrane is grooved deeply at regular intervals (arrows). Scale bar, 1 µm. M, mitochondrion; P, plastid; V, vacuole; W, cell wall. (c–g) 3D images showing distribution of plasma membrane (magenta), and underlying flattened vesicles (yellow) associated with microtubules (green) on cytoplasmic side. Not to scale. Arrows indicate that each bar-like groove of plasma membrane is covered by invagination of flattened vesicle. Arrowheads indicate slight overlapping of neighbouring flattened vesicles. (c) View with a tomographic image. For abbreviations of organelles, see (b). (d, e) View from cell wall side. (f, g) View from cytoplasmic side.

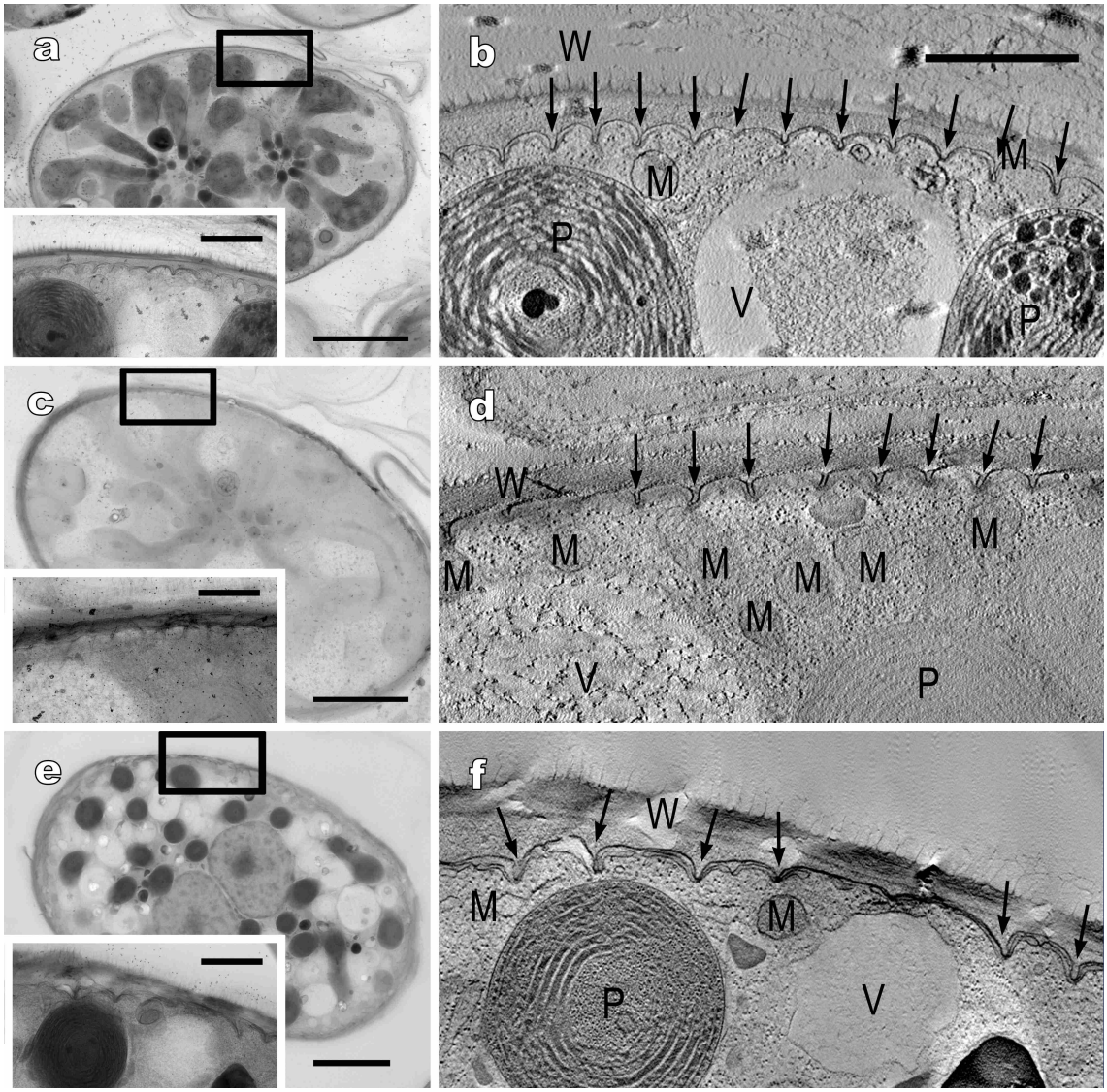

Figure 3.7. Electron tomography of protoplast periphery of vegetative cells of *Glaucocystis oocystiformis* strain 126 (a, b), *G. miyajii* sp. nov. strain Thu10 (c, d) and *G. bhattacharyae* sp. nov. strain 118 (e, f).

Note that *G. oocystiformis* exhibits periphery type A (Figure 3.10) whereas *G. miyajii* and *G. bhattacharyae* exhibit periphery type C (Figure 3.10). (a, c, e) Ultra-high voltage electron microscopic images. Insets show higher magnification image of the cell periphery (boxed area) at the same magnification. Scale bar, 5 μm and 1 μm (insets). (b, d, f) Tomographic images of boxed area in (a, c, e), respectively. Shown at the same magnification. Scale bar, 1 μm. M, mitochondrion; P, plastid; V, vacuole; W, cell wall.

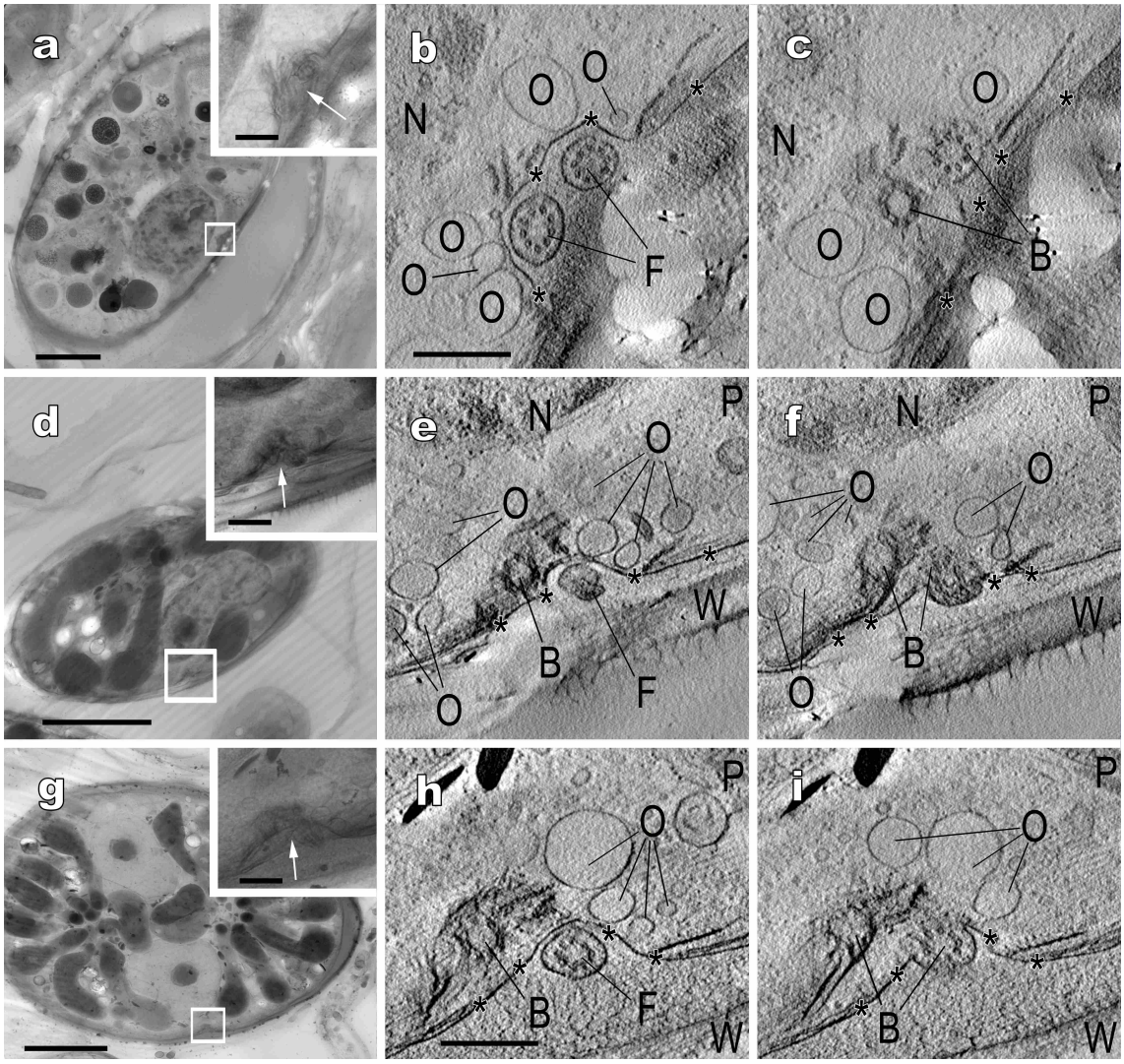

Figure 3.8. Electron tomography of the cell periphery near basal bodies of *Glaucocystis geitleri* sp. nov. SAG 229-1 (a–c), *G. nostochinearum* SAG 16.98 (d–f) and *G. incrassata* comb. & stat. nov. SAG 229-2 (g–i).

(a, d, g) Ultra-high voltage electron microscopic images of vegetative cells. Insets show higher magnification images in boxed area at the same magnification. Scale bar, 5 μm and 500 nm (insets). (b, c, e, f, h, i) Tomographic images of boxed area in (a, d, g), showing portions of cell periphery near basal bodies and vestigial flagella. Shown at the same magnification. Note that the cell periphery in these areas is composed of plasma membrane (asterisks) and ovoid-to-spherical vesicles surrounding basal bodies. Scale bar, 500 nm. B, basal body; F, vestigial flagellum; N, nucleus; O, ovoid-to-spherical vesicle; P, plastid; T, microtubule; W, cell wall.

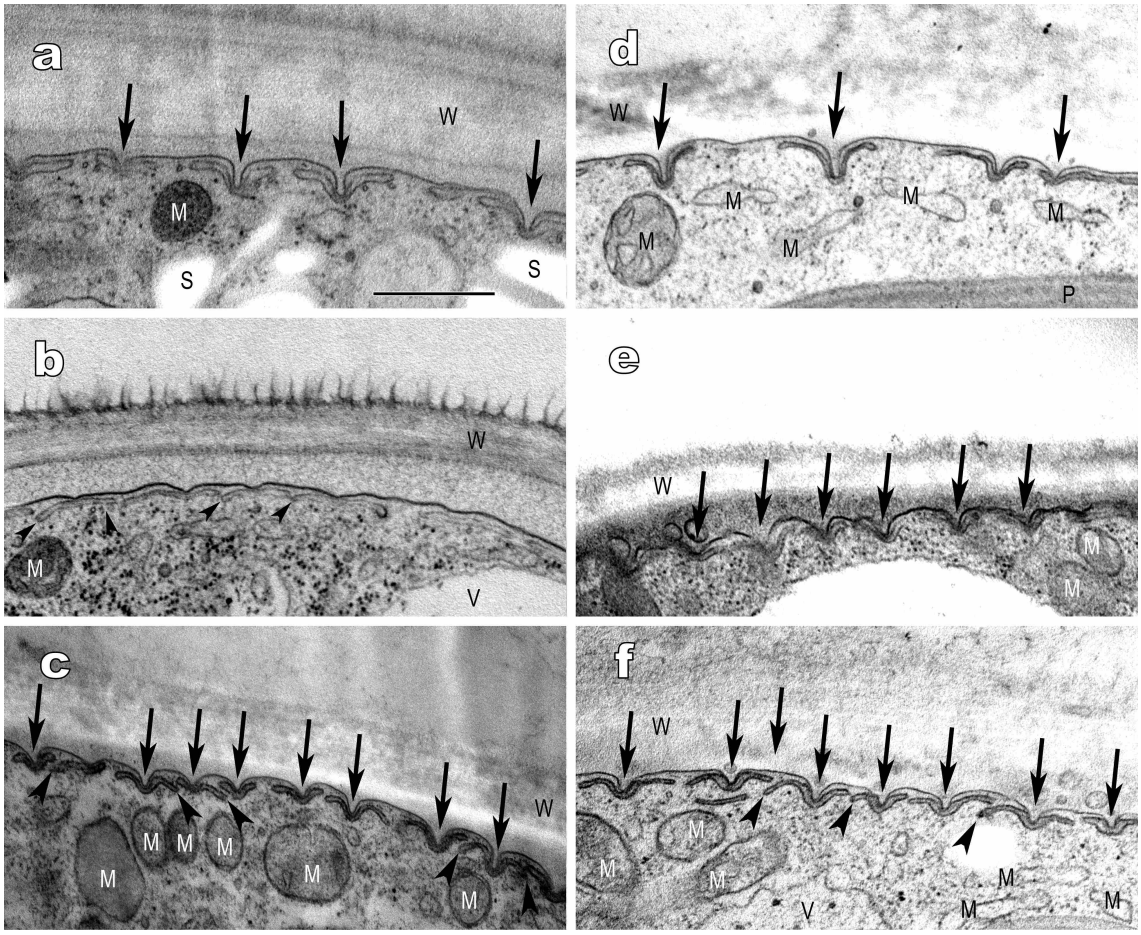

Figure 3.9. Ultrathin section transmission electron microscopy of six *Glaucocystis* species.

Shown at the same magnification. M, mitochondrion; S, starch; V, vacuole; W, cell wall. Scale bar, 500 nm. Note that the cell periphery consists of plasma membrane and underlying flattened vesicles lacking plate-like structure inside. (a) *G. geitleri* E.G.Pringsh. *ex* Tos.Takah. sp. nov. strain SAG 229-1, showing periphery type A (Figure 3.10). Note that both plasma membrane and underlying flattened vesicles are deeply grooved (black arrows). (b) *G. nostochinearum* Itzigs. *ex* Rabenh. strain SAG 16.98, showing periphery type B (Figure 3.10). Note that the plasma membrane lacks deep grooves and that the vesicles are slightly overlapping with one another (arrowheads). (c) *G. incrassata* (Lemmerm.) Tos.Takah. comb. & stat. nov. strain SAG 229-2, showing periphery type C (Figure 3.10). Note that the cell periphery consists of plasma membrane and underlying flattened vesicles both of which are deeply grooved (black arrows) and that the vesicles slightly overlap one another (arrowheads). (d) *G. oocystiformis* Prescott strain 126, showing periphery type A. (e) *G. miyajii* Tos.Takah. sp. nov. strain Thu10, showing periphery type C. (f) *G. bhattacharyae* Tos.Takah. sp. nov. strain 118, showing periphery type C.

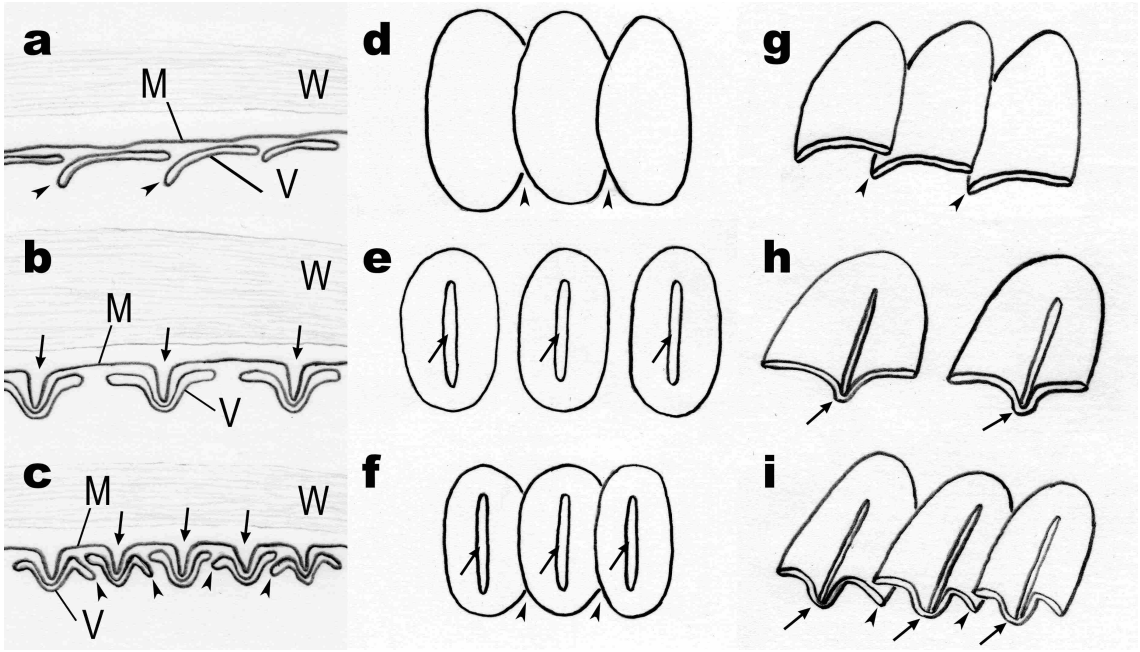

Figure 3.10. Diagrams of three types of the protoplast periphery in *Glaucocystis* species.

(a–c) Sectional views of protoplast periphery. M, plasma membrane; V, flattened vesicles; W, cell wall. (d–f) Surficial views of flattened vesicles. (g–i) 3D arrangements of flattened vesicles. (a, d, g) Periphery type B observed in *G. nostochinearum* Itzigs. *ex* Rabenh. Note that the flattened vesicles underneath the plasma membrane often overlap one another (arrowheads) and that the plasma membrane and flattened vesicles are almost smooth or flat, lacking grooves or invaginations. (b, e, h) Periphery type A observed in *G. geitleri* E.G.Pringsh. *ex* Tos.Takah. sp. nov. and *G. oocystiformis* Prescott. Note that the flattened vesicles are almost separated from one another and that the plasma membrane and the underlying flattened vesicles exhibit numerous bar-like grooves and invaginations (arrows) at longer intervals of 500–800 nm. (c, f, i) Periphery type C observed in *G. incrassata* (Lemmerm.) Tos.Takah. comb. & stat. nov., *G. miyajii* Tos.Takah. sp. nov. and *G. bhattacharyae* Tos.Takah. sp. nov. Note that the flattened vesicles often overlap one another (arrowheads) and that the plasma membrane and the underlying flattened vesicles exhibit numerous bar-like grooves and invaginations (arrows) at shorter intervals of 200–600 nm.

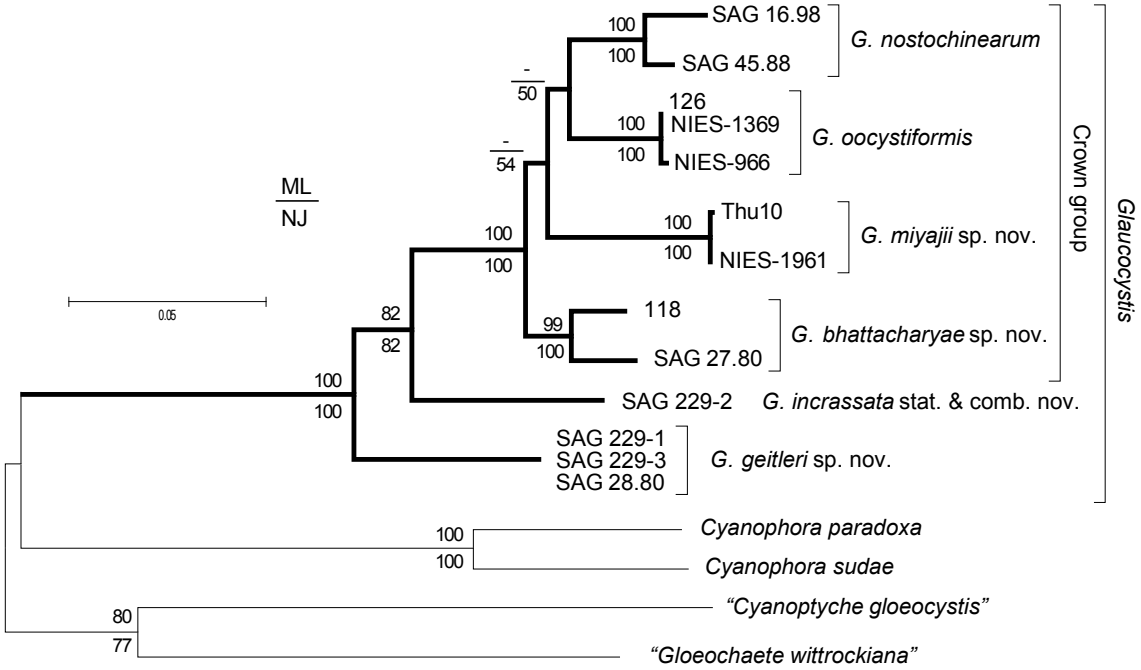

Figure 3.11. Maximum likelihood (ML) tree based on concatenated analyses of 1,461 and 750 base pairs of the coding regions of the plastid *psaB* and *psbA* genes, respectively, from 13 strains of six *Glaucocystis* species and four strains of other glaucophyte genera (Table 3.1).

Branch lengths are proportional to the genetic distances, which are indicated by the scale bar above the tree. Numbers above branches represent ≥50% bootstrap values (based on 1,000 replications) of the ML analyses and below branches are ≥50% bootstrap values (based on 1,000 replications) of neighbour-joining (NJ). For details of the phylogenetic methods, see Subsection 3.2.5.

a

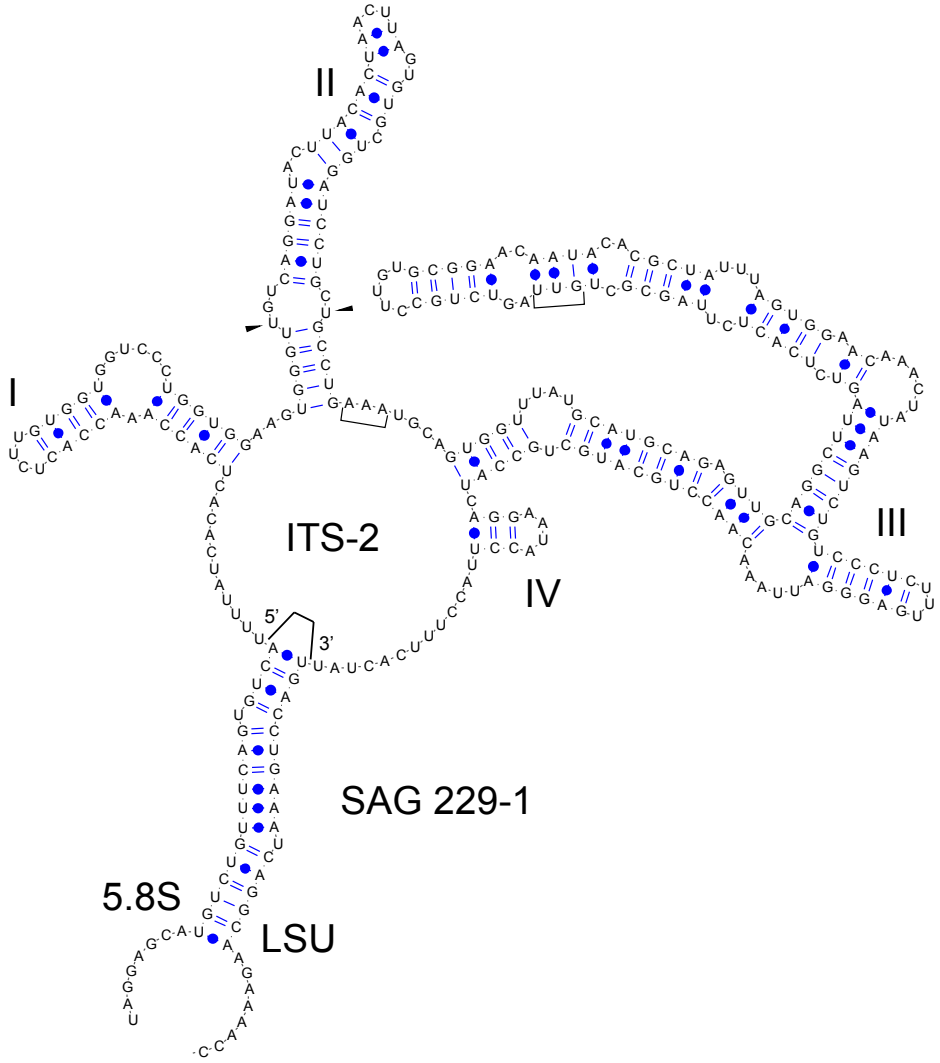

b

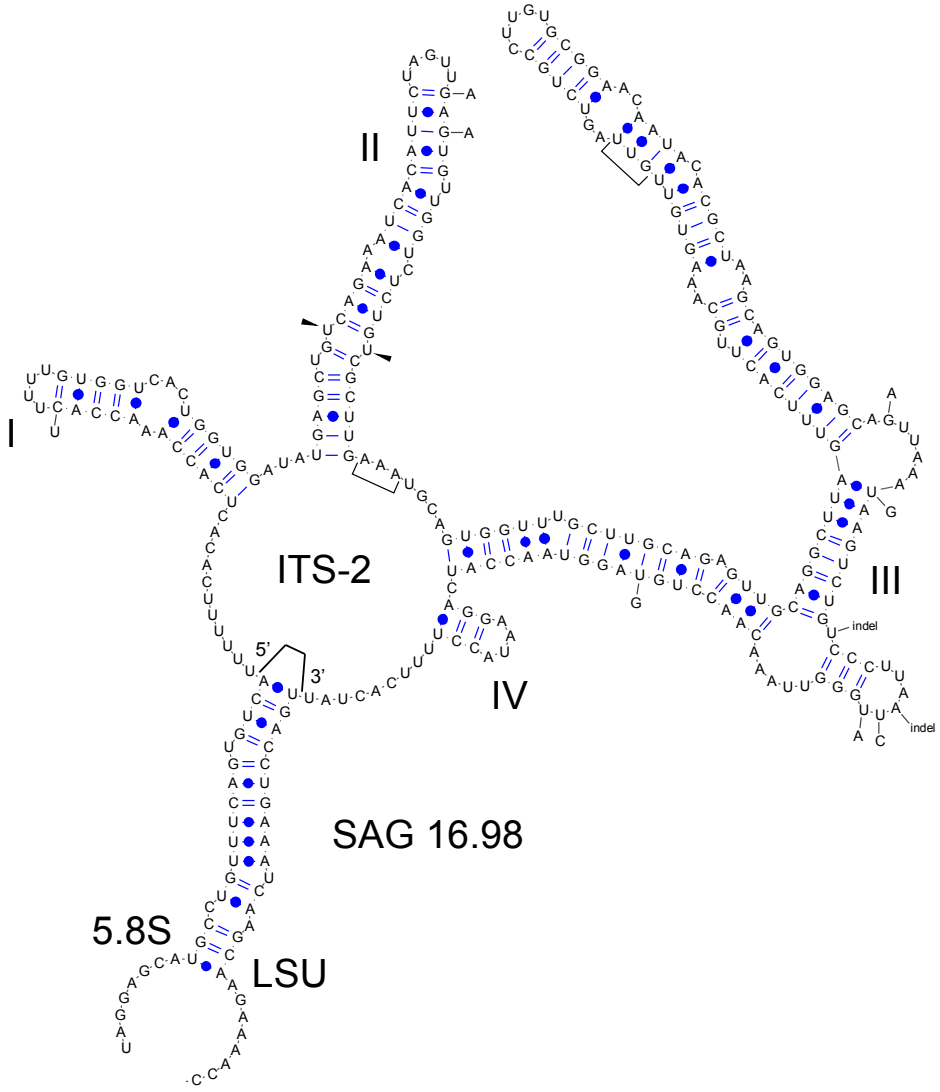

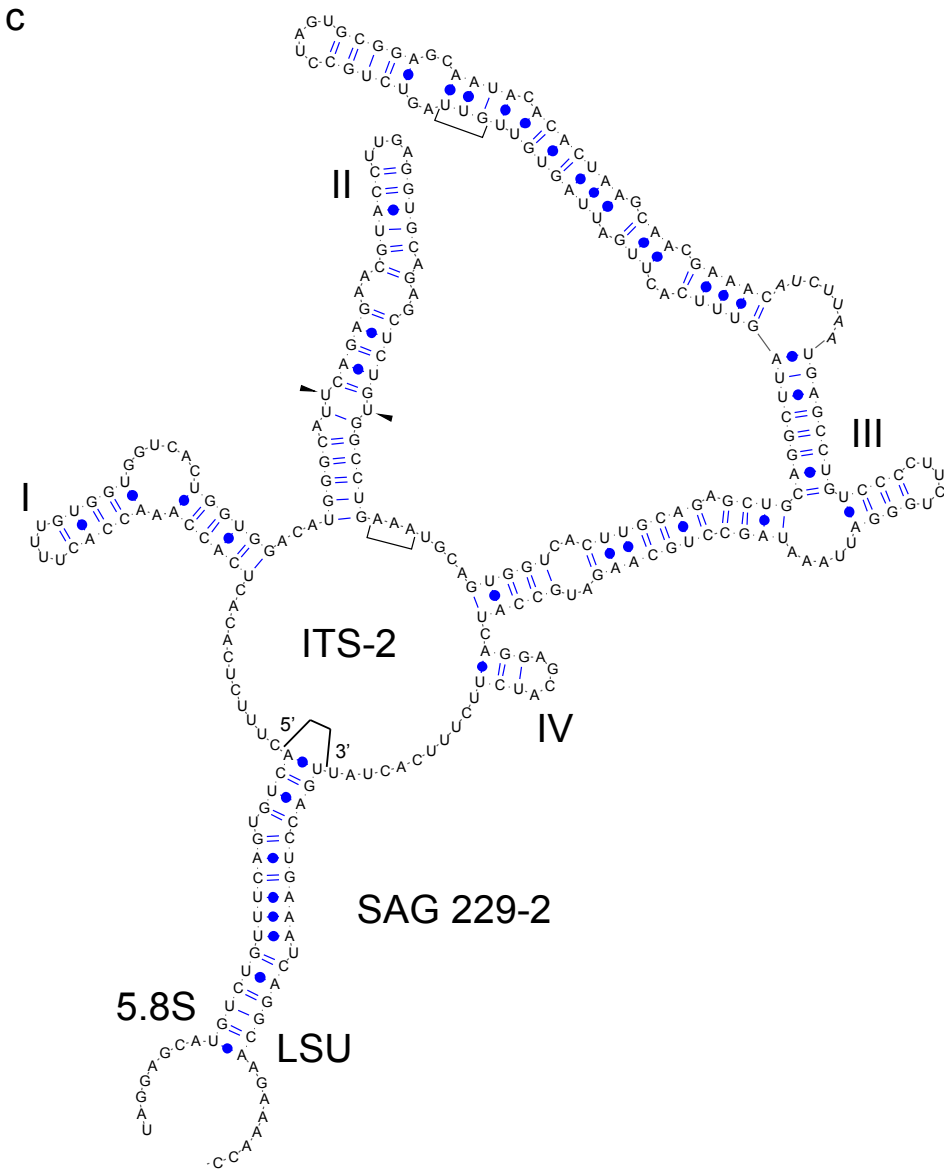
c
I
II
III
IV
ITS-2
SAG 229-2
5.8S
LSU
5'
3'

d

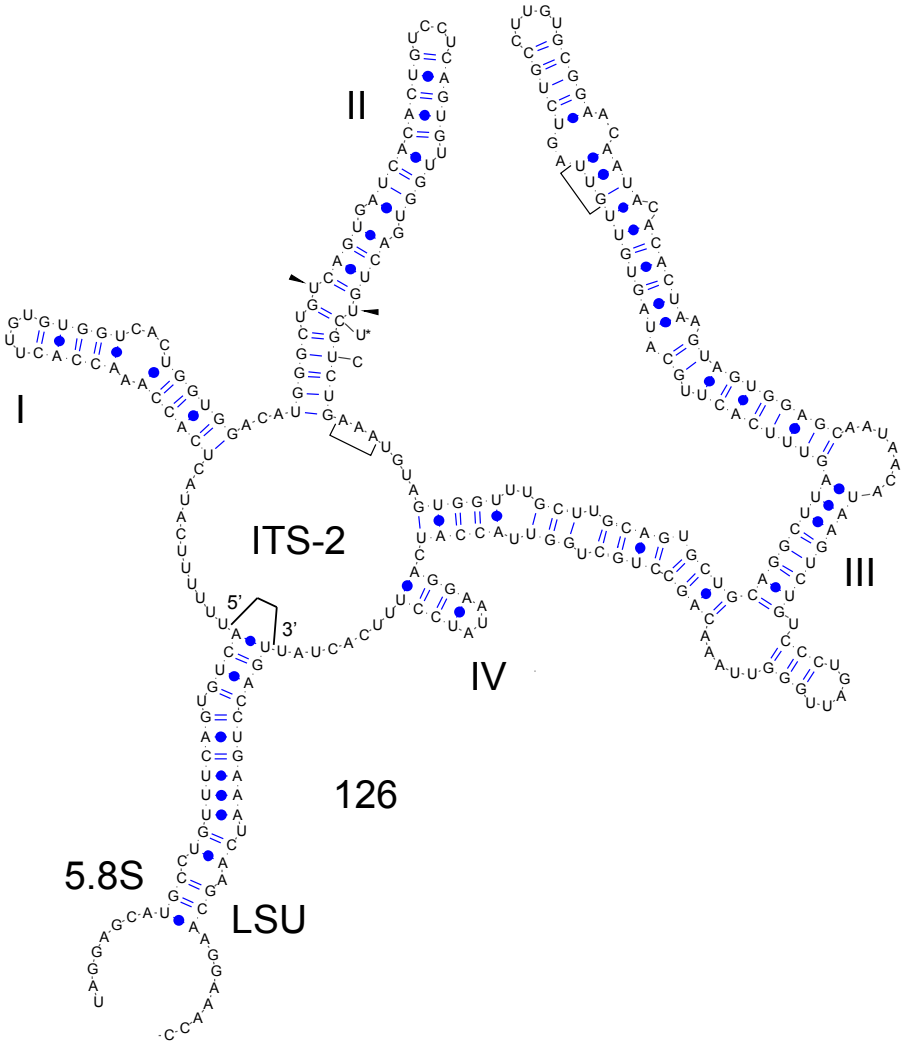

e

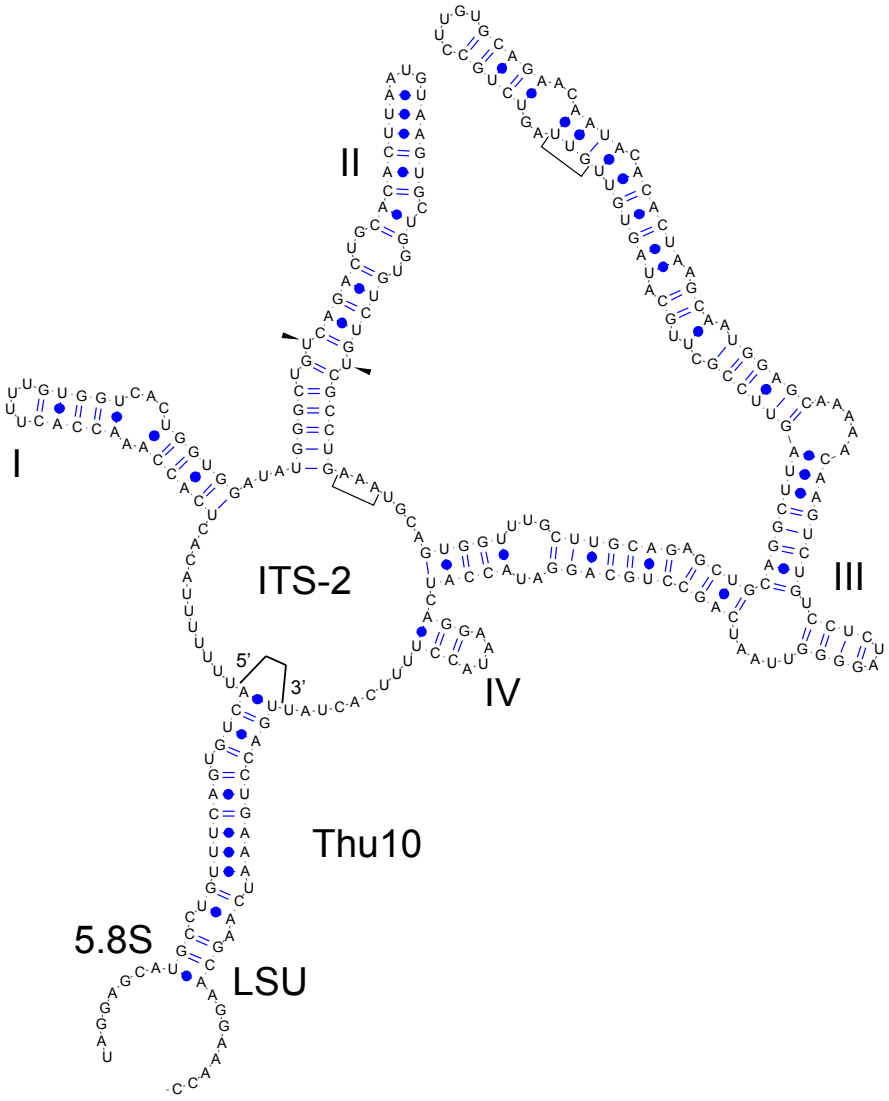

f

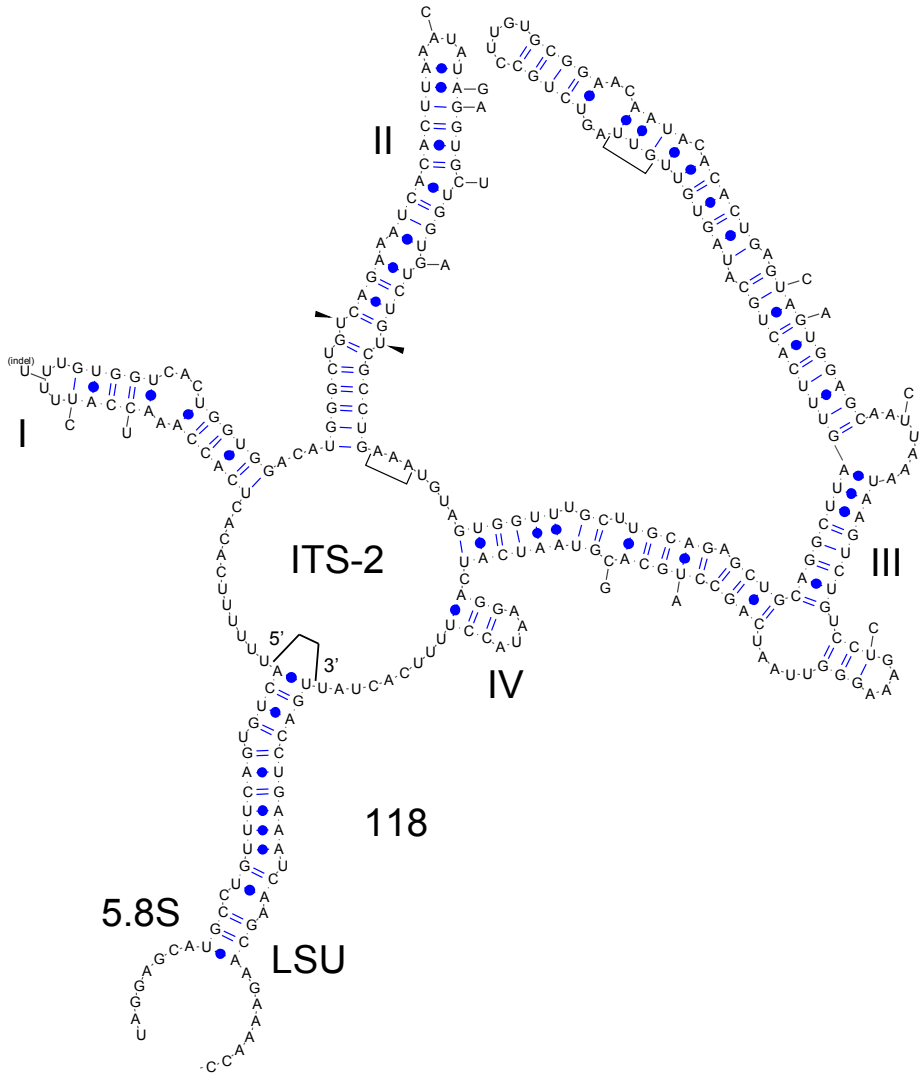

Figure 3.12. Secondary structures of nuclear *r*DNA ITS-2 of six species of *Glaucocystis*.

Note that ITS-2 secondary structures were highly conserved within the genus *Glaucocystis* and that they had four helices with helix III as the longest, U-U mismatches (arrowheads) in the helix II with AAA motif (bracket) between the helix II and III and GYU motif (bracket) near the 5' site apex of helix III. (a) *G. geitleri* E.G.Pringsh. *ex* Tos.Takah. sp. nov. strains SAG 229-1, SAG 229-3 and SAG 28.80. (b) *G. nostochinearum* Itzigs. *ex* Rabenh. strain SAG 16.98 with structural variations found in strain SAG 45.88 indicated by outside lines. (c) *G. incrassata* (Lemmerm.) Tos.Takah. comb. & stat. nov. strain SAG 229-2. (d) *G. oocystiformis* Prescott strain 126. Note that structural variations found in *G. oocystiformis* strains NIES-966 and NIES-1369 is indicated by outside lines. Asterisk indicating structural variation only found in strain NIES-1369. (e) *G. miyajii* Tos.Takah. sp. nov. strains Thu10 and NIES-1961. Note that no structural variation was found between the two. (f) *G. bhattacharyae* Tos.Takah. sp. nov. strain 118 with structural variations found in strain SAG 27.80 indicated by outside lines.

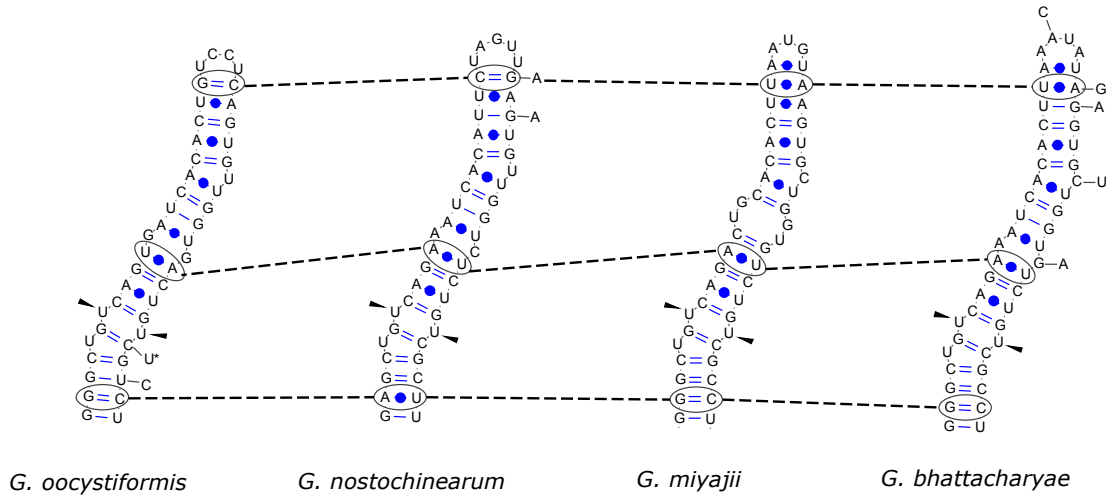

Figure 3.13. Comparison of the secondary structures of nuclear *r*DNA ITS-2 between species within crown group of *Glaucocystis* resolved in the present molecular phylogeny (Figure 3.11).

Dotted lines indicate compensatory base changes between the helices. For complete secondary structures and structural variations indicated by outside lines, see Figure 3.12.

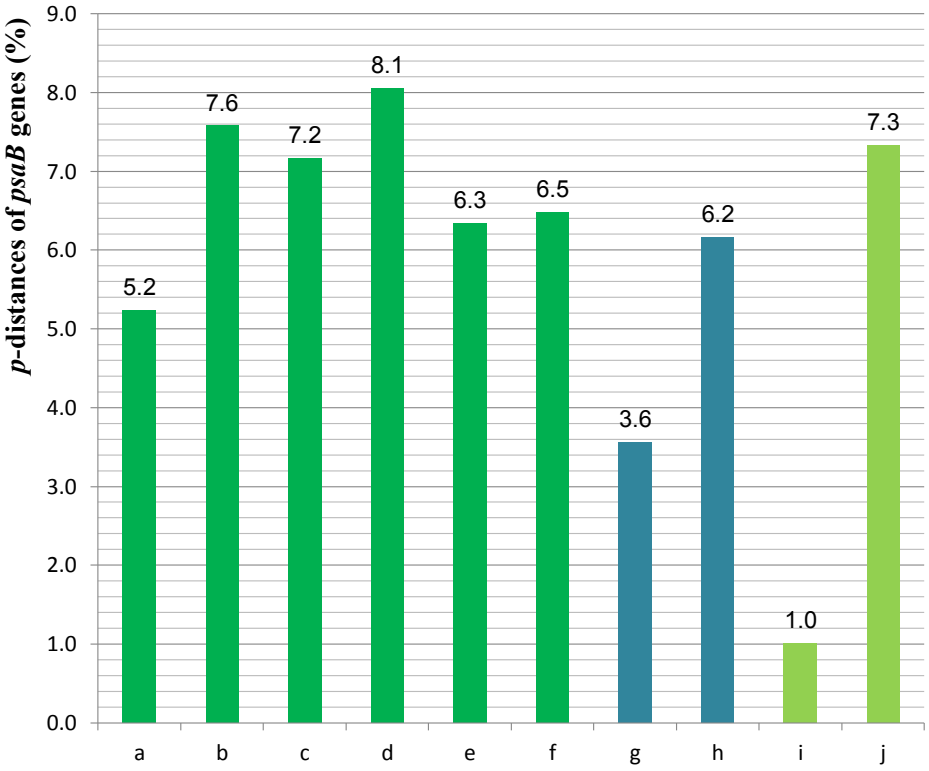

Figure 3.14. Nucleotide differences (%) or *p*-distances of *psaB* genes between *Glaucocystis* species within crown group resolved in the present molecular phylogeny (Figure 3.11) and *Cyanophora* and unicellular green algal genera.

The smallest difference is shown when multiple combinations of strains are present between sister species. For details of *psaB* gene sequence data of the green algal genera and *Cyanophora*, see Chapter 2. (a) *G. oocystiformis* and *G. nostochinearum*, (b) *G. nostochinearum* and *G. miyajii* sp. nov., (c) *G. oocystiformis* and *G. miyajii* sp. nov., (d) *G. bhattacharyae* sp. nov. and *G. miyajii* sp. nov., (e) *G. bhattacharyae* sp. nov. and *G. oocystiformis*, (f) *G. bhattacharyae* sp. nov. and *G. nostochinearum*, (g) *C. cuspidata* and *C. kugrensii*, (h) *C. biloba* and *C. sudae*, (i) *Hafniomonas conica* and *H. turbinea* and (j) *Chlorogonium capillatum* and *Ch. euchlorum*.

4. GENERAL DISCUSSION

4.1. THE NOVEL AND FUTURAL TAXONOMIC SYSTEMS OF GLAUCOPHYTES

The present dissertation aimed to reconstruct the taxonomic systems within the two glaucophyte genera representing the two of the three glaucophyte orders (Kies & Kremer, 1986; Table 1.1). In order to resolve morphologically delineated species, I applied advanced electron microscopy (EM) methodologies for comparative morphology. Ultra-high resolution (UHR) field emission (FE)-scanning electron microscopy (SEM) has recently been advanced to enable the ultrafine observation of entire cell surface; besides, numerous cells are observable at once (Nagatani, 1991; Osumi, 1998). The present UHR FE-SEM at low accelerating voltage (LV) clearly unveiled surface ornamentations of cell periphery and detailed cell shapes of the naked vegetative *Cyanophora* cells to delineate species by providing global and ultrafine information on cell surface (Figure 2.8). Within *Glaucocystis*, my LV FE-SEM was able to elucidate the two types of cellulose filament arrangements in mother cell wall. However, it cannot be applied for the native protoplast surfaces of *Glaucocystis* because the cell is enclosed by cell wall tightly although ultrastructural diversity was expected in cell periphery also in this genus as in *Cyanophora*. Alternatively, I applied three-dimensional (3D) ultra-high voltage electron microscopic (UHVEM) tomography which can provide *in situ* 3D ultrastructure of whole cells (Cyranoski, 2009; Nishida *et al.*, 2013) although 3D UHVEM has not previously been applied to microalgal taxonomy. The present 3D UHVEM clearly demonstrated morphological diversity of protoplast periphery within the genus to distinguish species, showing its utility for morphological classification in microalgae (Figures 3.4–3.8).

In Chapter 2, I delineated taxonomic species of *Cyanophora* using light microscopy

(LM) and EM of several globally distributed clonal strains, including one newly established (Chapter 2). Several molecular data supported this morphological delineation of five morphological species of *Cyanophora*. However, three of the five [*C. paradoxa* Korshikov (1924), *C. cuspidata* Tos.Takah. sp. nov. and *C. kugrensii* Tos.Takah. sp. nov.] could be identified to *C. paradoxa,* based on traditional taxonomic system (Korshikov, 1924; Bourrelly, 1985; Kugrens, 2002; Whitton, 2002; Barone *et al.*, 2006). Thus, the present novel taxonomical system of *Cyanophora* species (Table 2.2) suggests that the species diversity of glaucophytes may be significantly higher than previously believed. Through examining more strains novelly available, more *Cyanophora* species will be unveiled by my methodologies here established. Similarly, within the flagellate glaucophyte order Cyanophorales (Table 1.1), although *Peliaina* and *Strobilomonas* are indicated not to be glaucophytes (Kies & Kremer, 1986), *Cyanophora*-related algae, if exist, will also be revealed and belong to my system.

In Chapter 3, using molecular data combined with observation by LM and several EM, I reexamined the species of coccoid glaucophyte genus *Glaucocystis* that have a thick cell wall. The present 3D-modelling of *Glaucocystis* cells based on UHVEM tomography clearly showed that numerous, leaflet-like flattened vesicles are distributed throughout the protoplast periphery just underneath a single-layered plasma membrane; besides, *Glaucocystis* species exhibit morphological diversity in terms of their 3D ultrastructural features. On the basis of the 3D ultrastructures of the protoplast periphery, three periphery types were distinguished within *Glaucocystis* even by ultrathin section transmission electron microscopy (TEM). LV FE-SEM and LM elucidated the mother cell wall characters. The delineation of six morphological species was supported by several molecular data. Although several other *Glaucocystis* species as well as

Glaucocystopsis africana Bourr. (1961) have not been cultured (Philipose, 1967; Bayly, 1976; Patel & Isabella George, 1979; Chatterjee & Keshri, 2005) but they have clear LM difference between the species examined here (Table 3.2). In the near future, these species would be rediscovered and cultured to be examined at ultrastructural level, here unfolded, and to be integrated into my novel taxonomical system of the coccoid glaucophyte order Glaucocystales (Kies & Kremer, 1986; Table 1.1).

The other glaucophyte order is the palmelloid colonial Gloeochaetales which include four genera (Kies & Kremer, 1986; Table 1.1). The algae belonging to the order are characterised by having palmelloid immotile vegetative cells and some species are reported to have zoospores (Lagerheim, 1883, 1890; Dangeard, 1889; Kies, 1979, 1989). Recently, *Chalarodora azurea* Pascher (1929) was rediscovered but never has been cultured (Hindák, 2012; Hindák & Hindáková, 2012). Lagerheim (1890) considered that the three species of *Gloeochaete* Lagerh. (1883) and *Schrammia* P.-A.Dang. (1889) were composed of a same species (Table 1.1). Within the order, cultured strains labelled "*Cyanoptyche gloeocystis* Pascher (1929)" or "*Gloeochaete wittrockiana* Lagerh. (1883)" are available but not more than three in number (http://www.ccac.uni-koeln.de/; http://sagdb.uni-goettingen.de/; Schlösser, 1994); the two species are considered as cosmopolitan algae (Lagerheim, 1886a, 1888, 1890; Starmach, 1939, 1966; Bourrelly, 1957, 1961; Fenwick, 1966; Hirose & Yamagishi, 1977; Alvarez Cobelas & Gallardo, 1986; Simons, 2010; Cheraghpour *et al.*, 2013). However, taxonomic studies based upon molecular methods and comparative ultrastructure using various clonal strains, as in the two glaucophyte genera here examined, are also required within the order. Whereas vegetative cells of *Gloeochaete* and *Cyanoptyche* are immotile and enclosed by a non-cellulosic extracellular matrix, their zoospores are lacking extracellular matrix

(Kies, 1979, 1989). 3D UHVEM tomography will unveil the peripheral ultrastructures of their vegetative cells even though they are walled by extracellular matrix as *Glaucocystis* are. On the other hand, LV FE-SEM would be applicable to surface observation of their naked zoospores as of *Cyanophora*. These microscopy will reveal their diversity and essential difference in their peripheral ultrastructures and other structures, leading to understanding of the species diversity and taxonomy of the palmelloid glaucophytes.

In this dissertation, the two glaucophyte genera, *Cyanophora* and *Glaucocystis*, were clearly delineated on the basis of molecular data and comparative morphology. Therein my several EM methods were very efficient to reveal the essential difference between species because 3D UHVEM tomography and UHR FE-SEM surface observations provided the global information of characters entirely (Osumi, 1998; Kojima, 2008; Nishida *et al.*, 2013). As shown above, my UHR FE-SEM clarified the surface ornamentation which cannot be elucidated only by TEM; although 3D UHVEM tomography was applied to phycology or taxonomy at the first time, it is concluded that the 3D feature is very useful even to microbial taxonomic study as to classification of macroorganism whose 3D feature is observable by LM or even by the naked eye (Li, 1596; Linnaeus, 1753). These microscopic methods enable taxonomists to find microbial diversity as if they were observing macroscopic diversity by naked eye; therefore, these methods shall become the mainstream methods in the microbial taxonomy. For, the most of the organisms are in microorganism stage (Adl *et al.*, 2012). New generation EM including FE-SEM and UHVEM will become more and more popular hereafter (cf. Heymann *et al.*, 2006; de Oteyza *et al.*, 2013; Lee *et al.*, 2014;

Akashi *et al.*, 2015; Ichimura *et al.*, 2015). My glaucophyte taxonomy in this dissertation would become a model case of the microbial taxonomy, in the new age, including bacterial and archaeal taxonomy. Via such methods, microbial diversity in each glaucophyte genus will be unveiled. Based upon each taxonomy of the glaucophyte genera, the novel classification of glaucophytes will be reconstructed, as well as that of eukaryotes.

Indeed, molecular phylogenetic methods have been developed and become facilitated. However, only limited marker sequence can give a mere phylogeny and genetic distance between operational taxonomic units (OTUs) and never provide the delineation of species within the OTUs (Chong *et al.*, 2014). The present state of marker sequence is useful only when the species delineation or species concept has already been established; the utility of morphological data would become not less at all. On the contrary, the more important they will become, the more available the genomic data have got.

Whilst molecular data are going to change over to bioinformatical big data such as genomic and proteomic data, morphological data will transit into 3D ultrastructure of entire cells at molecular level (Kojima, 2008; Akashi *et al.*, 2015). Through such data transition, the molecular data which regulate the morphology will be more and more identified; genetic material carrying the molecular data itself and the primordial substance of life will become more and more observable directly, although they have been only imagined previously (Schrödinger, 1944). Extremely speaking, molecular and morphological data tie to each other closely and are two sides of the same coin. The ultimate goal is identical to both molecular information and morphological observation, hence I believe that on the basis of the combination of both supreme data, in the near

future, taxonomy could reach the system reflecting the native diagnosis of each species.

4.2. THE FIRST PHOTOSYNTHETIC EUKARYOTE

The primary plastids, possessed by Archaeplastida, are probably monophyletic and derived from those of the common ancestor of the primary photosynthetic eukaryotes [excluding chromatophores or endosymbionts of thecamoeba *Paulinella* (Bodył *et al.*, 2007, 2010)], which means a single primary endosymbiotic event in eukaryote lineages (Cavalier-Smith & Lee, 1985; Bhattacharya & Schmidt, 1997; Mackiewicz & Gagat, 2014). Similarly, Archaeplastida are widely believed to be a monophyletic lineage in the eukaryotes (Baldauf *et al.*, 2000; Moreira *et al.*, 2000; Rodríguez-Ezpeleta *et al.*, 2005; Hackett *et al.*, 2007; Reyes-Prieto & Bhattacharya, 2007; Jackson & Reyes-Prieto, 2014). However, some phylogenetic analyses showed that the primary photosynthetic eukaryotes are paraphyletic with respect to some secondary or higher-order photosynthetic eukaryotes that have lost their primary plastids (Bhattacharya & Schmidt, 1997; Nozaki *et al.*, 2003, 2007, 2009). Mackiewicz & Gagat (2014) argued that it is neither possible to confirm nor refute alternative evolutionary scenarios to a single primary endosymbiotic event based on results to date and that alternative approaches are needed.

Cavalier-Smith (1982) considered that the glaucophytes, dinophytes (Alveolata) and Euglenozoa (Excavata; Adl *et al.*, 2005, 2012) might be quite closely related because of the presence of alveolate pellicle (protoplast periphery with “flattened vesicles” and/or plates distributed just underneath the plasma membrane) in these three groups. He recently hypothesised that “cortical alveoli” (flattened vesicles) may have evolved in the common ancestor of a large eukaryotic group, “corticates” composed of primary phototrophs or Plantae *sensu* Cavalier-Smith (1981) (Archaeplastida; Adl *et al.*, 2005,

2012) and Chromista *sensu* Cavalier-Smith (2010) (including Chromalveolata and Rhizaria; Adl *et al.*, 2005, 2012) (Cavalier-Smith, 1982, 2002, 2010). Spiegel (2012) discussed that the first photosynthetic eukaryote may have been a *Cyanophora*-like flagellate.

Within alveolates, FE-SEM recently revealed that the surface ultrastructure of naked zoospores of *Chromera velia* is ornamented with angular fenestrations (Weatherby *et al.*, 2011), which are considered to reflect the alveolae underlying a plasma membrane as shown in the protoplast periphery of coccoid vegetative cells enclosed by a cell wall by ultrathin section TEM (Moore *et al.*, 2008; Oborník *et al.*, 2011; Weatherby *et al.*, 2011). Such a global peripheral structure is also expected in glaucophytes but FE-SEM has not previously been applied to glaucophyte cell surface. Although Kugrens *et al.* (1999) proposed that the periphery of vegetative cells in two species of *Cyanophora* are composed of the plasma membrane and underlying flattened vesicles as shown by ultrathin section and freeze-fracture TEM, the whole surface ornamentation was not unveiled because their conventional SEM could not reveal the native surficial feature. Moreover, in the coccoid glaucophyte genus *Glaucocystis*, the 3D ultrastructural features of the protoplast periphery were unclear, especially regarding the spatial relationship between the plasma membrane and flattened vesicles by ultrathin section and freeze-fracture TEM (Schnepf *et al.*, 1966; Robinson & Preston, 1971a; Willison & Brown Jr., 1978a). Especially, the Robinson and Preston (1971) proposed that the periphery of *Glaucocystis* consists of three sheets of plasma membrane, which is similar situation to that of apicomplexans (alveolates) (Adl *et al.*, 2005, 2012), and then such a peripheral ultrastructure could represent ancestral features of the first corticate, if consistent. Within glaucophyte lineage, *Cyanophora* and *Glaucocystis* represent the two

divergent clades, respectively (Chong *et al.*, 2014). Thus, to provide more detailed ancestral features of glaucophyte cells, ultrastructural characterisation of 3D structures of the whole protoplast periphery in both of the two divergent clades were required.

Here, I clearly showed as supported by ultrathin section and freeze-fracture TEM, as well as LV FE-SEM that the whole peripheral surface of naked vegetative cells in several species of *Cyanophora* is ornamented with angular fenestrations formed by ridges structured by overlapping, leaflet-like flattened vesicles underneath the plasma membrane (Figures 2.4, 2.5, 2.8, 2.9 and 2.11); this feature resembles to the zoospores of *Chromera velia* (Weatherby *et al.*, 2011).

On the other hand, the present UHVEM tomography study clearly demonstrated that the plasma membrane of periphery type A and C of *Glaucocystis* species represented a single, continuous sheet with numerous bar-like grooves that were distributed throughout the surface; the grooves were associated with numerous, leaflet-like flattened vesicles just underneath the plasma membrane (Figures 3.4 and 3.6). Except for the presence of grooves, these ultrastructural features of the protoplast periphery in periphery type A and C species were essentially the same as those of periphery type B species (Figure 3.5), as well as five species of the motile glaucophyte genus *Cyanophora* (Figure 2.8); a single plasma membrane is closely associated with numerous, leaflet-like flattened vesicles distributed throughout the periphery just underneath the membrane. Thus, these 3D structures can be considered common ancestral features of the glaucophytes (Figure 4.1). Even when 3D structures had not been clarified and molecular data were lacking, Kies (1979) already considered the peripheral flattened vesicles ("Lakunensystem") as a unifying morphological

characteristic of glaucophytes.

In dinophytes and *Chromera*, similar 3D structures of the plasma membrane and the underlying leaflet-like flattened vesicles or alveolae can be considered as a unifying morphological characteristic of alveolates based on observation by SEM/FE-SEM and ultrathin section TEM (Moore *et al.*, 2008; Oborník *et al.*, 2011; Weatherby *et al.*, 2011; Adl *et al.*, 2012). In addition, some haptophytes possess flattened-vesicle-like ultrastructures or peripheral endoplasmic reticulum (PER) just beneath the plasma membrane (Pienaar, 1994). Thus, fundamentally identical or homologous peripheral ultrastructures may be distributed in separate lineages or different supergoups within corticates or bikonts (corticates plus Excavata or eukaryotes excluding Amoebozoa and Opisthokonta; Adl *et al.*, 2012) (Figure 4.1). On the other hand, no organism in the other two groups of Archaeplastida (Chloroplastida and red algae) and unikonts (composed of opisthokonts and amoebozoans) contains such complicated peripheral ultrastructures. Given that the glaucophytes represent the most ancestral features of Archaeplastida (Price *et al.*, 2012; Spiegel, 2012), the leaflet-like flattened vesicles in the protoplast periphery in glaucophyte cells may have been retained from the first photosynthetic eukaryote in the Precambrian period or a more ancient ancestor within the bikonts, as suggested by Cavalier-Smith (2010) (Figure 4.1). In the ancestors of Chloroplastida and red algae, the flattened vesicles may have been lost during evolution.

In the present study, the 3D ultrastructural arrangement of the plasma membrane and the underlying leaflet-like flattened vesicles in the coccoid glaucophyte genus *Glaucocystis* were clearly observed by UHVEM tomography and 3D-modelling using HPF-FS method. Similar 3D ultrastructural arrangement is also indicated in motile glaucophyte

genus *Cyanophora* on the basis of the combination of ultrathin section and freeze-fracture TEM and LV FE-SEM. Although plates are lacking within the vesicles, the *Glaucocystis* periphery is essentially identical based on the 3D ultrastructural arrangement as that of motile glaucophyte genus *Cyanophora*, as well as alveolates, which suggests that such peripheral ultrastructures may represent ancestral features of the first photosynthetic eukaryote, as well as the first corticate (Figure 4.1), as suggested by Cavalier-Smith (2010). Further 3D UHVEM tomography and 3D-modelling of other genera of glaucophytes, as well as for other bikonts, will unveil the actual diversity and ancestral ultrastructural features of the bikonts.

4.3. THE POSSIBLE EVOLUTIONARY SCENARIO IN GLAUCOPHYTES

In Chaper 2, I classified five species of *Cyanophora* recognised by comparative morphology including several EM; besides, in Chaper 3, I produced the taxonomy of six *Glaucocystis* species on the basis of morphological characteristics including 3D ultrastructures. The precise observation was also undertaken to unveil the native feature of cell coverings in the two genera. *Cyanophora* and *Glaucocystis* represent the two divergent clades of glaucophytes, respectively (Chong *et al.*, 2014), and was diverged 400 – 800 million years ago (Parfrey *et al.*, 2011). Since variety of eukaryote cell coverings might reflect the lifestyle of each organism, the diversity has been examined extremely and the evolution has been discussed (Okuda, 2002). However, no speculation of evolutionary processes has been ventured within glaucophytes. Based upon the common characteristics between the two genera, I discussed the ancestral features of glaucophytes in Section 4.2. On the other hand, morphological diversity was also elucidated by microscopic observations within the each of the two genera. Here, a possible evolutionary scenario become worth speculating throughout glaucophytes.

The flattened vesicles of *Cyanophora* contained a plate and completely enclosed the protoplast by overlapping with one another at the protoplast periphery to form ridges on the cell surface under LV FE-SEM (Figures 2.8 and 2.11). In contrast, the present study also demonstrated that *Glaucocystis* species have flattened vesicles which lack the plate and are more or less separated from one another just underneath the plasma membrane to form spaces between the vesicles at the protoplast periphery (Figures 3.4–3.7). This difference may reflect the presence or absence of a cell wall in these two genera. Since

the *Cyanophora* cells lack cell walls, the function of tightly arranged flattened vesicles with plates may protect the protoplast or facilitate the formation of cell shape characteristics to the species. It is generally believed that the flagellate vegetative cells represent an ancestral form in the photosynthetic eukaryotes or algae (Leliaert *et al.*, 2012) and indeed, biflagellate cells exist polyphyletically throughout the bikonts (Adl *et al.*, 2005, 2012). Thus, it is possible that during evolutionary processes from the ancestral *Cyanophora*-like biflagellate to the immotile *Glaucocystis* cells, the flattened vesicles in the protoplast periphery may have lost their plates and the function as protector (Figure 4.1). Because of the presence of vestigial flagella in vegetative cells (Figure 3.8), *Glaucocystis* might have strayed into the initial evolutionary way into a "vegetal" phototroph that has obtained a cellulosic cell wall which can guard its protoplast and daughter cells (Figures 3.2 and 3.3). In exchange for obtaining a cell wall, the vegetative cells might have lost the motility and the plate within the vesicles.

In *Glaucocystis nostochinearum* (Figure 3.5) and *Cyanophora* species (Figures 2.5 and 2.11) the plasma membrane lacked grooves or invaginations. In contrast, the plasma membrane of the five species of *Glaucocystis* had numerous grooves throughout the protoplast surface (Figures 3.4, 3.6 and 3.7). The flattened vesicles without plate are closely associated with the plasma membrane at the grooves, which might have been obtained through such an evolutionary process. Vegetative cells of *G. geitleri*, exhibiting the most basal phylogenetic position within *Glaucocystis* (Figure 3.11), are far larger than vegetative cells of *Cyanophora* species as well as *G. nostochinearum* (Figures 2.7 and 3.1). Presence of the grooves or invaginations at the protoplast periphery in *G. geitleri* might contribute to expansion of the surficial area of the protoplast and consequently to their large cell size, considering that the surficial-area-to-volume ratio

in a cell is smaller (inversely proportional to the cell size) when the cell is larger and that the substance transportation across the plasma membrane is more limited. Through acquisition of plasma membrane grooves associated with flattened vesicles, *G. geitleri* might have kept their large cell size to be applied to immotile or vegetal lifestyle as a coccoid primary producer. For immotile unicellular phototrophs, large cell size is beneficial to plastid volume and photosynthesis rate in a whole cell. The function of the flattened vesicles might associate with the formation of the grooves. Whereas the other species sustain the grooves, *G. nostochinearum* might have lost the grooves because of its smallest cell size within the crown group (Figure 3.11).

Within *Cyanophora*, cells are flagellated form and do not exhibit such a mutation or adaptation. However, dorsoventrally compressed vegetative cells of Group B species might contribute to expansion of plastid volume per a cell volume and Group A species might retain the most primitive form of *Cyanophora* as well as glaucophytes (Figure 2.7).

In alveolates, although the coccoid vegetative cells of *Chromera velia* enclosed by a cell wall, as of coccoid glaucophyte *Glaucocystis*, the resemblance between biflagellated zoospores of *Ch. velia* and biflagellate glaucophyte *Cyanophora* indicate evolutionary convergence between alveolates and glaucophytes. The zoospores of *Ch. velia* might represent ancestral features of the first alveolate and vegetative cells of *Ch. velia* might be in such an initial evolutionary way into a "vegetal" phototroph. In Archaeplastida, all red algae lack motility without flagella and many of several chloroplastidal lineages have obtained a cell wall (Adl *et al.*, 2012). They might have evolved into hodiernal vegetal organisms through such a process. The evolutionary way to "vegetal" genus *Glaucocystis* within glaucophytes is very suggestive to consider the

initial evolutionary process within each of the other phototroph lineages.

In terms of *Glaucocystis* cell wall, mother cell wall may function to guard autospores or daughter cells even after cytokinesis but daughter cells cannot remain within it forever. By LV FE-SEM distinguished two types of filament arrangements; gauze fabric-like appearance with small spaces between fibrils or tightly arranged fibrils (Figure 3.3). Such filament arrangements corresponded to mother cell wall extension observed by LM (Figure 3.2). In four *Glaucocystis* species [*G. geitleri* E.G.Pringsh. *ex* Tos.Takah. sp. nov., *G. nostochinearum* Itzigs. *ex* Rabenh. (1866), *G. oocystiformis* Prescott (1944) and *G. miyajii* Tos.Takah. sp. nov.] the weave of whole of the mother cell wall fibrils may be easy to get loosed entirely and globally; at the same time, the cell wall would become extended prominently to form spaces between daughter cells within the colony. Such an extended mother cell wall with a loose open weave might be easily broken (Figure 3.3e). In the other species, *G. incrassata* (Lemmerm.) Tos.Takah. comb. & stat. nov. and *G. bhattacharyae* Tos.Takah. sp. nov., however, the weave of the mother cell wall fibrils may not get loosed globally, so as not to show an extended mother cell wall with a loose open weave. Alternatively, a local part of the mother cell wall could get pierced so that the content daughter cells can get out from the mother cell wall enclosing them tightly. For by my LV FE-SEM, locally pierced mother cell wall occasionally observed although the rest parts of colony surface keep exhibiting the tightly arranged fibrils (Figure 3.3c).

Whereas “ancestral” glaucophyte *Cyanophora* represents one of the two divergent clades, “vegetal” *Glaucocystis* belongs to the other divergent clade, that also includes the palmelloid glaucophytes *Cyanoptyche* and *Gloeochaete* (Chong *et al.*, 2014). The

palmelloid glaucophytes would play a key role to reveal the glaucophyte evolutionary process since their zoospores of *Gloeochaete* and *Cyanoptyche* can be induced easily (Kies, 1979, 1989). Their feature or lifestyle might exhibit the evolutionary intermediate stage between *Cyanophora* and *Glaucocystis*. The application of LV FE-SEM for naked zoospores as well as 3D UHVEM tomography for walled cells to palmelloid glaucophyte and other eukaryotic cells will unveil the peripheral ultrastructures and other essential structures, leading to understanding of the species diversity and taxonomy, which shall result in the elucidation of their evolutionary process.

4.4. FIGURE

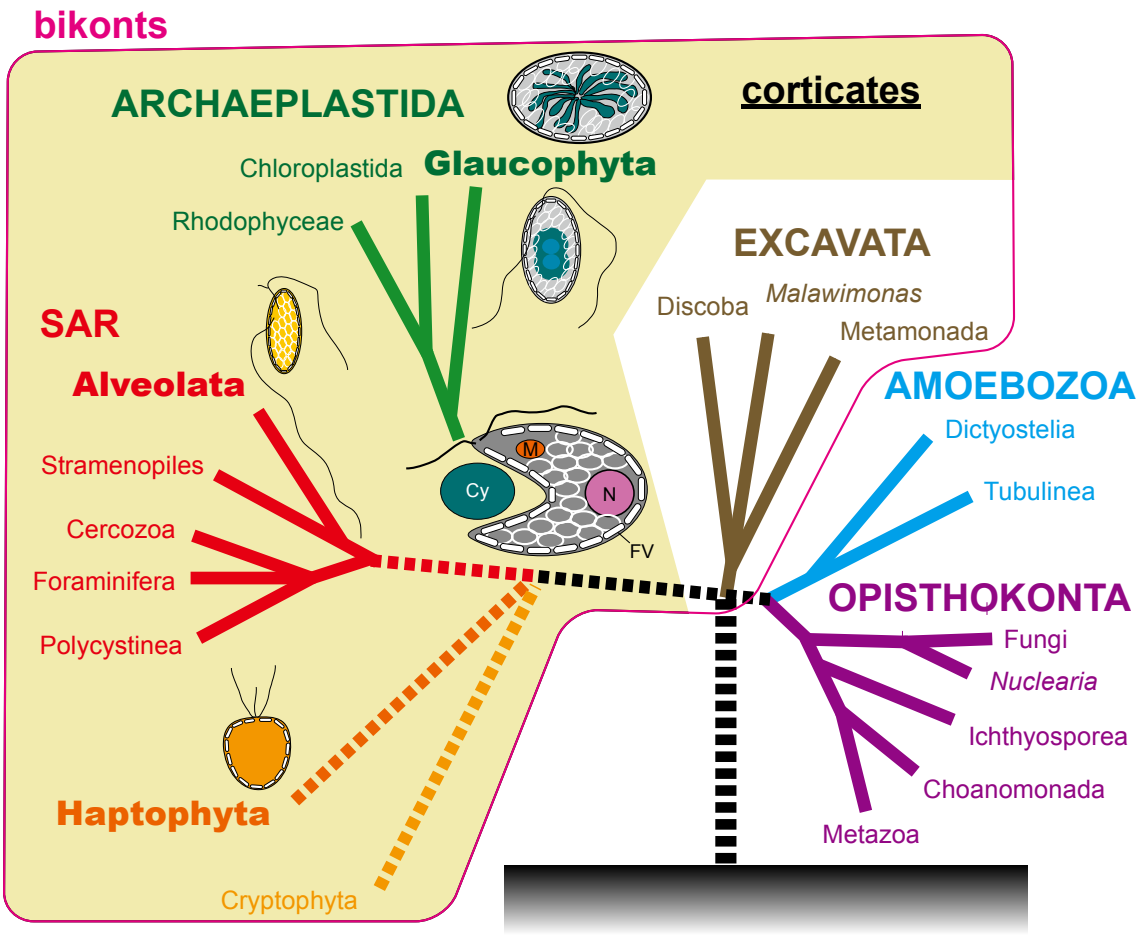

Figure 4.1. Diagram of a possible evolutionary scenario from an ancestral flagellate with leaflet-like flattened vesicles to extant primary photosynthetic eukaryotes (Archaeplastida).

Based on the present study, Adl *et al.* (2012) and Cavalier-Smith (1982, 2002, 2010). Extant organisms that possibly retain flattened vesicles are Glaucophyta, Alveolata and Haptophyta. The putative ancestral biflagellate of glaucophytes or the first primary photosynthetic eukaryote enslaved a cyanobacterium (Cy) as plastids might have contained nucleus (N), mitochondria (M) and leaflet-like flattened vesicles (FV).

ACKNOWLEDGEMENTS

First of all, I have to express my sincere gratitude to Assoc. Prof. Hisayoshi Nozaki (University of Tokyo) for all aspects as my supervisor during this study.

I am extremely grateful to Dr. Tomoki Nishida (QTEC, Japan Textile Products Quality and Technology Center) and Prof. Hidehiro Yasuda (Osaka University) for their kind technical help in ultra-high voltage electron microscopy. I wish to thank Drs. Mayuko Sato and Kiminori Toyooka (RIKEN Yokohama Institute) sincerely for their gentle guidance of scanning electron microscopy method and facility, Ms. Ayako Watanabe (University of Tokyo) for her kind guidance of critical point dryer JCPD-5 and Ms. Yukari Dan as well as Mr. Shunya Watanabe for using a demonstrated field emission scanning electron microscope SU8020 at Hitachi High-Technologies Corporation. I am also grateful sincerely to Dr. Chieko Saito (JST, Japan Science and Technology Agency) for her kind guidance about transmission electron microscopy techniques using freeze-substitution and high-pressure freezing, thanking Ms. Fumiko Ishitsuna (University of Tokyo) for her kind help for using the high-pressure freezing machine HPM010. I am deeply appreciative of Ms. Mai Kawamura as well as Prof. Kazuo Okuda (Kochi University) helping freeze fracture microscopic observation very kindly. I would like to thank Dr. Akihiro Tuji (Department of botany, National museum of nature and science, TNS) especially for his kind guidance about permanent slide preparation as well as Ms. Genevieve E. Tocci, Dr. Robert K. Edgar (Farlow Herbarium, University of Harvard, FH) and Prof. Jin Murata (Herbarium, University of Tokyo, TI) for the loan arrangement of *Glaucocystis nostochinearum* syntype material. I am sincerely appreciative of Prof. Kazuyuki Miyaji (Toho University) offering information and helping for collecting algae kindly. I also greatly acknowledge Dr. Kaoru Kawafune (Tokyo Institute of Technology) kindly providing soil samples, especially. I wish to

express my deepest thanks to Dr. Takashi Nakada (Keio University) especially for his kind nomenclatural advises. I wish to thank Ms. Yoko Arakaki as well as other current and former members in the Laboratory of Origin of eukaryote biodiversity greatly and sincerely for their kindness and help throughout this study. At last, I wish to express my sincere and great gratitude to Dr. Ryo Matsuzaki especially for his tender and helpful technical guidance about molecular methods and algal treatments. Besides, I would repeatedly like to acknowledge the favour, discussions and encouragement of all of them and everyone who have supported me during my graduate course.

A part of Chaper 3 was supported by "Nanotechnology Network Project of the Ministry of Education, Culture, Sports, Science and Technology (MEXT), Japan" at the Research Center for Ultrahigh Voltage Electron Microscopy, Osaka University (Handai multi-functional Nano-Foundry).

A part of Chapter 2 was reproduced from Takahashi *et al.* (2014) J. Phycol. (permitted under the License Number: 3742421220485 from John Wiley and Sons) and Takahashi *et al.* (2014) Cytologia (with permission from The Japan Mendel Society). A part of Chapter 3 and 4 was reproduced from Takahashi *et al.* (2015) Sci. Rep.

REFERENCES

Adl, S.M., Simpson, A.G.B., Farmer, M.A., Andersen, R.A., Anderson, O.R., Barta, J.R., Bowser, S.S., Brugerolle, G., Fensome, R.A., Fredericq, S., James, T.Y., Karpov, S., Kugrens, P., Krug, J., Lane, C.E., Lewis, L.A., Lodge, J., Lynn, D.H., Mann, D.G., McCourt, R.M., Mendoza, L., Moestrup, O., Mozley-Standridge, S.E., Nerad, T.A., Shearer, C.A., Smirnov, A.V., Spiegel, F.W. & Taylor, M.F.J.R. 2005. The new higher level classification of eukaryotes with emphasis on the taxonomy of protists. *J. Eukaryot. Microbiol.* **52**: 399–451.

Adl, S.M., Simpson, A.G.B., Lane, C.E., Lukeš, J., Bass, D., Bowser, S.S., Brown, M.W., Burki, F., Dunthorn, M., Hampl, V., Heiss, A., Hoppenrath, M., Lara, E., le Gall, L., Lynn, D.H., McManus, H., Mitchell, E.A.D., Mozley-Stanridge, S.E., Parfrey, L.W., Pawlowski, J., Rueckert, S., Shadwick, L., Schoch, C.L., Smirnov, A. & Spiegel, F.W. 2012. The revised classification of eukaryotes. *J. Eukaryot. Microbiol.* **59**: 429–514.

Aitken, A. & Stanier, R.Y. 1979. Characterization of peptidoglycan from the cyanelles of *Cyanophora paradoxa*. *J. Gen. Microbiol.* **112**: 219–223.

Akashi, T., Takahashi, Y., Tanigaki, T., Shimakura, T., Kawasaki, T., Furutsu, T., Shinada, H., Müller, H., Haider, M., Osakabe, N. & Tonomura, A. 2015. Aberration corrected 1.2-MV cold field-emission transmission electron microscope with a sub-50-pm resolution. *Appl. Phys. Lett.* **106**: 074101.

Alvarez Cobelas, M. & Gallardo, T. 1986. Catálogo de las algas continentales españolas. IV. Chlorophyceae Wille in Warming 1884. Prasinophyceae T. Christensen ex Silva 1980. *Acta Bot. Malac.* **11**: 17–38.

Ariyadej, C., Tansakul, R., Tansakul, P. & Angsupanich, S. 2004. Phytoplankton diversity and its relationships to the physico-chemical environment in the Banglang Reservoir, Yala Province. *Songklanakarin J. Sci. Technol.* **26**: 595–607.

Baldauf, S.L., Roger, A.J., Wenk-Siefert, I. & Doolittle, W.F. 2000. A Kingdom-level phylogeny of eukaryotes based on combined protein data. *Science* **290**: 972–977.

Barone, R., Marrone, F. & Naselli Flores, L. 2006. First record of *Cyanophora paradoxa* Koršikov (Glaucocystophyta) in Italy. *Naturalista Siciliano* **30**: 97–106.

Baudelet, P., Gagez, A., Bérard, J., Juin, C., Bridiau, N., Kaas, R., Thiéry, V., Cadoret, J. & Picot, L. 2013. Antiproliferative activity of *Cyanophora paradoxa* pigments in melanoma, breast and lung cancer cells. *Mar. Drugs* **11**: 4390–4406.

Bayer, M.G. 1986. Biosynthesis of proteins in *Cyanophora paradoxa* .1. Protein import into the endocyanelle analyzed by micro two-dimensional gel-electrophoresis. *Endocytobiosis & Cell Res.* **3**: 197–202.

Bayly, I. 1976. The plankton of Lake Eyre. *Mar. Freshwater Res.* **27**: 661–665.

Belkinova, D.S., Kirjakov, I.K. & Mladenov, R.D. 2002. Catalogue of the Strains of Plovdiv Algal Culture collection (PACC). *Trav. Sci. Univ. Plovdiv, Plantarum (2)* **38**: 3–78.

Bessey, C.E. 1907. A synopsis of plant phyla. *Univ. Stud. (Univ. Nebraska)* **7**: 1–99.

Bhattacharya, D. & Schmidt, H.A. 1997. Division Glaucocystophyta. in: Bhattacharya, D. (ed.), *The origin of algae and their plastid*. 139–148. Wien.

Bodył, A., Mackiewicz, P. & Stiller, J.W. 2007. The intracellular cyanobacteria of *Paulinella chromatophora*: endosymbionts or organelles? *Trends Microbiol.* **15**: 295–296.

Bodył, A., Mackiewicz, P. & Stiller, J.W. 2010. Comparative genomic studies suggest that the cyanobacterial endosymbionts of the amoeba *Paulinella chromatophora* possess an import apparatus for nuclear-encoded proteins. *Plant Biol.* **12**: 639–649.

Bohlin, K. 1897. Die Algen der ersten Regnell'schen Expedition. I. Protococcoiden. *Bih. K. Svensk. Vet. -Akad. Handl.* **23**: 1–47.

Bohlin, K. 1901. *Utkast till de gröna algernas och arkegoniaternas fylogeni*. Almqvist & Wiksells boktryckeri-a.-b., Upsala.

Bohnert, H.J., Michalowski, C., Bevacqua, S., Mucke, H. & Löffelhardt, W. 1985. Cyanelle DNA from *Cyanophora paradoxa*. *Mol. Genet. Genomics* **201**: 565–574.

Borge, O. 1906. Beiträge zur Alpenflora von Schweden. *Ark. Bot.* **6**: 1–88.

Borzì, A. 1914. Studi sulle mixoficee. I. Cenni generali—Systema Myxophycearum. *Nuovo Giorn. Bot. Ital. (Nuova serie)* **21**: 307–435.

Bourdu, R. & Lefort, M. 1967. Structure fine, observée en cryodécapage, des lamelles photosynthetiques des cyanophycées endosymbiotiques: *Glaucocystis nostochinearum* et *Cyanophora paradoxa*. *C. r. hebd. séances Acad. sci., D* **265**: 37–40.

Bourrelly, P. 1957. *Cyanoptyche gloeocystis* fo. *minor* nov. fo. Une algue rare de Rambouillet. *Rev. Algol., ns* **2**: 275–276.

Bourrelly, P. 1960. Un nouveau genre africain d'endocyanose: *Glaucocystopsis africana*: nov. gen. et nov. sp. *C. r. hebd. séances Acad. sci., D* **251**: 416–418.

Bourrelly, P. 1961. Algues d'eau douce de la République de Côte d'Ivoire. *Bull. Inst. franç. Afr. Noire, sér. A.* **23**: 283–398.

Bourrelly, P. 1985. *Les algues d'eau douce —Initiation à la Systématique— Tome Ⅲ: Les algues bleues et rouges —Les Eugléniens, Peridiniens et Cryptomonadines— Réimpression revue et augmemntée*. Paris.

Bresinsky, A. & Kaderkit, J.W. 2001. Systematik-Poster: Botanik. 2. überarbeitete Auflage. Heidelberg.

Bresinsky, A. & Kaderkit, J.W. 2006. Systematik-Poster: Botanik. 3. überarbeitete Auflage. München.

Briois, B., Saito, T., Pétrier, C., Putaux, J., Nishiyama, Y., Heux, L. & Molina-Boisseau, S. 2013. $I_\alpha \rightarrow I_\beta$ transition of cellulose under ultrasonic radiation. *Cellulose* **20**: 597–603.

Burey, S.C., Fathi-Nejad, S., Poroyko, V., Löffelhardt, W. & Bohnert, H.J. 2005. The central body of the cyanelles of *Cyanophora paradoxa*: a eukaryotic carboxysome? *Can. J. Bot.* **83**: 758–764.

Burey, S.C., Poroyko, V., Ergen, Z.N., Fathi-Nejad, S., Schüller, C., Ohnishi, N., Fukuzawa, H., Bohnert, H.J. & Löffelhardt, W. 2007. Acclimation to low [CO_2] by an inorganic carbon-concentrating mechanism in *Cyanophora paradoxa*. *Plant Cell Environ.* **30**: 1422–1435.

Caballero, F. 1945. Algas del macizo de Gredos. *Anales Jard. Bot. Madrid* **5**: 345–364.

Caisová, L., Marin, B. & Melkonian, M. 2013. A consensus secondary structure of ITS2 in the Chlorophyta identified by phylogenetic reconstruction. *Protist* **164**: 482–496.

Cărăuş, I. 2002. Algae of Romania. A distributional checklist of actual algae. *St. cerc. biol.* **7**: 1–694.

Cărăuş, I. 2012. Algae of Romania. A distributional checklist of actual algae. Third revision. *St. cerc. biol.* **7**: 1–809.

Cavalier-Smith, T. 1981. Eukaryote kingdoms: Seven or nine? *BioSys.* **14**: 461–481.

Cavalier-Smith, T. 1982. The origins of plastids. *Biol. J. Linn. Soc.* **17**: 289–306.

Cavalier-Smith, T. 1998. A revised six-kingdom system of life. *Biol. Rev.* **73**: 203–266.

Cavalier-Smith, T. 2002. Chloroplast evolution: secondary symbiogenesis and multiple losses. *Curr. Biol.* **12**: R62–R64.

Cavalier-Smith, T. 2010. Kingdoms Protozoa and Chromista and the eozoan root of the eukaryotic tree. *Biol. Lett.* **6**: 342–345.

Cavalier-Smith, T. & Lee, J.J. 1985. Protozoa as hosts for endosymbioses and the conversion of symbionts into organelles. *J. Protozool.* **32**: 376–379.

Chatterjee, S. & Keshri, J.P. 2005. New records of the genus *Glaucocystis* Itzigsohn (Glaucocystophyta) from West Bengal, India. *J. Econ. Taxon. Bot.* **29**: 378–381.

Cheraghpour, J., Afsharzadeh, S., Sharifi, M., Ramezannejad, G.R. & Masoudi, M. 2013 12 31: Phytoplankton diversity assessment of Gandoman wetland, West of Iran. *Iran. J. Bot.* **19**: 153–161.

Chodat, R. 1919. Sur un *Glaucocystis* et sa position systématique. *Bull. Soc. Bot. Genève* **2**: 42–49.

Chong, J., Jackson, C., Kim, J.I., Yoon, H.S. & Reyes-Prieto, A. 2014. Molecular markers from different genomic compartments reveal cryptic diversity within glaucophyte species. *Mol. Phylogenet. Evol.* **76**: 181–188.

Coleman, A.W. 2000. The significance of a coincidence between evolutionary landmarks found in mating affinity and a DNA sequence. *Protist* **151**: 1–9.

Coleman, A.W. 2003. ITS2 is a double-edged tool for eukaryote evolutionary comparisons. *Trends genet.* **19**: 370–375.

Coleman, A.W. 2009. Is there a molecular key to the level of "biological species" in eukaryotes? A DNA guide. *Mol. Phylogenet. Evol.* **50**: 197–203.

Compère, P. 1976. Algues de la région du lac Tchad. V — Chlorophycophytes (1re partie) (1). *Cah. O. R. S. T. O. M. sér. Hydrobiol.* **10**: 77–118.

Cyranoski, D. 2009. Microscopic marvels: the big and the bold. *Nature* **459**: 634–635.

Dangeard, P.-D. 1889. Mémoire sur les algues. *Le Botaniste* **1**: 127–174.

Day, J.G., Lukavský, J., Friedl, T., Brand, J.J., Campbell, C.N., Lorenz, M. & Elster, J. 2004. Pringsheim's living legacy: CCALA, CCAP, SAG and UTEX culture collections of algae. *Nova Hedwigia* **79**: 27–37.

Day, J.G., Pröschold, T., Friedl, T., Lorenz, M. & Silva, P.C. 2010. Conservation of microalgal type material: approaches needed for 21st century science. *Taxon* **59**: 3–6.

de Azevedo Barros, C.F. 2010. *Diversidade e ecologia do fitoplâncton em 18 lagoas*

naturais do médio Rio Doce. Univ. Federal de Minas Gerais, Belo Horizonte.

de Broglie, L. 1924. *Recherches sur la théorie des quanta*. Migration-université en cours d'affectation, Paris.

de Oteyza, D.G., Gorman, P., Chen, Y.C., Wickenburg, S., Riss, A., Mowbray, D.J., Etkin, G., Pedramrazi, Z., Tsai, H.Z., Rubio, A., Crommie, M.F. & Fischer, F.R. 2013. Direct imaging of covalent bond structure in single-molecule chemical reactions. *Science* **340**: 1434–1437.

Doweld, A. 2001. *Prosyllabus tracheophytorum: Tentamen systematis plantarum vascularium (Tracheophyta)*. Moscow.

Echlin, P. 1967. The biology of *Glaucocystis nostochinearum*. I. The morphology and fine structure. *Br. phycol. Bull.* **3**: 225–239.

Facchinelli, F., Pribil, M., Oster, U., Ebert, N., Bhattacharya, D., Leister, D. & Weber, A.M. 2013. Proteomic analysis of the *Cyanophora paradoxa* muroplast provides clues on early events in plastid endosymbiosis. *Planta* **237**: 637–651.

Fathinejad, S., Steiner, J.M., Reipert, S., Marchetti, M., Allmaier, G., Burey, S.C., Ohnishi, N., Fukuzawa, H., Löffelhardt, W. & Bohnert, H.J. 2008. A carboxysomal carbon-concentrating mechanism in the cyanelles of the 'coelacanth' of the algal world, *Cyanophora paradoxa*? *Physiol. Plantarum* **133**: 27–32.

Felsenstein, J. 1985. Confidence limits on phylogenies: an approach using bootstrap. *Evolution* **38**: 16–24.

Fenwick, M.G. 1966. Some rare and interesting algae from Port Radium, N. W. T. Canada. *Trans. Am. Microsc. Soc.* **85**: 477–480.

Frassanito, A.M., Barsanti, L., Passarelli, V., Evangelista, V. & Gualtieri, P. 2010. A rhodopsin-like protein in *Cyanophora paradoxa*: gene sequence and protein immunolocalization. *Cell Mol. Life Sci.* **67**: 965–971.

Frassanito, A.M., Barsanti, L., Passarelli, V., Evangelista, V. & Gualtieri, P. 2013. A second rhodopsin-like protein in *Cyanophora paradoxa*: gene sequence and protein expression in a cell-free system. *J. Photochem. Photobiol. B, Biol.* **125**: 188–193.

Gärtner, G. & Ingolić, E. 2001. Über *Glaucocystis nostochinearum* Itzigsohn (Algae, Glaucocystophyta) in Nordtirol und Bemerkungen zur Systematik der Gattung. *Ber. nat. -med. Verein Innsbruck* **88**: 99–105.

Geitler, L. 1923. Der Zellbau von *Glaucocystis Nostochinearum* und *Gloeochaete Wittrockiana* und die Chromatophoren-Symbiosetheorie von Mereschkowsky. *Arch. Protistenkd.* **47**: 1–24.

Geitler, L. 1924. Kleinere Mitteilungen. Ein Fall von scheinbarer Kalkfeindlichkeit. *Arch. Hydrobiol.* **15**: 280–281.

Geitler, L. 1959. Eine neue Endocyanose, *Cyanoptyche dispersa* n. sp., und Bemerkungen über ähnliche Syncyanosen. *Österr. Bot. Z.* **106**: 464–471.

Gordon, D.P. 2013. New Zealand's genetic diversity. in: Dymond, J.R. (ed.), *Ecosystem services in New Zealand—conditions and trends*. 162–191. Lincoln (New Zealand).

Griffiths, B.M. 1915. On *Glaucocystis Nostochinearum*, Itzigsohn. *Ann. Bot.* **29**: 423–432.

Gross, J., Wajid, S., Price, D.C., Zelzion, E., Li, J., Chan, C.X. & Bhattacharya, D. 2013.

Evidence for widespread exonic small RNAs in the glaucophyte alga *Cyanophora paradoxa*. *PLoS ONE* **8**: e67669.

Gross, L. & Kneucker, A. 1901. Unsere Reise nach Istrien, Dalmatien, Montenegro, der Hercegovina und Bosnien im Juli und August 1900. *Allg. Bot. Zeitschrift* **Jahrg. 7**: 125–130.

Gutwiński, R. 1901. Additamenta ad floram algarum Indiae Batavorum cognoscendam. Algae a cl. D^{re} M. Raciborski in montibus Vulcaniis: Krakatau et Slamat anno 1897 collectae. *Rozpr. Akad. Umiej. Wydział Mat. -Przyr.* **39**: 287–307.

Gutwiński, R. 1909. Flora algarum montium Tatrensium. *Bull. Intern. Acad. Sci. Cracovie, Classe Sci. Math. Nat.* **9**: 415–560.

Hackett, J.D., Yoon, H.S., Li, S., Reyes-Prieto, A., Rümmele, S.E. & Bhattacharya, D. 2007. Phylogenomic analysis supports the monophyly of cryptophytes and haptophytes and the association of Rhizaria with chromalveolates. *Mol. Biol. Evol.* **24**: 1702–1713.

Hall, W.T. & Claus, G. 1963. Ultrastructural studies on blue-green algal symbiont in *Cyanophora paradoxa* Korschikoff. *J. Cell Biol.* **19**: 551–563.

Hall, W.T. & Claus, G. 1967. Ultrastructural studies on the cyanelles of *Glaucocystis nostochinearum* Itzigsohn. *J. Phycol.* **3**: 37–51.

Hansgirg, A. 1892. Prodromus der Algenflora von Böhmen: Zweiter Theil, welcher die blaugrünen Algen (Myxophyceen, Cyanophyceen), nebst Nachträgen zum ersten Theile und einer systematischen Bearbeitung der in Böhmen verbreiteten saprophytischen Bacterien und Euglenen enthält. Prague.

Hayama, M., Nakada, T., Hamaji, T. & Nozaki, H. 2010. Morphology, molecular

phylogeny and taxonomy of *Gonium maiaprilis* [sic] sp. nov. (Goniaceae, Chlorophyta) from Japan. *Phycologia* **49**: 221–234.

Herdman, M.M. & Stanier, R.Y. 1977. The cyanelle: chloroplast or endosymbiotic prokaryote? *FEMS Microbiol. Lett.* **1**: 7–11.

Heymann, J.A.W., Hayles, M., Gestmann, I., Giannuzzi, L.A., Lich, B. & Subramaniam, S. 2006. Site-specific 3D imaging of cells and tissues with a dual beam microscope. *J. Struct. Biol.* **155**: 63–73.

Hieronymus, G. 1892. Beitrage zur Morphologie und Biologie der Algen. I. *Glaucocystis nostochinearum* Itzigsohn. *Beitr. Biol. Pfl.* **5**: 461–495.

Hindák, F. 2012. Cyanobaktérie/sinice rašeliniska Klin, Horná Orava. *XVI. Konf. SLS a ČLS zborník príspevkov* 43–45.

Hindák, F. & Hindáková, A. 2012. *Chalarodora azurea* Pascher 1929 —a rare glaucophyte found in the peat— bog Klin (Orava, northern Slovakia). in: Wołowski, K., Kaczmarska, I., Ehrman, J.M. & Wojtal, A.Z. (eds.), *Current advances in algal taxonomy and its applications: phylogenetic, ecological and applied perspective*. 53–60. Kraków.

Hirose, H. & Yamagishi, T. 1977. *Illustrations of the Japanese fresh-water algae*. Tokyo.

Hoffmann, L. & Kostikov, I. 2004. New record of *Glaucocystis nostochinearum* (Glaucophyta) in Belgium. *Belg. J. Bot.* **137**: 205–208.

Hu, H. & Wei, Y. 2006. *The freshwater algae of China: systematics, taxonomy and ecology*. Beijing.

Hu, Z., Ling, Y., Liang, L. & Bi, L. 1996. The new record of genera, species, varieties and form of Chlorococcales from China. *J. Wuhan Bot. Res.* **14**: 231–239.

Ichimura, K., Miyazaki, N., Sadayama, S., Murata, K., Koike, M., Nakamura, K., Ohta, K. & Sakai, T. 2015. Three-dimensional architecture of podocytes revealed by block-face scanning electron microscopy. *Sci. Rep.* **5**: 8993.

Imai, T., Sugiyama, J., Itoh, T. & Horii, F. 1999. Almost pure I_α cellulose in the cell wall of *Glaucocystis*. *J. Struct. Biol.* **127**: 248–257.

Islam, A.K.M.N. & Irfanullah, H.M. 1998. New records of three green algal genera for Bangladesh: *Desmatractum*, *Glaucocystis* and *Groenbladia*. *J. Plant Taxon* **5**: 91–95.

Jackson, C.J. & Reyes-Prieto, A. 2014. The mitochondrial genomes of the glaucophytes *Gloeochaete wittrockiana* and *Cyanoptyche gloeocystis*: multilocus phylogenetics suggests a monophyletic Archaeplastida. *Genom. Biol. Evol.* **6**: 2774–2785.

Kapustin, D.A. 2014. Freshwater algae of the Polessian Nature Reserve (Ukraine). *Internat. J. Alg.* **16**: 57–67.

Kasai, F., Kawachi, M., Erata, M., Mori, F., Yumoto, K., Sato, M. & Ishimoto, M. 2009. *NIES-Collection. List of strains 8th edition*. Tsukuba.

Kato, S. 1982. Laboratory culture and morphology of *Colacium vesiculosum* Ehrb. (Euglenophyceae). *Jpn. J. Phycol.* **30**: 63–67.

Keller, A., Schleicher, T., Schultz, J., Müller, T., Dandekar, T. & Wolf, M. 2009. 5.8S-28S rRNA interaction and HMM-based ITS2 annotation. *Gene* **430**: 50–57.

Kern, R., Eisenhut, M., Bauwe, H., Weber, A.P.M. & Hagemann, M. 2013. Does the *Cyanophora paradoxa* genome revise our view on the evolution of photorespiratory enzymes? *Plant Biol.* **15**: 759–768.

Kies, L. 1979. Zur systematischen Einordnung von *Cyanophora paradoxa*, *Gloeochaete wittrockiana* und *Glaucocystis nostochinearum*. *Ber. Dtsch. Bot. Ges.* **92**: 445–454.

Kies, L. 1984. Cytological aspects of blue-green algal endosymbiosis. in: Wiessner, W., Robinson, D.G. & Starr, R.C. (eds.), *Compartments in algal cells and their interaction*. 191–199. Berlin.

Kies, L. 1988. The effect of penicillin on the morphology and ultrastructure of *Cyanophora*, *Gloeochaete* and *Glaucocystis* (Glaucocystophyceae) and their cyanelles. *Endocyt. Cell Res.* **5**: 361–372.

Kies, L. 1989. Ultrastructure of *Cyanoptyche gloeocystis* f. *dispersa* (Glaucocystophyceae). *Plant Syst. Evol.* **164**: 65–73.

Kies, L. 1992. Glaucocystophyceae and other protists harbouring procaryotic endocytobionts. in: Reisser, W. (ed.), *Algae and symbioses: plants, animals, fungi, viruses, interactions explored*. 353–377. Bristol.

Kies, L. & Kremer, B.P. 1986. Typification of the Glaucocystophyta. *Taxon* **35**: 128–133.

Kies, L. & Kremer, B.P. 1990. Phylum Glaucocystophyta. in: Margulis, L. *et al.* (eds.), *Handbook of Protoctista: the structure, cultivation, habitats and life histories of the eukaryotic microorganisms and their descendants exclusive of animals, plants, and fungi: a guide to the algae, ciliates, foraminifera, sporozoa, water*

molds, slime molds, and the other protoctists. 152–166. Boston.

Kim, H.S. & Chung, J. 1994. Fresh-water algae new to Korea(IV). *Kor. J. Phycol.* **9**: 1–6.

Kirchner, O. 1888. Nachträge zur Algenflora von Württemberg. *Jahresh. Vereins vaterl. Naturkd. Württ.* **44**: 143–166.

Koch, W. 1964. Verzeichnis der Sammlung von Algenkulturen am Pflanzenphysiologischen Institut der Universität Göttingen. *Arch. Microbiol.* **47**: 402–432.

Koetschan, C., Förster, F., Keller, A., Schleicher, T., Ruderisch, B., Schwarz, R., Müller, T., Wolf, M. & Schultz, J. 2010. The ITS2 database III—sequences and structures for phylogeny. *Nucleic Acids Res.* **38**: D275–D279.

Kojima, K. 2008. *A systematic survey of the technical development of transmission electron microscopes*. Tokyo.

Komárek, J. & Fott, B. 1983. *Chlorophyceae (Grünalgen); Ordnung: Chlorococcales*. Stuttgart.

Коршиков, А.А. (= Korschikov, A.A. [*sic*]) 1924. Протистологические заметки. (= Protistologische Beobachtungen.) *Рус. Арх. Протистол. (=Arch. Rus. Protistol.)* **3**: 57–74.

Korshikov, A.A. 1930. *Glaucosphaera vacuolata*, a new member of the Glaucophyceae. *Arch. Protistenkd.* **70**: 217–222.

Korshikov, A.A. 1941. On some new or little known flagellates. *Arch. Protistenkd.* **95**: 22–44.

Коршиков, О.А. (= Korshikov, O.A.). 1953. *Підклас Протококові (Protococcineae): Вакуольні (Vacuolales) та Протококові (Protococcales) [=Pidklas Protokokovi (Protococcineae): Vakuoljni (Vacuolales) ta Protokokovi (Protococcales)]*. Kyiv.

Kugrens, P. 2002. Structure and phylogeny of *Cyanophora* species. in: Seckbach, J. (ed.), *Symbiosis: mechanisms and model systems*. 257–272. Dordrecht.

Kugrens, P., Clay, B.L., Meyer, C.J. & Lee, R.E. 1999. Ultrastructure and description of *Cyanophora biloba,* sp. nov., with additional observations on *C. paradoxa* (Glaucophyta). *J. Phycol.* **35**: 844–854.

Kühn, F.S. & Schnepf, E. 2002. Infection of *Glaucocystis nostochinearum* (Glaucophyta) by *Lagenidium* sp. (Oomycota) and its hyperparasite *Pythiella* sp. (Oomycota). *Hydrobiologia* **481**: 165–171.

Kützing, F.T. 1836. *Algarum aquae dulcis germanicum. Decas 15*. Halle (Saale).

Kützing, F.T. 1843. *Phycologia generalis oder Anatomie, Physiologie und Systemkunde der Tange—Mit 80 farbig gedruckten Tafeln, gezeichnet und gravirt vom Verfasser*. Leipzig.

Kützing, F.T. 1849. *Species algarum*. Leipzig.

Lagerheim, G. 1883. Bidrag till Sveriges algflora. *Öfvers. Kgl. Svensk. Vetensk.* **Årgang 40**: 37–78.

Lagerheim, G. 1884. Ein nenes Beispiel des Vorkommens von Chromatophoren bei den Phycochromaceen. *Ber. dtsch. Bot. Ges.* **2**: 302–304.

Lagerheim, G. 1886a. Algologiska bidrag. I. Contributions algologique à la flore de la

Suède. *Botaniska Notiser* **1886**: 44–50.

Lagerheim, G. 1886b. Bidrag till Amerikas Desmidié-flora. *Öfversigt af Kongl.* **42**: 225–255.

Lagerheim, G. 1888. Sopra alcune Alghe d'acqua dolce, nuove rimarchevoli. *Notarisia* **3**: 590–595. *[seen in the top page and the cited Italian in Lagerheim (1890)]*.

Lagerheim, G. 1890. *Gloeochaete* et *Schrammia*. *Nouva Notarisia* **1**: 227–231.

Lambert, D.H., Bryant, D.A., Stirewalt, V.L., Dubbs, J.M., Stevens, S.E. & Porter, R.D. 1985. Gene map for the *Cyanophora paradoxa* cyanelle genome. *J. Bacteriol.* **164**: 659–664.

Leblond, J.D., Dodson, J., Khadka, M., Holder, S. & Seipelt, R.L. 2012. Sterol composition and biosynthetic genes of the recently discovered photosynthetic alveolate, *Chromera velia* (Chromerida), a close relative of apicomplexans. *J. Eukaryot. Microbiol.* **59**: 191–197.

Leblond, J.D., Timofte, H.I., Roche, S.A. & Porter, N.M. 2011. Sterols of glaucocystophytes. *Phycol. Res.* **59**: 129–134.

Lee, C.M., Kafle, K., Park, Y.B. & Kim, S.H. 2014. Probing crystal structure and mesoscale assembly of cellulose microfibrils in plant cell walls, tunicate tests, and bacterial films using vibrational Sum Frequency Generation (SFG) spectroscopy. *Phys. Chem. Chem. Phys.* **16**: 10844–10853.

Lefort, M. 1965. Sur le chromatoplasme d'une Cyanophycée endosymbiotique, *Glaucocystis nostochinearum* Itzigs. *C. r. Acad. Sci.* **261**: 233–236.

Lefort, M. & Pouphile, M. 1967. Données cytochimiques sur l'organisation structurale

du chromatoplasma de *Glaucocystis nostochinearum*. *Soc. Biol.* **161**: 992–994.

Leliaert, F., Smith, D.R., Moreau, H., Herron, M.D., Verbruggen, H., Delwiche, C.F. & De Clerck, O. 2012. Phylogeny and molecular evolution of the green algae. *Crit. Rev. Plant Sci.* **31**: 1–46.

Lemmermann, E. 1908. Algologische Beiträge. *Arch. Hydrobiol. Planktonkd.* **4**: 165–192.

Li, S. 1596. *Compendium of materia medica*. Nanjing. *[in classical Chinese]*.

Linnaeus, C. 1753. *Species plantarum, exhibentes plantas rite cognitas, ad genera relatas, cum differentiis specificis, nominibus trivialibus, synonymis selectis, locis natalibus, secundum systema sexuale digestas*. Stockholm.

Löffelhardt, W. 1987. The cyanelle genome of *Cyanophora paradoxa*. *Ann. N. Y. Acad. Sci.* **503**: 550–552.

Löffelhardt, W., Mucke, H., Crouse, E.J. & Bohnert, H.J. 1983. Comparison of the cyanelle DNA from two different strains of *Cyanophora paradoxa*. *Curr. Genet.* **7**: 139–144.

Mackiewicz, P. & Gagat, P. 2014. Monophyly of Archaeplastida supergroup and relationships among its lineages in the light of phylogenetic and phylogenomic studies. Are we close to a consensus? *Acta Soc. Bot. Pol.* **83**.

Mangeney, E., Hawthornthwaite, A.M., Codd, G.A. & Gibbs, S.P. 1987. Immunocytochemical localization of phosphoribulose kinase in the cyanelles of *Cyanophora paradoxa* and *Glaucocystis nostochinearum*. *Plant Physiol.* **84**: 1028–1032.

Matsuzaki, R., Hara, Y. & Nozaki, H. 2014. A taxonomic study of snow *Chloromonas* species (Volvocales, Chlorophyceae) based on light and electron microscopy and molecular analysis of cultured material. *Phycologia* **53**: 293–304.

Matsuzaki, R., Nakada, T., Hara, Y. & Nozaki, H. 2010. Light and electron microscopy and molecular phylogenetic analyses of *Chloromonas pseudoplatyrhyncha* (Volvocales, Chlorophyceae). *Phycol. Res.* **58**: 202–209.

Mayr, E. 1942. *Systematics and the origin of species, from the viewpoint of a zoologist*. London.

Mereschkowsky, C. 1905. Über Natur und Ursprung der Chromatophoren im Pflanzenreiche. *Biol. Cbl.* **25**: 593–604.

Mignot, J.P., Joyon, L. & Pringsheim, E.G. 1969. Quelques particularités structurales de *Cyanophora paradoxa* Korsch., protozoaire flagellé. *J. Eukaryot. Microbiol.* **16**: 138–145.

Miyagishima, S., Kabeya, Y., Sugita, C., Sugita, M. & Fujiwara, T. 2014. *DipM* is required for peptidoglycan hydrolysis during chloroplast division. *BMC Plant Biol.* **14**: 57.

Miyamura, S., Hori, T. & Nagumo, T. 2003. Eyespot behavior during the fertilization of gametes in *Ulva arasakii* Chihara (Ulvophyceae, Chlorophyta). *Phycol. Res.* **51**: 143–146.

Mogi, Y., Kagami, Y., Kuwano, K., Miyamura, S., Nagumo, T. & Kawano, S. 2008. Asymmetry of eyespot and mating structure positions in *Ulva compressa* (Ulvales, Chlorophyta) revealed by a new FE-SEM method. *J. Phycol.* **44**: 1290–1299.

Moore, R.B., Oborník, M., Janouškovec, J., Chrudimský, T., Vancová, M., Green, D.H., Wright, S.W., Davies, N.W., Bolch, C.J.S., Heimann, K., Šlapeta, J., Hoegh-Guldberg, O., Logsdon, J.M. & Carter, D.A. 2008. A photosynthetic alveolate closely related to apicomplexan parasites. *Nature* **451**: 959–963.

Moreira, D., le Guyader, H. & Philippe, H. 2000. The origin of red algae and the evolution of chloroplasts. *Nature* **405**: 69–72.

Mori, F., Erata, M. & Watanabe, M.M. 2002. Cryopreservation of cyanobacteria and green algae in the NIES-Collection. *Microbiol. Cult. Coll.* **18**: 45–55.

Müller, T., Philippi, N., Dandekar, T., Schultz, J. & Wolf, M. 2007. Distinguishing species. *RNA* **13**: 1469–1472.

Nagatani, T. 1991. High resolution scanning electron microscopy—Microscopic observation of surface fine morphology. *CACS Forum* **11**: 28–37.

Nakada, T. 2010. Culture dependent research of microalgae and typification under the International Code of Botanical Nomenclature (Vienna Code). *Microbiol. Cult. Coll.* **26**: 109–116.

Nakada, T. & Nozaki, H. 2007. Re-evaluation of three *Chlorogonium* (Volvocales, Chlorophyceae) species based on 18S ribosomal RNA gene phylogeny. *Eur. J. Phycol.* **42**: 177–182.

Nakada, T., Nozaki, H. & Pröschold, T. 2008. Molecular phylogeny, ultrastructure, and taxonomic revision of *Chlorogonium* (Chlorophyta): emendation of *Chlorogonium* and description of *Gungnir* gen. nov. and *Rusalka* gen. nov. *J. Phycol.* **44**: 751–760.

Nishida, T., Yoshimura, R. & Endo, Y. 2013. Three-dimensional distribution of TrkA

neurotrophin receptors in neurite varicosities of differentiated PC12 cells treated with NGF determined by immunoelectron tomography. *Cell Tissue Res.* **351**: 1–13.

Nozaki, H., Iseki, M., Hasegawa, M., Misawa, K., Nakada, T., Sasaki, N. & Watanabe, M. 2007. Phylogeny of primary photosynthetic eukaryotes as deduced from slowly evolving nuclear genes. *Mol. Biol. Evol.* **24**: 1592–1595.

Nozaki, H., Maruyama, S., Matsuzaki, M., Nakada, T., Kato, S. & Misawa, K. 2009. Phylogenetic positions of Glaucophyta, green plants (Archaeplastida) and Haptophyta (Chromalveolata) as deduced from slowly evolving nuclear genes. *Mol. Phylogenet. Evol.* **53**: 872–880.

Nozaki, H., Matsuzaki, M., Takahara, M., Misumi, O., Kuroiwa, H., Hasegawa, M., Shin-i, T., Kohara, Y., Ogasawara, N. & Kuroiwa, T. 2003. The phylogenetic position of red algae revealed by multiple nuclear genes from mitochondria-containing eukaryotes and an alternative hypothesis on the origin of plastids. *J. Mol. Evol.* **56**: 485–497.

Nozaki, H., Misawa, K., Kajita, T., Kato, M., Nohara, S. & Watanabe, M.M. 2000. Origin and evolution of the colonial Volvocales (Chlorophyceae) as inferred from multiple, chloroplast gene sequences. *Mol. Phylogenet. Evol.* **17**: 256–268.

Oborník, M., Vancová, M., Lai, D., Janouškovec, J., Keeling, P.J. & Lukeš, J. 2011. Morphology and ultrastructure of multiple life cycle stages of the photosynthetic relative of Apicomplexa, *Chromera velia*. *Protist* **162**: 115–130.

Okuda, K. 2002. Structure and phylogeny of cell coverings. *J. Plant Res.* **115**: 283–288.

Okuda, K., Tsekos, L. & Brown Jr., R.M. 1994. Cellulose microfibril assembly in *Erythrocladia subintegra* Rosenv.: an ideal system for understanding the relationship between synthesizing complexes (TCs) and microfibril crystallization. *Protoplasma* **180**: 49–58.

Osumi, M. 1998. The ultrastructure of yeast: cell wall structure and formation. *Micron* **29**: 207–233.

Palm, L.C. 2008. Antoni van Leeuwenhoek [*sic*] 1632–1723. in: Kox, A.J. (ed.), *Van Stevin tot Lorentz. Portretten van achttien Nederlandse natuurwetenschappers. (2e herziene uitgave)*. 49–60. Amsterdam.

Parfrey, L.W., Lahr, D.J.G., Knoll, A.H. & Katz, L.A. 2011. Estimating the timing of early eukaryotic diversification with multigene molecular clocks. *Proc. Natl. Acad. Sci. USA* **108**: 13624–13629.

Pascher, A. 1906. Neuer Beitrag zur Algenflora des südlichen Böhmerwaldes. *Lotos* **54**: 147–182.

Pascher, A. 1914. Über Symbiosen von Spaltpilzen und Flagellaten mit Blaualgen. *Ber. Dtsch. Bot. Ges.* **32**: 339–352.

Pascher, A. 1929. Über einige Endosymbiosen von Blaualgen in Einzellern. *Jahrb. Wiss. Bot.* **71**: 386–462.

Patel, R.J. 1981. *Glaucocystis indica* Patel sp. nov. from India. *Geophytology* **11**: 259–261.

Patel, R.J. & Isabella George 1979. Chlorococcales of Gujarat—India. *Vidya. B, Sci.* **22**: 1–9.

Philipose, M. 1967. *Chlorococcales*. New Delhi.

Pienaar, R.N. 1994. Ultrastructure and calcification of coccolithophores. in: Winter, A. & Siesser, W.G. (eds.), *Coccolithophores*. 13–37. Cambridge.

Prasad, B.N. 1961. *Glaucocystis nostochinearum* (Itzig.) Rabenhorst in India. *Bull. Bot. Soc.* **13**: 44–45.

Prasad, B.N., Mehrotra, R.K. & Misra, P.K. 1984. *Glaucocystis reniformis* sp. nov. from Andaman Islands. *Cryptogamie, Algologie* **5**: 79–84.

Prescott, G.W. 1944. New species and varieties of Wisconsin algae. *Farlowia* **1**: 347–385.

Prescott, G.W. 1962. *Algae of the western Great Lakes area*. Dubuque.

Price, D.C., Chan, C.X., Yoon, H.S., Yang, E.C., Qiu, H., Weber, A.P.M., Schwacke, R., Gross, J., Blouin, N.A., Lane, C., Reyes-Prieto, A., Durnford, D.G., Neilson, J.A.D., Lang, B.F., Burger, G., Steiner, J.M., Löffelhardt, W., Meuser, J.E., Posewitz, M.C., Ball, S., Arias, M.C., Henrissat, B., Coutinho, P.M., Rensing, S.A., Symeonidi, A., Doddapaneni, H., Green, B.R., Rajah, V.D., Boore, J. & Bhattacharya, D. 2012. *Cyanophora paradoxa* genome elucidates origin of photosynthesis in algae and plants. *Science* **335**: 843–847.

Pringsheim, E.G. 1946. *Pure cultures of algae*. Cambridge.

Pringsheim, E.G. 1958. Organismen mit blaugrünen Assimilatoren. in: Prat, S. (ed.), *Studies in plant physiology*. 165–184. Prague.

Rabenhorst, L.G. 1866. *Die Algen Europa's, Fortsetzung der Algen Sachsens, resp. Mittel-europa's. Decades 94–95, Number 1935*. Dresden. *[in Fraktur]*.

Rabenhorst, L.G. 1868. *Flora Europaea algarum aquae dulcis et submarinae. III. Algas Chlorophyllophyceas, Melanophyceas et Rhodophyceas, complectens*. Leipzig.

Reyes-Prieto, A. & Bhattacharya, D. 2007. Phylogeny of nuclear-encoded plastid-targeted proteins supports an early divergence of glaucophytes within Plantae. *Mol. Biol. Evol.* **24**: 2358–2361.

Robinson, D.G. & Preston, R.D. 1971a. Studies on the fine structure of *Glaucocystis nostochinearum* Itzigs. II. Membrane morphology and taxonomy. *Br. Phycol. J.* **6**: 113–128.

Robinson, D.G. & Preston, R.D. 1971b. Studies on the fine structure of *Glaucocystis nostochinearum* Itzigs. I. Wall structure. *J. Exp. Bot.* **22**: 635–643.

Rodríguez-Ezpeleta, N., Brinkmann, H., Burey, S.C., Roure, B., Burger, G., Löffelhardt, W., Bohnert, H.J., Philippe, H. & Lang, B.F. 2005. Monophyly of primary photosynthetic eukaryotes: green plants, red algae, and glaucophytes. *Current Biology* **15**: 1325–1330.

Rybalka, N., Wolf, M., Andersen, R.A. & Friedl, T. 2013. Congruence of chloroplast- and nuclear-encoded DNA sequence variations used to assess species boundaries in the soil microalga *Heterococcus* (Stramenopiles, Xanthophyceae). *BMC Evol. Biol.* **13**: 1–15.

Sagan, L. 1967. On the origin of mitosing cells. *J. Theor. Biol.* **14**: 225–274.

Saito, C. 2013. Ultrastructural analysis of single-membrane-bound organelles in plant cells: A comparison of high-pressure freezing versus chemical fixation. *Plant Morphol.* **25**: 11–14.

Saitou, N. & Nei, M. 1987. The neighbor-joining method: a new method for

reconstructing phylogenetic trees. *Mol. Biol. Evol.* **4**: 406–425.

Sato, M., Mogi, Y., Nishikawa, T., Miyamura, S., Nagumo, T. & Kawano, S. 2009. The dynamic surface of dividing cyanelles and ultrastructure of the region directly below the surface in *Cyanophora paradoxa*. *Planta* **229**: 781–791.

Sato, M., Nishikawa, T., Kajitani, H. & Kawano, S. 2007. Conserved relationship between FtsZ and peptidoglycan in the cyanelles of *Cyanophora paradoxa* similar to that in bacterial cell division. *Planta* **227**: 177–187.

Sato, M., Nishikawa, T., Yamazaki, T. & Kawano, S. 2005. Isolation of the plastid *FtsZ* gene from *Cyanophora paradoxa* (Glaucocystophyceae, Glaucocystophyta). *Phycol. Res.* **53**: 93–96.

Saunders, G.W. & Hommersand, M.H. 2004. Assessing red algal supraordinal diversity and taxonomy in the context of contemporary systematic data. *Am. J. Bot.* **91**: 1494–1507.

Schaffner, J.H. 1922. The classification of plants. XII. *Ohio J. Sci.* **22**: 129–139.

Schenk, H.E.A. 1970. Nachweis einer lysozymempfindlichen Stützmembran der Endocyanellen von *Cyanophora paradoxa* Korschikoff. *Z. Naturforsch. B.* **B25**: 656.

Schenk, H.E.A. 1992. Cyanobacterial symbioses. in: Balows, A. (ed.), *The prokaryotes: a handbook on the biology of bacteria: ecophysiology, isolation, identification, applications*. 3819–3854. New York.

Schenk, H.E.A. 1994. Glaucocystophyta model for symbiogenous evolution of new eukaryotic species. in: Seckbach, J. (ed.), *Evolutionary pathways and enigmatic algae: Cyanidium caldarium (Rhodophyta) and related cells*. 19–52.

Dordrecht.

Schenk, H.E.A. 2002. Glaucocystophytes. *ELS*.

Schenk, H.E.A., Bayer, M.G. & Zook, D. 1987. Cyanelles—From symbiont to organelle. *Ann. N. Y. Acad. Sci.* **503**: 151–167.

Schiller, J. 1954. Neue Mikrophyten aus künstlich betonierten Wasserbehältern. *Arch. Protistenkd.* **100**: 116–126.

Schimper, A.F.W. 1883. Ueber die Entwickelung der Chlorophyllkörner und Farbkörper. *Bot. Zeitung* **41**: 105–162.

Schlösser, U.G. 1994. SAG—Sammlung von Algenkulturen at the University of Göttingen. Catalogue of Strains 1994. *Bot. Acta* **107**: 111–186.

Schmidle, W. 1902. Berichte über die botanischen Ergebnisse der Nyassa-See- und Kinga-Gebirgs-Expedition der Hermann- und Elise- geb. Heckmann-Wentzel-Stiftung. V. Algen, insbesondere solche des Plankton, aus dem Nyassa-See und seiner Umgebung, gesammelt von Dr. Fülleborn. *Bot. Jahrb. Syst.* **32**: 55–88.

Schnepf, E. 1965. Struktur der Zellwände und Cellulosefibrillen bei *Glaucocystis*. *Planta* **67**: 213–224.

Schnepf, E. & Brown Jr., R.M. 1971. On relationships between endosymbiosis and the origin of plastids and mitochondria. in: Ursprung, H. & Reinert, J. (eds.), *Origin and development of cell organelles*. Heidelberg.

Schnepf, E. & Koch, W. 1966. Golgi Apparat und Wasserausscheidung bei *Glaucocystis*. *Z. PflPhysiol.* **55**: 97–109.

Schnepf, E., Koch, W. & Deichgräber, G. 1966. Zur Cytologie und taxonomischen Einordnung von *Glaucocystis*. *Arch. Microbiol.* **55**: 149–174.

Schouteden-Wéry, J. 1911. Quelques recherches sur les facteurs qui règlent la distribution géographique des algues dans la Veurne Ambacht. *Rec. Inst. Bot. Leo Errera* **8**: 101–212.

Schrödinger, E. 1944. *What is life?—The physical aspect of the living cell.* Cambridge.

Scott, J., Yang, E.C., West, J.A., Yokoyama, A., Kim, H.J., Loiseaux de Goër, S., O'Kelly, C.J., Orlova, E., Kim, S.Y., Park, J.K. & Yoon, H.S. 2011. On the genus *Rhodella*, the emended orders Dixoniellales and Rhodellales with a new order Glaucosphaerales (Rhodellophyceae, Rhodophyta). *Algae* **26**: 277–288.

Scott, O.T., Castenholz, R.W. & Bonnett, H.T. 1984. Evidence for a peptidoglycan envelope in the cyanelles of *Glaucocystis nostochinearum* Itzigsohn. *Arch. Microbiol.* **139**: 130–138.

Sekida, S., Horiguchi, T. & Okuda, K. 2001. Development of the cell covering in the dinoflagellate *Scrippsiella hexapraecingula* (Peridiniales, Dinophyceae). *Phycol. Res.* **49**: 163–176.

Simons, J. 2010. Glaucophyta. in: Noordijk, J., Kleukers, R.M.J.C., van Nieukerken, E.J. & van Loon, A.J. (eds.), *Overzicht van de Nederlandse biodiversiteit*. 61. Nederland.

Skuja, H.L. 1948. Taxonomie des Phytoplanktons einiger Seen in Uppland. *Symb. Bot. Ups.* **9**: 1–399.

Skuja, H.L. 1949. Zur Süßwasser Algenflora Burmas. *Nov. Act. Reg. Soc. Sci. Ups. (IV)* **14**: 1–188.

Skuja, H.L. 1954. Abteilung Glaucophyta. in: Melchior, H. & Werdermann, E. (eds.), *Allgemeiner Teil, Bakterien bis Gymnospermen*. 56–57. Berlin-Nikolassee.

Skuja, H.L. 1956. Taxonomische und biologische Studien über das Phytoplankton schwedischer Binnengewässer. *Nov. Act. Reg. Soc. Sci. Ups. (IV)* **16**: 1–404.

Smit, P. & Heniger, J. 1975. Antoni van Leeuwenhoek [*sic*] (1632–1723) and the discovery of bacteria. *Antonie van Leeuwenhoek* [sic] **41**: 217–228.

Smith, G.M. 1933. *The fresh-water algae of the United States*. New York.

Smith, D.R., Jackson, C.J. & Reyes-Prieto, A. 2014. Nucleotide substitution analyses of the glaucophyte *Cyanophora* suggest an ancestrally lower mutation rate in plastid vs mitochondrial DNA for the Archaeplastida. *Mol. Phylogenet. Evol.* **79**: 380–384.

Smith, M.A., Eveleigh, E.S., McCann, K.S., Merilo, M.T., McCarthy, P.C. & Van Rooyen, K.I. 2011. Barcoding a quantified food web: crypsis, concepts, ecology and hypotheses. *PLoS ONE* **6**: e14424.

Spiegel, F.W. 2012. Contemplating the first Plantae. *Science* **335**: 809–810.

Spurr, A.R. 1969. A low viscosity epoxy resin embedding medium. *J. Ultrastruct. Res.* **26**: 31–43.

Starmach, K. 1939. O zakwicie neustonowym w jednym stawków Rybackiej Stacji Doświadczalnej U. J. w Mydlnikach pod Krakowem. *Acta Soc. Bot. Pol.* **16**: 127–153.

Starmach, K. 1966. Flora słodkowodna Polski. Tom 2. *Cyanophyta—Sinice. Glaucophyta—Glaukofity.* Warszawa.

Starr, R.C. & Zeikus, J.A. 1993. UTEX—the culture collection of algae at the University of Texas at Austin. *J. Phycol.* **29**(Suppl): 1–106.

Stirewalt, V., Michalowski, C., Löffelhardt, W., Bohnert, H. & Bryant, D.A. 1995. Nucleotide sequence of the cyanelle genome from *Cyanophora paradoxa*. *Plant Mol. Biol. Rep.* **13**: 327–332.

Sugiyama, J., Persson, J. & Chanzy, H. 1991. Combined infrared and electron diffraction study of the polymorphism of native celluloses. *Macromolecules* **24**: 2461–2466.

Takahashi, T. 2013. *A taxonomic study of* Cyanophora *(Cyanophorales, Glaucophyta), on the basis of molecular phylogeny and comparative morphology.* The University of Tokyo, Tokyo.

Tamura, K. 1992. Estimation of the number of nucleotide substitutions when there are strong transition-transversion and G+C-content biases. *Mol. Biol. Evol.* **9**: 678–687.

Tamura, K., Peterson, D., Peterson, N., Stecher, G., Nei, M. & Kumar, S. 2011. MEGA5: Molecular evolutionary genetics analysis using maximum likelihood, evolutionary distance, and maximum parsimony methods. *Mol. Biol. Evol.* **28**: 2731–2739.

Tao, H. 718. *Bencaojizhu.* Xi'an. *[m.s., in classical Chinese, seen in several pieces, originally published ca. 500, Nanjing]*.

Тарноградский, Д.А. (=Tarnogradskij, D.A.). 1957. Микрофлора и микрофауна торфяников Кавказа. 6. Девдоракское сфагновое болотце (= Mikroflora i mikrofauna torfjanikov Kavkaza. 6. Djevdorakskoje sfagnovoje bolotcje).

Работы Северокавказ. гидробиол. станции (= Raboty Severokavkaz. gidrobiol. stantsii) **6**: 3–55. *[not seen in original; cited after Komárek & Fott (1983)]*.

Тарноградский, Д.А. (=Tarnogradskij, D.A.). 1959. Микрофлора и микрофауна торфяников Кавказа. 8. Осоковосфагновое озеро в верховьях Балкараской реки Терек (=Mikroflora i mikrofauna torfjanikov Kavkaza. 8. Osokovosfagnovoje ozjero v verchov'ach Balkaraskoj rjeki Tjerjek). *Тр. Сев. -Осет. с. -х. ин-та. Орджоникидзе (=Rab. Severo-Kavkaz. Gidrobiol. Stancij Ordzhonikidze)* **20**: 2–17.

Theophrastus. 1483. *Historia plantarum. [translated into Latin by Theodorus Gaza, original title: Θεόφραστος, Περὶ φυτῶν ἱστορία (ca. B.C. 300), Athens]*.

Thompson, A. 1973. The flagella of *Cyanophora paradoxa* Korsch. *J. S. Afr. Bot.* **39**: 35–39.

Thompson, J., Higgins, D. & Gibson, T. 1994. CLUSTAL W: improving the sensitivity of progressive multiple sequence alignment through sequence weighting, position-specific gap penalties and weight matrix choice. *Nucleic Acids Res.* **22**: 4673–4680.

Trench, R.K., Pool, R.R., Logan, M. & Engelland, A. 1978. Aspects of the relation between *Cyanophora paradoxa* (Korschikoff) and its endosymbiotic cyanelles *Cyanocyta korschikoffiana* (Hall & Claus). I. Growth, ultrastructure, photosynthesis and the obligate nature of the association. *Proc. Royal Soc. B.* **202**: 423–443.

Trench, R.K. & Siebens, H.C. 1978. Aspects of the relation between *Cyanophora paradoxa* (Korschikoff) and its endosymbiotic cyanelles *Cyanocyta korschikoffiana* (Hall & Claus). IV. The effects of rifampicin, chloramphenicol and cycloheximide on the synthesis of ribosomal ribonucleic acids and chlorophyll. *Proc. Royal Soc. B.* **202**: 473–482.

Ueda, K. 1961. Structure of plant cells with special reference to lower plants; VI. Structure of chloroplasts in algae. *Cytologia* **26**: 344–358.

Van Leewenhoeck, A. 1677. Obſervations, communicated to the Publiſher by Mr. Antony van Leewenhoeck [*sic*], in a Dutch Letter of the 9th of Octob. 1676. here Engliſh'd: Concerning little Animals by him obſerved in Rain-Well-Sea- and Snow- water; as alſo in water wherein pepper had lain infuſed. *Phil. Trans.* **12**: 821–831.

Van Meel, L. 1939. Matériaux pour servir à la flore algologique de la province d'Anvers. *Bull. Soc. Roy. Bot. Belg.* **71**: 186–192.

Van Meel, L. 1944. Contributions à la flore algologique de la Belgique. *Bull. Soc. Roy. Bot. Belg.* **76**: 51–59.

Van Wichelen, J., Declerck, S., Louette, G., Hoste, I., Denayer, S., Denys, L., de Meester, L. & Vyverman, W. 2008. Grootschalig natuurherstel in de Kraenepoel, een geëutrofieerd ondiep meer te Aalter (Oost-Vlaanderen). *Natuur. focus* **7**: 46–53.

Vasconcelos, V. & Morais, J. 2009. *Relatório. 1º Ensaio laboratorial de fitoplâncton*. Lisbon.

Watanabe, M., Kubota, H., Wada, H., Narikawa, R. & Ikeuchi, M. 2011. Novel

supercomplex organization of photosystem I in *Anabaena* and *Cyanophora paradoxa*. *Plant Cell Physiol.* **52**: 162–168.

Watanabe, M., Sato, M., Kondo, K., Narikawa, R. & Ikeuchi, M. 2012. Phycobilisome model with novel skeleton-like structures in a glaucocystophyte *Cyanophora paradoxa*. *BBA, Bioenerg.* **1817**: 1428–1435.

Weatherby, K., Murray, S., Carter, D. & Šlapeta, J. 2011. Surface and flagella morphology of the motile form of *Chromera velia* revealed by field-emission scanning electron microscopy. *Protist* **162**: 142–153.

Wełnicz, W., Grohme, M.A., Kaczmarek, Ł., Schill, R.O. & Frohme, M. 2011. ITS-2 and 18S rRNA data from *Macrobiotus polonicus* and *Milnesium tardigradum* (Eutardigrada, Tardigrada). *J. Zool. Syst. Evol. Res.* **49**: 34-39.

West, G.S. 1904. *British freshwater algae*. London.

Whitton, B.A. 2002. Phylum Glaucophyta. in: John, D.M., Whitton, B.A. & Brook, A.J. (eds.), *The freshwater algal flora of the British Isles: an identification guide to freshwater and terrestrial algae*. 613. London.

Wille, J.N.F. 1919. Algologische Notizen XXV–XXIX. XXIX. Studien in Agardh's Herbarium 8–15. 9. Über *Microcystis bullosa* (Kütz.) Menegh. und *M. gelatinosa* Menegh. (p.33–60). *Nyt Mag. f. Naturv.* **56**: 1–60.

Willison, J.H.M. & Brown Jr., R.M. 1978a. Cell wall structure and deposition in *Glaucocystis*. *J. Cell Biol.* **77**: 103–119.

Willison, J.H.M. & Brown Jr., R.M. 1978b. A model for the pattern of deposition of microfibrils in the cell wall of *Glaucocystis*. *Planta* **141**: 51–58.

Wolf, M., Chen, S., Song, J., Ankenbrand, M. & Müller, T. 2013. Compensatory base changes in ITS2 secondary structures correlate with the biological species concept despite intragenomic variability in ITS2 sequences—a proof of concept. *PLoS ONE* **8**: e66726.

Xu, D., Sun, P., Shin, M.K. & Kim, Y.O. 2012. Species boundaries in Tintinnid ciliates: a case study—morphometric variability, molecular characterization, and temporal distribution of *Helicostomella* species (Ciliophora, Tintinnina). *J. Eukaryot. Microbiol.* **59**: 351–358.